Going with the Flow

A study on the impact of stratified North Sea coastal currents on energy consumption in dredging projects

S.E. Schless
Delft University of Technology
27-06-2023

Van Oord
Marine ingenuity

TU Delft

Going with the Flow

A study on the impact of stratified North Sea coastal currents on energy consumption in dredging projects

Master thesis submitted to Delft University of Technology

in partial fulfilment of the requirements for the degree of

MASTER OF SCIENCE

in **Hydraulic Engineering**

Faculty of Civil Engineering

by

S.E. Schless

Student number: 5185378

To be defended in public on July 6th 2023

Graduation committee

Chairperson	: Prof. dr. ir. J.D. Pietrzak,	TU Delft
First Supervisor	: Prof. dr. ir. M. Van Koingsveld,	TU Delft, Van Oord
External Supervisor	: Dr. ir. G. J. de Boer,	Van Oord

Acknowledgement

This thesis research is carried out to complete the Hydraulic Engineering master at the TU Delft Faculty Of Civil Engineering and Geosciences. The research was done in collaboration with Van Oord, a maritime contracting company specializing in dredging and offshore wind farms, in the form of a graduation internship. Van Oord provided funding and a workspace to facilitate the research process. The total duration of the thesis research was approximately 11 months, starting from the 15th of august 2022 until the 6th of july 2023.

First of all, I want to thank my supervisor at Van Oord, Gerben de Boer. From start to finish we had a weekly meeting in which he gave me new ideas for improvement, helpful feedback and overall knowledge on how to conduct a research. He also showed enthusiasm and support throughout the 11 months of my process, which helped with my motivation and made my research feel important and relevant. Secondly, I would like to thank my TU Delft thesis committee members, consisting of my chair Julie Pietrzak and second reader Mark van Koningsveld. They helped me to look outside the scope of my research and see the valuable implications it has. I would also like to thank Martin de Geus, who helped me to translate the interaction between currents and a dredging vessel into a python-based model. Lastly, I want to thank my colleagues and other graduates at Van Oord that were always helpful and kind to me.

Abstract

The goal of achieving net-zero emissions by 2050 requires innovative ways to reduce energy consumption in all sectors. This thesis presents an in-depth analysis on the effect of coastal currents on energy consumption of sailing dredging vessels and the potential to make use of these currents to minimize energy consumption in dredging projects. To model the highly dynamic and time-dependent currents of the North Sea, an analytical solution for the tidal-induced currents and residual density-driven currents was used to create a synthetic 3D flow field, respectively derived by Prandle and Heaps. To quantify the energy consumption of dredging vessels sailing through a 3D flow field, a python-based model was developed. This model utilizes the Holtrop and Mennen method to calculate the sailing speed corresponding to a desired engine power, with a modification to account for current-induced drag resistance on the rudder caused by currents perpendicular to the sailing direction. The model was validated with sensory vessel data of Van Oord containing information of a dredging project in the North Sea, in combination with measured data for the currents at the location of the project. The validated model was used to explore a dredging strategy for a sand nourishment project that minimizes energy consumption by waiting for favourable marine currents before sailing. A sand nourishment project was chosen because the primary cross-shore movement of the vessel interacts with the bi-weekly occurrence of alternating cross-shore currents. Two cases were simulated, a hypothetical case in which the vessel does not consume energy when waiting, and a realistic case in which the vessel's energy consumption continues due to utilities such a lighting and heating of the on-board hotel. The hypothetical case showed a reduction of energy consumption of 3% when sailing with the cross-shore currents as opposed to neglecting these currents, which is at the lower boundary of the energy reduction due to voyage optimization predicted by IMO (1% - 10%). However, the energy reduction was outweighed by energy consumption during waiting in the realistic case, making this strategy unsuitable for conventional dredging vessels. The model developed in this thesis can be of significant value for both dredging companies as well as researchers. These stakeholders can use the model to plan and optimize dredging activities, reduce environmental impact, and identify areas for innovation and improvement in the dredging industry.

Summary

The net-zero emissions goal presented in the Paris Agreement requires a reduction of carbon emissions, which is a complex effort that benefits from innovation and research. Global shipping's total share of greenhouse gas emissions is estimated to be 3% according to the IMO. With over a hundred marine vessels and projects all around the world, Van Oord is one of the largest contractors in the dredging and offshore wind park industry and has a part to play in this effort to reduce emissions. The net-zero emissions goal is causing a shifting paradigm in this industry from project design based on the lowest costs, towards project design based on the lowest carbon emissions (i.e. lowest energy consumption). To inform decision-making and develop effective energy-efficient measures, it is necessary to gain insight into the factors that contribute the most to the energy consumption of the vessels. This thesis explores the effects of stratified coastal currents in the North Sea on the energy consumption of dredging vessels, presenting a python-based model that can quantify the energy consumption while also being able to provide insight into the various parameters and their effect on savings and adaptive sailing approaches. The main research question is:

> *What is the effect of a dynamic and time-dependent stratified coastal current on the energy consumption of dredging vessels, and how can these currents be harnessed to reduce energy consumption?*

To conduct the research and create the python-based model, a research was done on the various existing methodologies that determine energy consumption and emissions for sailing ships. This existing method should be able to account for currents by means of a modification while simultaneously provide insight into the different components influencing energy consumption. The Holtrop and Mennen method was chosen as the most suitable approach because it includes parameters such as the water depth and the draught amongst various other ship dimensions and characteristics. It contains an elaborate set of input variables, providing the most detailed calculation of energy consumption and the ability to identify the largest contributors.

The model presented in this thesis provides a means to calculate the energy consumption of the free sailing part of a dredging vessel by accounting for additional factors beyond those considered in the Holtrop and Mennen method. Namely an extra drag resistance on the rudder of the dredging vessel, caused by the drift angle, and an altered sailing time. The model takes as input a desired engine power, in combination with the vessel dimensions, sailing path, water depth and draught, to calculate the sailing speed of the vessel. Furthermore, the model was validated with data from a sea access dredging project consisting of information on ship activity and coastal currents in the North Sea. It was concluded that the model underestimates the sailing speed. By introducing a calibration factor, the average error between the model prediction and the measurements was reduced to less than 5.5%.

The model uses a synthetic flow field containing realistic velocity magnitudes to get a first order estimate of the effect of currents on the energy consumption of sailing vessels. This flow field is based on an analytical solution for the tidal-induced currents and the residual density-driven flow. The analytical solution for tidal-induced currents was derived by Prandle in 1982, the solution is a time-dependent vertical velocity structure that oscillates with the tidal period. The analytical solution for the density-driven residual flow was derived by Heaps in 1972, it resulted in a time-independent vertical velocity structure. The 3D flow field that was used in the energy consumption calculations combines the two analytical solutions to represent the currents of a neap tide and spring tide scenario in the North Sea. This produces a vertical velocity structure with counter-rotating elliptical currents at the surface and at the bed. In essence, these currents are a Kelvin Wave with vertical cross-shore exchange currents. The figure below provides a highly simplified depiction of the interaction between these currents and the dredging vessel.

With the model working and validated, the effectiveness of waiting for the current to become favourable in the sailing direction was explored with the Prandle and Heaps flow field. This was done for two cases; a hypothetical case where the vessel does not consume energy while waiting, and a realistic case in which the vessel consumes energy during waiting due to the presence of other utilities such as the energy consumption of an on-board hotel. The main finding was a reduction of energy consumption of 3% for a scenario with maximum stratification and an infinite allowable waiting time in the hypothetical case.

The model can be used directly by dredging companies to plan and optimize dredging and wind installation projects and to present accurate energy estimations in tenders. It can also be used it to explore innovative strategies that make use of the currents to reduce energy consumption of sailing on a project scale. Moreover, it can be used by researchers to study the impact of marine currents in other coastal systems. A limitation of this research is the use of an analytical solution to represent the North Sea currents. This creates a possibility for further research with a more accurate representation, for instance by means of a numerical model. A second research possibility is to add a component that accounts for weather conditions, such as an added resistance due to wind and waves.

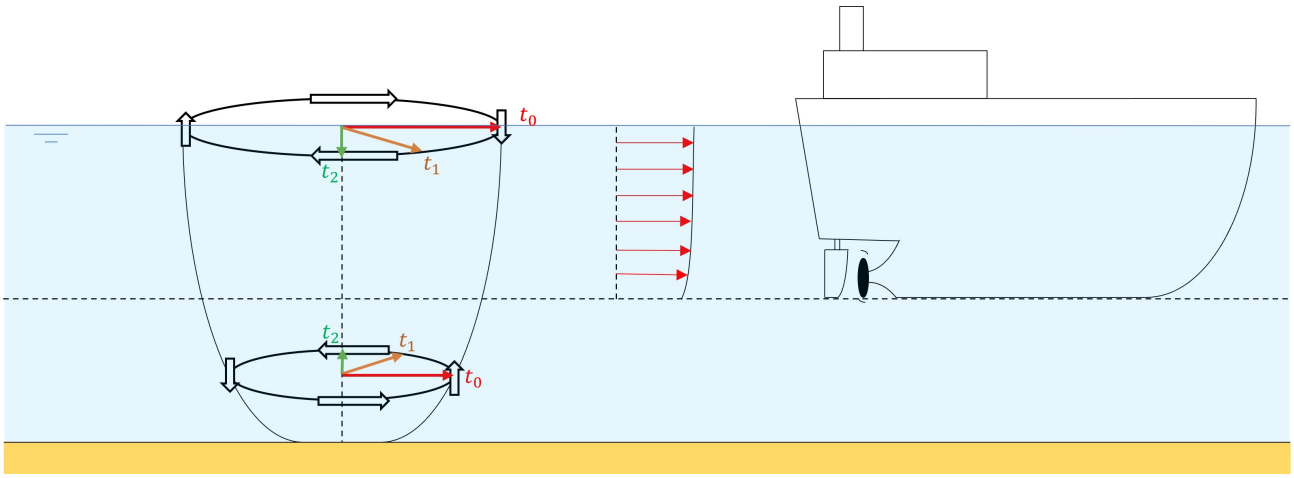

Schematization of a dredging vessel sailing through the vertical velocity structure (left), with counter-rotating elliptical currents at the surface and bed, and the part affecting the vessel at t0 (middle).

Contents

Chapter 1

Introduction

The Earth is on the brink of irreversible damage due to rising greenhouse gas emissions, the Intergovernmental Panel on Climate Change gave their final warning in the latest assessment report (IPCC, 2023). With increasing regulations aiming to reduce the greenhouse emissions, whereas the initial reduction of 40% by 2030 compared to 1990 was set (European Commission, 2013), this has recently been increased to a reduction of 55% by 2030 compared to 1990 (Council of the European Union, 2021). Achieving these ambitious targets set by governments and international organizations requires innovative and sustainable solutions across all sectors. To keep global warming below 1.5 degrees Celsius, a goal set in the Paris Agreement (United Nations, 2016), all sectors should meet the net-zero emissions requirement by 2050.

The shipping industry contributes to 3% of the global production of greenhouse gas emissions (Olmer, 2017), which comes down to approximately 1 billion metric tonnes in 2018 (IMO, 2020). Sectors such as energy supply, industry and the residential sector, show a decrease in greenhouse gas emissions that even exceeds the targets set by the European Commission. However, the transport sector, including maritime transport, has demonstrated a slower pace in reductions (Forster et al., 2021). Furthermore, the world trade continues to increase generating a growing need for shipping (Cullinane and Cullinane, 2018). This causes the shipping industry to have an expected share of 17% of the global human-caused greenhouse gas emissions by 2050 (Comer et al., 2018). Achieving the goal of net-zero emissions from marine vessels requires the implementation of energy-efficient measures and innovation, making research an essential factor in the process.

Van Oord, a major player in the dredging and offshore wind park industry, operates across the globe with a fleet of over a hundred marine vessels and numerous ongoing projects. With the undertaking of achieving net-zero emissions, and the tender market shifting towards a demand for minimal emissions, an energy estimation tool is of significant importance.

The aim of this thesis is to investigate the impact of marine currents on the energy consumption of marine vessels and develop a reliable tool for estimating the energy consumption for specific ships in combination with marine currents. Furthermore, it explores the energy-efficient strategy, to allow for a waiting time to harness the marine currents, that can be implemented to reduce the greenhouse gas emissions. Keep in mind that this research only addresses one aspect that possibly contributes to the goal of achieving net-zero emissions. It aims to offer valuable insights into the practicality of harnessing marine currents and assessing the significance of the impact of the marine currents on energy consumption, thus contributing to the collective efforts to combat climate change.

1.1 Background Information

One of the sectors within the shipping industry that makes use of marine vessels for large-scale projects on a global scale is the dredging and offshore wind farm industry. Van Oord has projects ranging from dredging ports and waterways, coastal protection, offshore constructions and land reclamation. A common factor among these projects is the usage of large marine vessels, which consume significant amounts of energy, leading to a notable contribution to global greenhouse gas emissions. Van Oord is considered to be one of the key players in the dredging industry, with a large fleet of over a hundred marine vessels and projects on a global scale.

With the new regulation from the European Commission to decrease the greenhouse gas emissions to 55% by 2030 compared to 1990, also referred to as the "Fit for 55" or "The Green Deal" (Fetting, 2020), there is an urgency to decrease the energy consumption in the dredging industry. Van Oord released the sustainability programme "Sustainable Earth Actions" (S.E.A.) (Van Oord, 2019), which contains four sustainability pillars: Enhancing the energy transition, accelerating climate actions, empowering nature and communities and achieving net-zero emissions. The first pillar, enhancing the energy transition, is being achieved by facilitating offshore wind farms that generate renewable energy. The second and third pillars, accelerating climate actions and empowering nature and communities, are realized through projects that provide coastal protection and restore ecosystems.

Meeting the final goal of achieving net-zero emissions in the dredging industry is proving to be a task for the long term due to the fact that the majority of the vessels currently in operation rely on old designs with engines that run on conventional marine gas oil (MGO). While Van Oord has taken steps towards reducing emissions by introducing three new dredging vessels to their fleet with engines that run on LNG, which emits less CO_2 for the same operations, this solution also presents additional challenges such as the potential for methane leakage (Pavlenko et al., 2020), (Baresic, 2018) that must be taken into consideration. Therefore, further research and innovation are necessary to overcome these challenges and achieve the ambitious goal of net-zero emissions in the dredging industry.

1.2 Problem description

The regulations and climate awareness caused an increased demand for sustainable project strategies as opposed to conventional strategies, thus having the ability to quantify energy consumption becomes an increasingly significant incentive for competing in the tender market. This caused several previous research theses to be carried out at Van Oord with the aim to analyse the energy consumption of the dredging industry. Van der Bilt (2019) conducted research on different dredging strategies on a project level and their impact on emissions, Lamers (2022) provided a tool that is able to estimate the energy consumption for dredging vessels in a stationary condition and Janssen (2023) assessed the energy consumption during the loading phase of a dredging vessel. Another relevant thesis was conducted at Rijkswaterstaat, where Segers (2021) conducted research in which a method was developed that is able to map emission levels of inland shipping.

This thesis can be seen as a follow-up on the research of Lamers (2022), who studied the energy consumption for free sailing vessels. The sailing part of dredging vessels can be subdivided in three components: acceleration, free sailing and deceleration. Free sailing is defined as the part where the vessel has a constant effective engine power, constant thrust and constant pitch. Lamers did not take currents into consideration when estimating the energy consumption. This thesis therefore aims to improve the estimation of energy consumption by quantifying the effect of marine currents on the resistance, power and energy consumption of the vessel when free sailing.

The main problem statement is formulated as follows: With the shifting paradigm from projects based on the lowest costs towards projects based on the lowest emissions, a reliable estimation tool is necessary to quantify the energy consumption and explore alternative and innovative dredging strategies. Currently, the estimation is not sufficiently accurate and therefore can only be used for rough estimations. An improved energy estimation tool therefore strengthens Van Oord's position in the tender market. Additionally, there is insufficient basic research on the impact of currents on a marine vessel's energy consumption. This study aims to build a foundational understanding that can be applied by government agencies and researchers.

1.3 Research questions

The problem statement can be subdivided in several sub-goals that contribute to achieving the objective. The first sub-goal concerns the dynamic and time-dependent coastal currents, and specifically, the currents in the North Sea. Since Van Oord is located in The Netherlands and undertakes numerous projects along the Dutch coastline, the estimation tool should be capable of forecasting these currents to be able to explore various dredging strategies. The first sub-question is therefore formulated as follows:

> *How can the essential physical features of the dynamic and time-dependent coastal currents in the North Sea be represented in a continuous three-dimensional space?*

The second sub-goal regards the method to quantify energy consumption of a sailing vessel that incorporates coastal currents. To address this sub-goal, it is necessary to conduct a thorough research on the existing methodologies that determine energy consumption. The method should be modifiable to include the marine currents. This resulted in the second sub-question:

> *How can the energy consumption of sailing dredging vessels be quantified, taking into account the influence of dynamic and time-dependent coastal currents?*

The last sub-goal addresses the development of the model that can quantify the energy consumption. After the suitable methodology to quantify energy consumption is chosen and the currents in the North Sea can be represented in a 3D space, this has to be combined in a model which can be utilized by Van Oord in tender assessments. The model should be practical and user-friendly to use given project-specific conditions, such as the vessel type and location of the project. The third sub-question is therefore:

> *How can a practical and user-friendly model be developed to estimate the energy consumption of dredging vessels in project-specific conditions?*

After the model has been developed and validated, it can be utilized to study the effects of stratified coastal currents on the energy consumption of dredging vessels. The dredging strategy to allow for a waiting time to be incorporated in a dredging project, such that the currents can be harnessed to reduce energy consumption, is assessed. Therefore, by answering the three sub-goals, the main research question can be answered. The main research question is formulated as follows:

> *What is the effect of a dynamic and time-dependent stratified coastal current on the energy consumption of dredging vessels, and how can these currents be harnessed to reduce energy consumption?*

1.4 Research scope

The python-based model is firstly verified with trivial test cases and using the representative coastal currents for the North Sea, which is an analytical solution for the tidal-induced and residual density-driven currents. Note that by adjusting the input parameters of this analytical solution, the calculated cross-shore and alongshore components can represent the physical features ranging from a neap tide scenario to a spring tide scenario. To verify the the model, a neap tide scenario was selected as it is known to be characterized by the largest stratification and cross-shore components of the currents. The choice of this neap tide scenario is important as the large cross-shore components of the currents can be utilized to reduce energy consumption for sand replenishment projects. This is because the primary movement of the vessel during such projects is also cross-shore and therefore interacts with these currents.

After the model verification has been completed, the model is validated by comparing the model results to actual on-board data measurements during free sailing, i.e. stationary conditions, in combination with databases containing coastal currents in the North Sea. The verified model is used for the characteristics and dimensions of a dredging vessel owned by Van Oord. These dredging vessels are designed and equipped with measuring sensors and are subject to rigorous monitoring and maintenance protocols, which ensures that the data collected is accurate and reliable. The obtained data is collected in the in-house database called "Vessellog" which consists of a wide variety of parameters such as the sailing speed, water depth, draught and location. The project chosen to validate the model is a dredging project concerning the sea acces at IJmond in 2019. At this location a current measuring pole from Rijkswaterstaat is present, containing the magnitude and the direction of the marine currents at the exact time of the project.

After the model has been verified and validated, it is used to explore an energy-efficient dredging strategy, namely allowing for a dredging vessel to wait for the currents to increase in the sailing direction. The fictitious dredging project concerns a sand nourishment in the proximity of the Rhine ROFI (region of freshwater influence). The sailing activities are repetitive cycles consisting of sailing from deep water to the coast and back to deep water, the primary movement of the dredging vessel is cross-shore. Upon returning, the dredging vessel is allowed to wait for the cross-shore component to increase in the sailing direction, thus harnessing these currents to decrease the energy consumption. This will be carried out under two scenarios: the first will assume that there is no energy consumption during waiting. The second scenario will consider the more realistic case where energy is continuously consumed during waiting due to other on-board utilities such as the energy use for electricity (e.g. lighting) and heating for the crew members on the dredging vessel.

1.5 Report structure

In the introduction chapter, the relevance and importance for the study is presented, which centered on meeting the climate change goals and the shift towards sustainable dredging practices. Van Oord does not have an estimation tool that takes into account the effect of currents on the energy consumption of dredging vessels, this research aims to provide a python-based model that does take into account currents in calculating the energy consumption. The python-based model is utilized to asses the significance of the impact of marine currents on the energy consumption of marine vessels and to explore an alternative sustainable dredging strategy.

The literature review chapter is divided into two sections, namely, energy calculation methods and North Sea currents. The first section provides a comprehensive analysis of the existing methodologies used to estimate the energy consumption of marine vessels, with the aim of identifying the most appropriate method to account for the impact of marine currents on energy consumption. The second section seeks to identify a suitable approach to represent the fundamental physical characteristics of the coastal currents in the North Sea.

In the chapter on model development, the selected method for calculating energy consumption is described in detail, followed by an explanation of how the impact of coastal currents is incorporated into this method through modifications. Furthermore, the Python-based model, which facilitates the interaction between the energy consumption model and the representation of North Sea currents, is explained in great detail. It is worth emphasizing that the model is designed as an adaptable tool that can be employed for different types of dredging projects and a wide range of dredging vessels.

In the chapter Model Implementation and Results, the model is verified, validated and used to explore a sustainable dredging strategy. The model is tested through various test cases that change parameters such as water depth, vessel draught, and currents to understand their impact on vessel resistance and energy consumption. The most complex test case involves using the dynamic and time-dependent currents in the North Sea, as defined in the literature review. Validation is then conducted to assess the model's accuracy by comparing it with on-board measurements during a dredging project and marine current measurements. Additionally, a sustainable dredging strategy is proposed for a sand nourishment project where the vessel waits for the marine currents to increase in the sailing direction, theoretically reducing energy consumption. However, in practice, the vessel still consumes energy when not sailing, so the overall energy consumption on a dredging project scale may increase when allowing for waiting time.

In the discussion chapter, a summary of the research findings will be presented, followed by a critical analysis of these findings and the implications and limitations of the study. The conclusion chapter will provide a definitive answer to the main research question and offer further recommendations for future research. Furthermore, practical recommendations for improving the energy consumption model and enhancing sustainable dredging practices will be presented.

Chapter 2

Literature review

Section 2.1 aims to identify the most appropriate energy calculation method for developing a python-based model capable of calculating the energy consumption of a vessel navigating through a flow field. Section 2.2 explores relevant research to address the effective representation of the fundamental physical features of the dynamic and time-varying coastal currents in the North Sea in a continuous three-dimensional space.

2.1 Energy calculation methods

2.1.1 Introduction

In this section, an evaluation and comparison of the various techniques to calculate the energy consumption of a sailing vessel is made with the aim to select the most appropriate method for this research. Specifically, this method should depend on significant parameters that are under the control of Van Oord, such as engine power or speed, while also allowing for the addition of an ambient flow field by means of a minor modification
In subsection 2.1.2, a differentiation is made between two distinct methodologies, namely the top-down and bottom-up approach. The top-down approach relies on determining the total yearly energy consumption based on the marine fuel sales data. On the other hand, the bottom-up approach determines the energy consumption on an operational level, incorporating factors such as engine performance, sailing speed and weather conditions. A comparison is made by discussing the advantages and disadvantages of both methodologies, after which the bottom-up approach is chosen based on this comparison.
In the following subsections, from subsection 2.1.3 until subsection 2.1.7, an evaluation of different existing models within the bottom-up approach will be presented. Lastly in subsection 2.1.8 a choice for the most appropriate calculation method will be made based on the models and the aim and scope of this research.

2.1.2 Evaluation of Top-Down and Bottom-Up approaches

Top-Down

The top-down method is based on marine fuel sales data and quantifies the global emissions based on internationally-accepted emission factors, expressed as kg pollutants/kg fuel used (Moreno-Gutiérrez and Durán-Grados, 2021). The total emissions are calculated without considering the characteristics of individual vessels and are subsequently geographically located and assigned to different ships (Miola and Ciuffo, 2011) using ship traffic density proxies (Goldsworthy and Goldsworthy, 2015). The method neglects the ship characteristics and the performance factors, both of which are of significant influence on the energy consumption of a vessel.

The top-down approach is a fast and straightforward method that requires only the analysis of yearly fuel expenses to determine the total fuel consumption. This approach is highly efficient and cost-effective, as it does not require a large investment in monitoring and data collection.

However, the top-down approach has several disadvantages, including a lack of detail, inaccuracies, and limited insight. The broad overview of global energy consumption provided by the top-down approach fails to identify the specific factors or patterns that contribute significantly to overall energy consumption. Furthermore, the method might not be accurate, as fuel expenses can include costs that are not directly related to energy consumption. It can also be inaccurate because there are uncertainties in the global estimates used and the way the data is collected can lead to bias (Wang et al., 2006). Last but not least, the top-down approach also fails to take into account important factors such as engine power, sailing speed, and weather conditions, making it less suitable for research purposes.

Bottom-Up

The bottom-up approach contains two different methods. The first method employs on-board real-time data of fuel consumption, reported by individual vessels in the so-called noon report. The second method uses data sources that describe the shipping activities in combination with each vessels technical characteristics (Moreno-Gutiérrez and Durán-Grados, 2021). This second model is also considered to be a hybrid of the top-down and bottom-up approach as it uses global information of shipping activities in combination with individual ship attributes (Goldsworthy and Goldsworthy, 2015). One way to collect the shipping activities in real-time is by means of AIS, Automatic Identification System, consisting of static and dynamic information. Static AIS information contains ship fundamental information such as ship name, ship type and ship length, dynamic AIS information contains a recording of the ship movements, such as location, speed over ground and course of vessel (Huang et al., 2020).

The bottom-up approach offers several advantages in the analysis of energy consumption in shipping. Firstly, it provides a highly detailed understanding of energy consumption patterns by including the impact of various ship characteristics and other factors such as engine performance and weather conditions. Secondly, the approach boasts high accuracy due to the

detailed understanding of the system. Finally, the in-depth analysis and identification of significant contributors to energy consumption can inform decision-making and the development of targeted energy-efficient measures to reduce energy consumption.

However, the bottom-up approach has certain disadvantages making the top-down approach favourable in certain scenarios. One of the disadvantages of utilizing the bottom-up approach is that it is resource-intensive, the bottom-up approach requires significant resources in terms of time, manpower and technical expertise making it a relative cost-ineffective method. The bottom-up approach is also of complex nature and requires vast knowledge on the subject to understand all the factors that play a role and to interpret the results. This complexity can make it challenging for decision-makers who may not possess the necessary technical knowledge to effectively use the results of a bottom-up analysis. Finally, although the bottom-up is generally more precise than the top-down approach, large-scale bottom-up energy calculation can be uncertain because they estimate engine performance, ship speed and the locations of the routes (Wang et al., 2006).

Conclusion

Taking into account the advantages and disadvantages of the two distinct approaches, and the aim of this research to study the effects of density-driven currents on the energy-consumption of vessels, the bottom-up approach is an obvious choice as the most appropriate method for this research. The top-down approach is more suitable for energy consumption calculations on a global scale, for instance to study the impact of the shipping industry on the global greenhouse gas emissions. These calculations are known to be correct to assess the fuel consumption, however, they lack detailed information on vessel- and flow-related parameters and their influence on energy consumption. To study small-scale shipping activities and identify the effects of external factors, such as density-driven currents, on the energy consumption, the bottom-up approach is more appropriate. By taking into account the various ship characteristics and other factors influencing the energy consumption, it can be used to identify specific areas of improvement to minimize the energy consumption of vessels. The bottom-up based model can also be used to study the effects of different dredging strategies on the energy consumption.

2.1.3 STEEM

One of the widely recognized bottom-up methodologies for determining energy consumption of seagoing vessels is STEEM (Ship Traffic Energy and Environmental Model) (Corbett, 2007). The method is considered to be a hybrid of the top-down and bottom-up approaches. It utilizes advanced GIS tools to build an empirical waterway network based on shipping routes for the spatial and temporal information. It uses historical ship movements, ship attributes and the distances of the shipping routes to estimates the energy, fuel use and emissions (Corbett, 2007).

The formula to calculate the fuel consumption can be seen in Equation 2.1 (Moreno-Gutiérrez and Durán-Grados, 2021).

$$Fuel \quad Consumption = P_{transient} * t * SFOC \tag{2.1}$$

This equation is not specific to STEEM, however, the procedure to calculate the transient power $P_{transient}$ [kW] is. This is the instantaneous power produced by the engine of the vessel, i.e. the engine power. The fuel consumption [g] is in grams, t [h] is the time duration of the sailing vessel and SFOC [g/kWh] is the Specific Fuel Oil Consumption. The SFOC is a value between 0 and 1 that represents the amount of fuel consumed per unit of time (Moreno-Gutiérrez and Durán-Grados, 2021). The value for the SFOC is determined as follows:

$$SFOC = SFOC_{relative} * SFOC_{base} \tag{2.2}$$

$$SFOC_{relative} = 0.455LF^2 - 0.71LF + 1.28 \tag{2.3}$$

in which the $SFOC_{base}$ [g/kWh] is a constant value based on the engine type of a vessel and $SFOC_{relative}$ is a unitless paramater that depends on the engine load factor LF. The engine load factor, which changes in real-time, is the most important factor in determining SFOC. However, calculating the engine load factor is the most difficult of all variables (Moreno-Gutiérrez and Durán-Grados, 2021). The engine load factor depends on several factors including speed, weather conditions, currents, ship dimensions, draught and the state of the hull. It is defined as follows:

$$LF = \frac{P_{transient}}{P_{reference}} \tag{2.4}$$

The formula used to calculate the delivered power for the STEEM method can be seen below:

$$P_{transient} = P_{reference} \left(\frac{V_{transient}}{V_{reference}} \right)^3 \tag{2.5}$$

where $P_{reference}$ [kW] and $V_{reference}$ [m/s] are respectively the power and speed of the ship at 100% Maximum Continuous Rating (MCR). $V_{transient}$ [m/s] is the instantaneous sailing speed (speed over ground) determined by analysing the historical data of the waterway network containing shipping activities. It can be noted that the STEEM method only needs three parameters to be able to calculate the engine load factor, namely the reference power [kW] and speed [m/s] and the transient speed [m/s].

2.1.4 STEAM

A second model to calculate energy consumption for vessels is called STEAM (Ship Traffic Emission Assessment Model). The STEAM method was introduced by Jalkanen et al. (2009), who expanded on the STEEM method by using AIS data for the recorded identification and location of ships and including a safety margin of 0.5 knots to account for ship speeds that

exceed the stated maximum (Moreno-Gutiérrez and Durán-Grados, 2021). The formula used in calculating the transient power is shown below:

$$P_{transient} = \varepsilon_p * P_{installed} \left(\frac{V_{transient}}{V_{reference} + V_{safety}} \right)^3 \tag{2.6}$$

where $P_{installed}$ [kW] is the total installed power of the main engine(s) and ε_p [-] is assumed to be equal to 0.8 because the maximum continuous rating of the engine is taken to be 80% of the total installed main engine power (Moreno-Gutiérrez and Durán-Grados, 2021). The load factor again only depends on the power and speed while neglecting the external factors such as weather conditions, currents and draught.

2.1.5 IMO

A new model was proposed by the International Maritime Organization (IMO) after a Greenhouse Gases study by Smith et al. (2014). This model improved upon the STEAM model by introducing additional parameters such as a time-dependent draught, a parameter representing the modification of the propulsion efficiency due to weather and a parameter representing the modification of the propulsion efficiency due to fouling. The draught is determined with the loading condition at that time, which depend on the amount of cargo and variable loads. A larger draught generally increases the resistance due to the increased wetted surface area. The formula as proposed by Smith et al. (2014) can be seen below:

$$P_{transient} = \frac{P_{ref} \left(\frac{t_t}{t_{ref}} \right)^{\frac{2}{3}} \left(\frac{V_t}{V_{ref}} \right)^n}{\eta_w \eta_f} \tag{2.7}$$

where t_t [m] is the draught in real-time and t_{ref} [m] is the reference draught, the propulsion efficiency parameters for the weather conditions and fouling of the hull are respectively η_w [-] and η_f [-]. n is assumed to be 3, which gives the same relationship between power and speed as the STEEM and STEAM models. This formula created a new complete methodology to calculate the transient power demand, however, although the propulsion efficiency parameters are included in the formula, the procedure for calculating the values for η_w and η_f has not been specified (Moreno-Gutiérrez and Durán-Grados, 2021).

2.1.6 SENEM

Finally, Moreno-Gutierrez and Duran-Grados combined the principles of the STEEM, STEAM and IMO models to create a complete model to calculate the main energy output and subsequently with Equation 2.1 the energy and fuel use. This model is called SENEM (Ships Energy and Emissions Model) (Moreno-Gutiérrez and Durán-Grados, 2021). The proposed equation to determine the transient power demand is:

$$P_{\text{transient}} = \frac{P_{\text{ref}} \left(\frac{t_{\text{transient}}}{t_{\text{ref}}}\right)^{\left(\frac{2}{3}\right)} \left[\left(\frac{V_{\text{transient}} + \Delta V_{\text{windandwaves}} + \Delta V_{\text{fouling}} \pm V_{\text{current}}}{V_{\text{ref}}}\right)^{n}\right]}{\eta_j} \tag{2.8}$$

It can be noted that the draught is treated similarly as in the model proposed by IMO, the propulsion efficiency parameters η_w and η_f have been combined to one propulsion efficiency parameter η_j [-]. This parameter is now defined with the form of: $y = a + bx^2$, where y is the propulsion efficiency and x the ship's speed (Moreno-Gutiérrez and Durán-Grados, 2021). The intersect and slope, respectively a and b, are predefined for varying ship types. This updated model also considers the impacts of wind, waves, fouling, and marine currents on the vessel's speed, providing a comprehensive representation of all the factors that affect energy consumption. Additionally, unlike previous models that used a constant for the exponent n to describe the relationship between a ship's power and speed, this model allows for the adjustability of the exponent based on different types of vessels. The value for n increases as the vessel size gets larger.

This methodology provides a complete representation of all the influences on the vessel's energy consumption, however, the procedure to determine the effects of wind and waves, currents and fouling is not defined. This requires an additional model to calculate the total ΔV.

2.1.7 Holtrop and Mennen

Prior to the widespread availability of data collection methods, an entirely different approach was introduced by Holtrop and Mennen (1982). This approach calculates the transient power demand of a vessel based on the speed of the vessel, its characteristics and dimensions and the water depth. The method was developed through a regression analysis of model experiments and full-scale data (Holtrop and Mennen, 1982). It is a well-established method for designing and evaluating the performance of ship hulls. The principle of this method is to calculate the total resistance and determining the required power based on the relationship:

$$P_e = R_{tot} * V \tag{2.9}$$

In this equation, the effective power P_e [kW] represents the engine power minus the losses resulting from the propeller efficiency. The effective power provides a measure of the power required to overcome the resistance encountered by the ship as it moves through the water. Subsequently, the actual engine power required to reach the desired sailing speed is determined by first calculating the delivered horse power P_d [kW] and eventually the brake horse power P_b [kW]. The brake horse power is equal to the engine power. The effective power is related to the engine power as shown by the following formulae:

$$P_d = \frac{P_e}{\eta_0 \eta_r \eta_h} \tag{2.10}$$

$$P_b = \frac{P_d}{\eta_t \eta_g} = P_{transient} \tag{2.11}$$

Where in Equation 3.4 the different efficiency factors η_0, η_r and η_h respectively account for the open water efficiency of propeller, relative rotative efficiency and the hull efficiency. The relation between the delivered horse power P_d and the brake horse power (or engine power) P_b can be seen in Equation 3.5, where η_t and η_g are respectively the efficiency of the shaft and gearbox. The brake horse power is therefore the effective power P_e including the losses at the propeller (i.e. P_d), the shaft and the gearbox.

The total resistance is subdivided in different components, which are all calculated using the empirical relations based on the model experiments. The total resistance is calculated with the formula:

$$R_{total} = R_F(1 + k_1) + R_{APP} + R_W + R_B + R_{TR} + R_A \tag{2.12}$$

where:

R_F = Frictional resistance [kN]

$(1 + k_1)$ = The form factor describing the relationship between the frictional resistance and the viscous resistance [-]

R_{APP} = Appendage induced resistance [kN]

R_W = Wave-making and wave-breaking resistance, not to be confused with the (wind) wave resistance [kN]

R_B = Pressure induced resistance caused by a bulbous bow [kN]

R_{TR} = Additional pressure resistance of immersed transom stern [kN]

R_A = Model-ship correlation resistance [kN]

By decomposing the total resistance into its constituent parts, more insight can be obtained by analysing the effects of different parameters on these components. The water depth is also taken into account in determining the resistance components. This parameter is of significant importance for this thesis because the sand nourishment projects in the North Sea consist of relatively shallow water.

2.1.8 Conclusion

The methods that were first evaluated in this analysis (STEEM, STEAM, IMO and SENEM) generally rely on Automatic Identification System (AIS) data to estimate ship speed and position, they can also be used for small-scale research by incorporating data captured on individual vessels. SENEM is considered the most complete model of these methods, as it includes the engine efficiency, weather conditions and transient draught, making it a theoretically comprehensive model. However, determining some of these factors, particularly the load factor (LF), remains ambiguous, leading to significant uncertainty. Additionally, the effect of water depth on the required engine power for a vessel is not taken into account, which is a crucial parameter for the sand nourishment project in the North Sea.

the Holtrop and Mennen method decomposes the total resistance into its constituent parts, allowing for a more detailed analysis of the effects of different parameters on the ship's energy consumption. Additionaly, the Holtrop and Mennen method differentiates between effective power [kW] and engine power [kW], which is important for accurately estimating the power requirements of a ship under different operating conditions. Last but not least, the Holtrop and Mennen method allows for a comprehensive customization of varying types of dredging vessels that goes beyond only the vessel's dimensions, providing a more accurate representation of specific dredging vessels.

In conclusion to the analysis of the various bottom-up approaches, the Holtrop and Mennen method is found to be the most suitable for the current research purpose of this thesis, being a study on the effect of marine currents on energy consumption of vessels.

2.2 3D ocean currents

2.2.1 Introduction

The present study has a specific focus on the region of freshwater influence (ROFI) where the Rhine River flows into the North Sea. This section describes the derivation of the analytical solution for a dynamic and time-dependent vertical velocity structure, representing realistic magnitudes for the currents at said location. The ROFI is a region of high freshwater inflow that experiences significant density differences, leading to stratification and complex circulation patterns that are important to understand because these interact with sailing dredging vessels.

The analytical solution aims to capture the essential physical features of water movement in the ROFI, specifically tidal-induced currents and residual density-driven flow. Tidal-induced currents and residual density-driven flow are most important in the ROFI because they are the dominant physical processes that govern water movement and circulation patterns in the region. These therefore can be used as a first order estimate to determine the influence of these currents on activities such as dredging operations.

Subsection 2.2.2 outlines the general equations that describe the hydrodynamics in the North sea and explains its corresponding simplifications and assumptions. Hereafter, in subsection 2.2.3 and subsection 2.2.4, the analytical solutions for the tidal-induced currents and residual density-driven flow are derived, respectively. These analytical solutions are in the form of a vertical velocity structure. To produce a flow field that represents the essential physical features of the currents in the North Sea, the tidal-induced vertical structure is added to the vertical structure of the density-driven flow. This is done is subsection 2.2.5. The vertical velocity structure has horizontal differences due to spatially varying input parameters such as the water depth D.

2.2.2 North Sea

To describe the full system of the Rhine region of fresh water 6 equations are necessary, namely the continuity equation, 3 equations of motion (in three directions) and 2 conservation equations (one for temperature and one for salinity). These equations are shown on the next page, namely Equation 2.13 up to and including Equation 2.18. Various simplifications and assumptions are made in deriving these equations, namely the hydrostatic pressure, f-plane, Boussinesq, turbulent eddy viscosity and diffusivity and incompressibility assumptions. There are 6 unknowns in these equations, namely the velocities u, v and w, respectively in x, y and z direction, water surface level η, salinity S and temperature T. A Cartesian co-ordinate system is used to describe the fluid motion in x, y and z direction; x, y are measured in the horizontal plane representing the on-shore (eastward) and alongshore (northward) directions respectively, z is positive in upward direction increasing from $-D(x, y, t)$ at the bed to $\eta(x, y, t)$ at the surface. This is commonly known as the right handed coordinate system.

$$\frac{\partial u}{\partial t} + \frac{\partial u^2}{\partial x} + \frac{\partial uv}{\partial y} + \frac{\partial uw}{\partial z} - fv + \frac{1}{\rho_0}\frac{\partial p}{\partial x} - F_x - \frac{\partial}{\partial z}\left(E_z \frac{\partial u}{\partial z}\right) = 0 \tag{2.13}$$

$$\frac{\partial v}{\partial t} + \frac{\partial vu}{\partial x} + \frac{\partial v^2}{\partial y} + \frac{\partial vw}{\partial z} + fu + \frac{1}{\rho_0}\frac{\partial p}{\partial y} - F_y - \frac{\partial}{\partial z}\left(E_z \frac{\partial v}{\partial z}\right) = 0 \tag{2.14}$$

$$\frac{\partial p}{\partial z} = -\rho g \tag{2.15}$$

$$\frac{\partial u}{\partial x} + \frac{\partial v}{\partial y} + \frac{\partial w}{\partial z} = 0 \tag{2.16}$$

$$\frac{\partial S}{\partial t} + \frac{\partial uS}{\partial x} + \frac{\partial vS}{\partial y} + \frac{\partial wS}{\partial z} - F_S - \frac{\partial}{\partial z}\left(D_t \frac{\partial S}{\partial z}\right) = S_{SS} \tag{2.17}$$

$$\frac{\partial T}{\partial t} + \frac{\partial uT}{\partial x} + \frac{\partial vT}{\partial y} + \frac{\partial wT}{\partial z} - F_T - \frac{\partial}{\partial z}\left(D_t \frac{\partial T}{\partial z}\right) = \frac{1}{\rho} Q_H + T_{SS} \tag{2.18}$$

2.2.3 Prandle

Prandle (1982) provided a time-dependent vertical structure of the velocity for a given eddy viscosity that is uniform in the water column, this produced an elliptical current at the surface rotating clockwise (anti-cyclonic) and an opposing elliptical current at the bed rotating anti-clockwise (cyclonic) for a Kelvin wave. The starting point for the analytical solution of Prandle are the equations of motion in x and y direction, respectively Equation 2.13 and Equation 2.14. In studying first-order tidal propagation it is generally allowed to neglect vertical components of the velocity and acceleration, the convective terms and density effects (Prandle, 1982). This is allowed because the vertical motion length scale of the tidal wave is significantly smaller than the horizontal motion length scale, and the convection terms and density effects are relatively small when compared to the other terms in the equations of motion. Moreover, the nonlinear terms are neglected and the pressure term are expressed in change of water surface level. This results in the two following coupled equations of motion:

$$\frac{\partial u}{\partial t} - fv = -g\frac{\partial \eta}{\partial x} + \frac{\partial}{\partial z}\left(E_z \frac{\partial u}{\partial z}\right) \tag{2.19}$$

$$\frac{\partial v}{\partial t} + fu = -g\frac{\partial \eta}{\partial y} + \frac{\partial}{\partial z}\left(E_z \frac{\partial v}{\partial z}\right) \tag{2.20}$$

The boundary conditions are specified along the z-axis, namely at the bottom and the surface (de Boer, 2009), as follows:

$$z = 0: \quad \frac{\partial u}{\partial z} = 0, \quad \frac{\partial v}{\partial z} = 0 \tag{2.21}$$

$$z = -D: \quad \frac{\partial u}{\partial z} = su, \quad \frac{\partial v}{\partial z} = sv \tag{2.22}$$

This again is a simplification of reality. In Equation 2.21 the velocity is assumed to not be influenced at the water surface, i.e. neglecting the forcing of wind and waves. The boundary conditions at the bottom in Equation 2.22 are based on the linearised bottom friction $s = \frac{8}{3\pi}\frac{kU}{E}$, in which k is a friction factor introduced by Prandle (1982).

To solve these two equations analytically for u and v, the equations of motion have to be decoupled by means of rephrasing the equations in terms of rotating phasors. The derivation of this is presented in Appendix A, the solution is shown here:

$$i(f+\omega)R^+ = G^+ + \frac{\partial}{\partial z}\left(E_z \frac{\partial R^+}{\partial z}\right) \tag{2.23}$$

$$i(f-\omega)R^- = G^- + \frac{\partial}{\partial z}\left(E_z \frac{\partial R^-}{\partial z}\right) \tag{2.24}$$

with the relation between the rotating phasors R^+ and R^- and the cross-shore and alongshore velocity components of the currents, respectively u and v as follows:

$$R = R^+ + R^- = u + iv \tag{2.25}$$

R^+ and R^- are the counter-clockwise and clockwise rotating phasors, respectively. These equations can be solved by assuming a general solution of the form $R^\pm = [c_1 e^{-\alpha z} + c_2 e^{\alpha z}]e^{\pm iwt}$ in combination with the boundary conditions as given in Equation 2.21 and Equation 2.22, neglecting the surface water elevation η and dividing by the depth-averaged velocity $\langle u \rangle = \int_{-D}^{0} u(z)dz$. The following solution is obtained:

$$\frac{R^\pm}{\langle R^\pm \rangle} = \frac{\cosh\left(\alpha^\pm[z-D]\right) - \left[\cosh\left(\alpha^\pm D\right)\right] - \frac{\alpha^\pm}{s} \cdot \left[\sinh\left(\alpha^\pm D\right)\right]}{-\left[\cosh\left(\alpha^\pm D\right)\right] + \left(\frac{1}{\alpha^\pm D} - \frac{\alpha^\pm}{s}\right) \cdot \left[\sinh\left(\alpha^\pm D\right)\right]} \tag{2.26}$$

in which $\alpha^\pm$ is defined as the inverse of the boundary layer height as follows:

$$\alpha^\pm = (1+i)\sqrt{\frac{f \pm w}{2E_z}} = \frac{1}{\delta^\pm} \tag{2.27}$$

The Ekman boundary layer as described by Soulsby (1983) gives a prediction of the vertical scale of influence of the bottom friction on the bottom upward development of the horizontal velocity. The two components δ^+ and δ^- respectively represent the boundary layer for a cyclonic rotation and a anti-cyclonic rotation, whereas $\delta^+ \ll \delta^-$. This can be explained by taking into account the rotation of the earth, the boundary layer corresponding to the cyclonic phasor (R^+) rotates in the same direction as the earth and thus has a relative lower influence of the bottom friction, i.e. less shear to overcome. The opposite applies to the boundary layer corresponding to the anti-cyclonic phasor (R^-), whereas it rotates against the rotation of the earth and thus experiences a relative larger effect of the bottom friction resulting in a larger vertical scale in which the horizontal velocity develops.

Equation 2.26 can now be used to produce a time-dependent vertical structure of the velocity in a 3D flow field. The values for each parameter shown in Table 2.1 will be used to recreate a neap tide scenario in the North Sea, these values are based on the work of de Boer (2009) and produce realistic velocity magnitudes.

Parameter	**Value**	**Unit**
E_z (Neap)	0.0028	$m^2 s^{-1}$
D	25	m
ω (M2)	$1.4 * 10^-4$	rad/s
f	$1.15 * 10^-4$	rad/s
U	0.43	m/s
k	0.0025	-

Table 2.1: Parameters neap tide scenario, Prandle

By substituting the values from Table 2.1 in the solution (Equation 2.26), the normalized amplitudes for both the anti-clockwise and clockwise phasors can be determined (respectively R^+ and R^-). Hereafter these normalized amplitudes are multiplied by the depth averaged velocity U of the North Sea location for a neap tide scenario (de Boer, 2009), the resulting vertical structure of the phasor amplitude is shown in Figure 2.1.

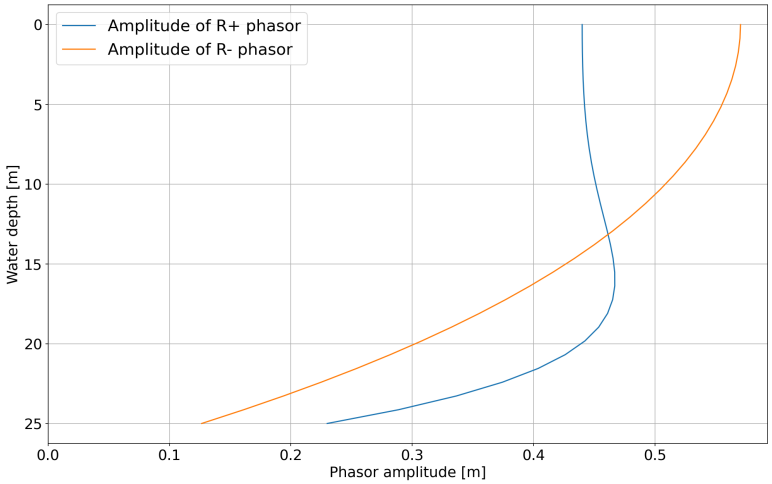

Figure 2.1: Vertical structure phasor amplitude

The previously explained difference in Ekman boundary layer scale for the cyclonic phasor (R^+) and the anti-cyclonic phasor (R^-) can be recognized in the graph, whereas the cyclonic phasor has a vertical section in the upper layer of the water column which represents a fully developed velocity while the anti-cyclonic does not have a sufficient vertical length scale to be fully developed. It can also be seen that in the upper part of the water column the anti-cyclonic phasor is larger than the cyclonic phasor, after summation this results in a anti-cyclonic or clockwise rotating elliptical current over a tidal period. In the lower part the opposite is visible resulting in a cyclonic or anti-clockwise elliptical current over a tidal period, hence, counter-rotating elliptical horizontal velocities at the surface and bottom of the water column.

To create a 3D time-dependent flow field, the phasor amplitudes R^+ and R^- have to be multiplied with, respectively, e^{iwt} and e^{-iwt} to let them rotate in the complex plane with the angular frequency of the M2 tide. Subsequently, the total complex vector representing the velocity at a certain time t is obtained by means of summation of the two counter-rotating phasors. Applying Equation 2.25, the velocities u and v in the real coordinate system as prescribed previously can be obtained by taking the real part and imaginary part of the summation. Figure 2.2 presents the evolution of the 3D velocity structure for a neap tide scenario, dividing the M2 tidal period in four time steps.

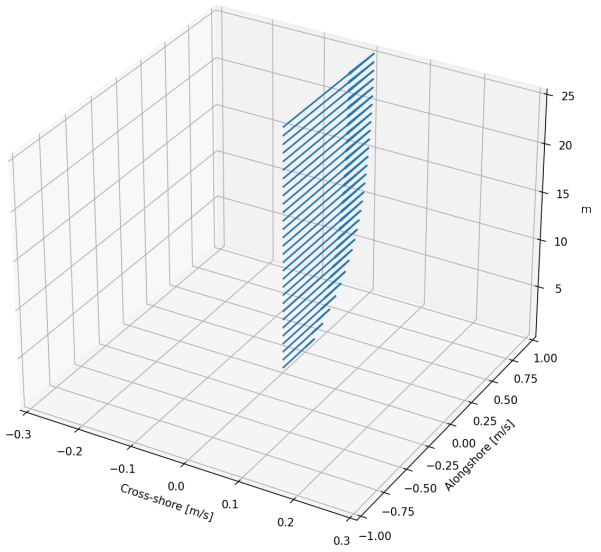

(a) $t = 0$

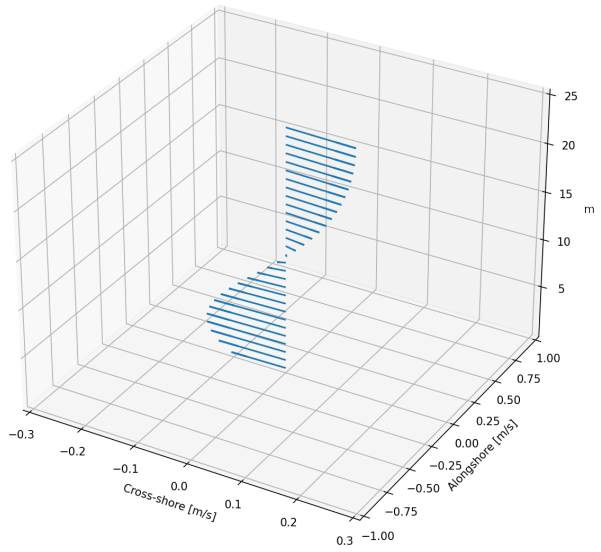

(b) $t = \frac{1}{4}T$

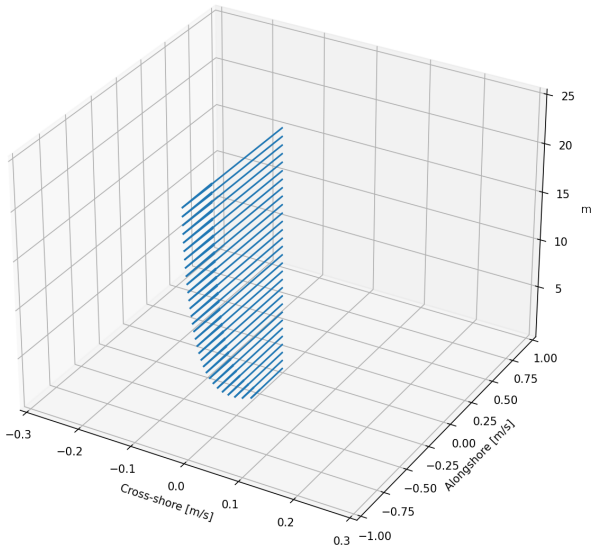

(c) $t = \frac{1}{2}T$

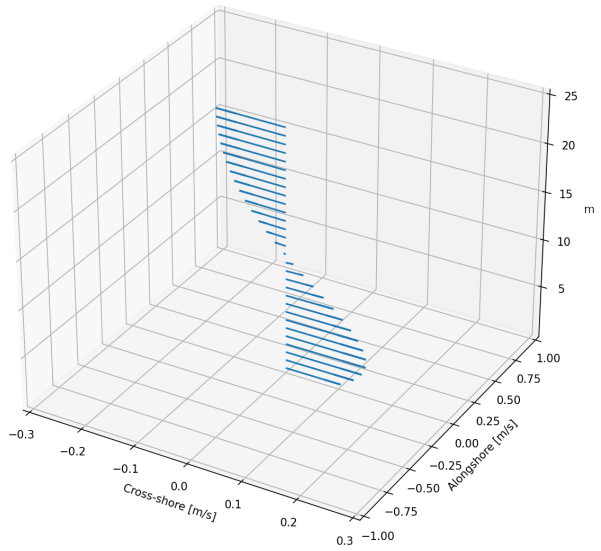

(d) $t = \frac{3}{4}T$

Figure 2.2: Evolution of 3D velocity structure over a tidal period

2.2.4 Heaps

Heaps (1972) published a paper on density driven-currents in the Liverpool Bay, specifically on the vertical velocity structure of the steady-state solution of the density-driven flow. His paper produced a theoretical model of density-driven flow in a two-layer system, this is a general theory that is not only bound to Liverpool Bay but can also be applied to other coastal areas where a ROFI is present. The vertical structure obtained with Heaps (1972) model can be explained as a combination of thermal wind and estuarine circulation (de Boer, 2009).

In the alongshore direction the thermal wind balance exists in the form of a residual northward velocity shear, this vertical shear structure results from the geostrophic balance and the cross-shore baroclinic and barotropic pressure gradient. However, due to the shallow water in the coastal area, the thermal wind can not fully develop because of friction and thus deviates from a classic thermal wind balance known from meteorology.

In the cross-shore direction a density gradient exists that is caused by, amongst other factors, the freshwater discharge of the Rhine river and the saline water in the North Sea. This causes an estuarine circulation to develop consisting of a seaward surface currents and landward currents at the bed.

The residual velocity profile is a balance between the alongshore thermal wind balance and cross-shore estuarine circulation. The structure of the vertical velocity depends on the specifics of the location, namely the water depth, wind-induced residuals, tidal amplitude, density differences and the degree of stratification in the water column. For this thesis research the wind is neglected and the water depth and tidal amplitude are known. The density differences and degree of stratification are translated as the vertical eddy viscosity, which is a measure of vertical mixing. It is generally observed that as the mixing energy within an estuary increases, i.e more friction, the vertical velocity structure of the water column becomes more characteristic of estuarine circulation. Conversely, as mixing energy decreases, i.e. less friction, the vertical velocity structure is more consistent with the dynamics predicted by the thermal wind balance. Due to the scope of this research, only the analytical solution to steady-state solutions of the continuity and momentum equations derived by Heaps (1972) is presented here. The analytical solution is:

$$u = (gH/f)(XQ - YP)(\partial\rho/\partial x)/\rho + (fq/k)(MP - LQ)/S \tag{2.28}$$

$$v = (gH/f)(XP + YQ + \Lambda + \eta)(\partial\rho/\partial x)/\rho + (fq/k)(1 - LP - MQ)/S. \tag{2.29}$$

The various parameters seen in the analytical solution are defined as follows:

$$Z = z + \zeta, H = D + \zeta, \eta = Z/H,$$
$$a = \pi H/D, a_1 = a(1-\eta), a_2 = a\eta, b = kH/E_z,$$
$$C = a(\sinh a \cos a - \cosh a \sin a) + b \cosh a \cos a,$$
$$E = a(\sinh a \cos a + \cosh a \sin a) + b \sinh a \sin a$$
$$L = b \cosh a_2 \cos a_2, M = b \sinh a_2 \sin a_2,$$
$$P = C/\left(C^2 + E^2\right), Q = E/\left(C^2 + E^2\right),$$
$$R = P \cosh a \cos a + Q \sinh a \sin a, S = 1 - Rb,$$
$$\Lambda = (R - P - S)/S, \lambda = 1 + b + b\Lambda,$$
$$X = \cosh a_1 \cos a_1 + (b/2a)\left(\sinh a_1 \cos a_1 + \cosh a_1 \sin a_1\right) - \lambda \cosh a_2 \cos a_2$$
$$Y = \sinh a_1 \sin a_1 + (b/2a)\left(\cosh a_1 \sin a_1 - \sinh a_1 \cos a_1\right) - \lambda \sinh a_2 \sin a_2$$

In Equation 2.28 and Equation 2.29 the first term in the right-hand side is the influence of the density gradient and the second term represents the influence of the coastal discharge, in this case the Rhine River discharge. The second term is found to be very small and can thus be neglected (Heaps, 1972). The input variables for these equations are:

η = elevation of the water surface above its undisturbed level $[m]$

D = depth from undisturbed surface to bed $[m]$

E_z = vertical eddy viscosity coefficient $[m^2 s^{-1}]$

k = friction coefficient $[-]$

f = Coriolis parameter $[rad/s]$

g = gravitational acceleration $[m/s^2]$

$\partial\rho/\partial x$ = density gradient in cross-shore direction $[kg/m^4]$

ρ = fluid density $[kg/m^3]$

q = coastal discharge $[m^3/s]$

Parameter	Value	Unit
E_z	0.0028	$m^2 s^{-1}$
D	25	m
f	$1.15 * 10^{-}4$	rad/s
k	0.0025	-
η	0.2	m
g	9.81	m/s^2
ρ	1000	kg/m^3
$\partial\rho/\partial x$	$-2 * 10^{-4}$	kg/m^4

Table 2.2: Parameters neap tide scenario, Heaps

The vertical eddy viscosity coefficient represents the mixing energy in this case, a larger value meaning a higher mixing energy. The input values are given in Table 2.2 below. The values are consistent with the input parameters used in the analytical solution of Prandle (1982). The density gradient is a new input parameter and is based on the research of de Boer (2009) for a neap tide scenario.

The resulting residual flow pattern using the values as prescribed in Table 2.2 is plotted in Figure 2.3. Note that the scale in cross-shore and alongshore direction is different than the scale shown in the vertical structure of Prandle (1982). The residual flow magnitude is significantly smaller than the tidal propagation induced flow.

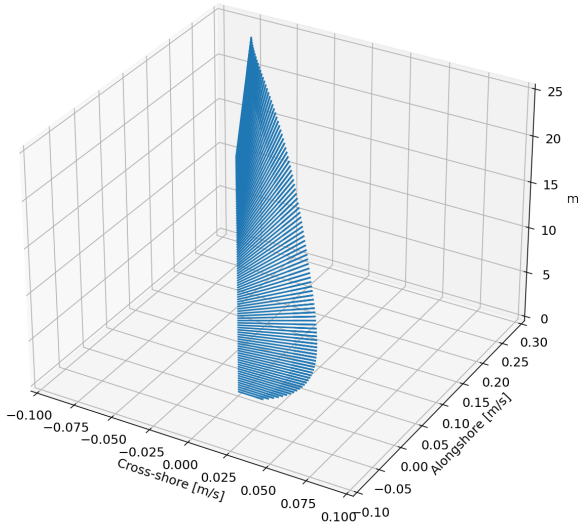

Figure 2.3: Vertical structure residual flow Heaps

The mentioned hypothesis states that a low mixing energy tends to result in a vertical velocity structure resembling the thermal wind balance and a low mixing energy results in a vertical structure that looks more like a estuarine circulation. Two more plots are made shown in Figure 2.4 on the next page to illustrate this.

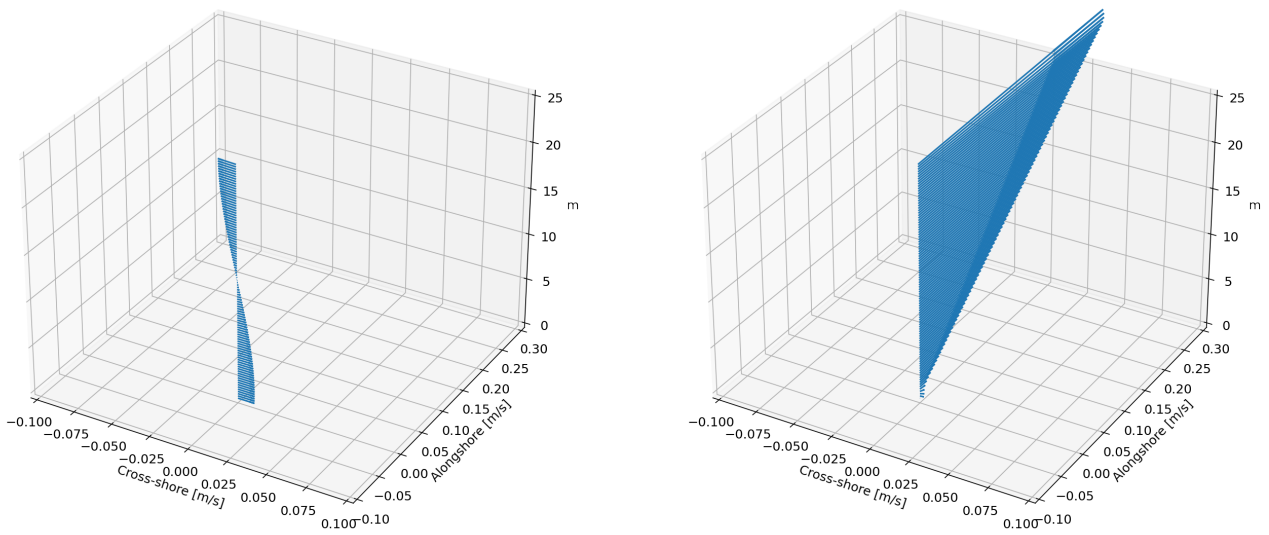

(a) $E_z = 0.1$ (b) $E_z = 1 * 10^{-5}$

Figure 2.4: Vertical structure Heaps for low and high mixing energy

It can indeed be seen that for an eddy viscosity coefficient of 0.1 the vertical structure of the residual flow looks like an estuarine circulation whereas the vertical structure for an eddy viscosity coefficient of $1 * 10^{-5}$ represents a thermal wind balance. Note that the thermal wind balance known from meteorology generally has the point of 0 velocity at approximately half the height of the vertical length scale, whereas here the point of 0 velocity is defined at the bottom boundary condition and with an increasing height from the bed the velocity increases in alongshore direction.

2.2.5 Vertical structure: Prandle and Heaps

To create the total vertical velocity structure including Prandle's (1982) time-dependent flow pattern and Heaps (1972) time-independent flow pattern, the previously shown vertical structures can simply be added. The tidal evolution as shown in Figure 2.2 is shown again below in Figure 2.5, this time the residual density-driven flow of Heaps is added.

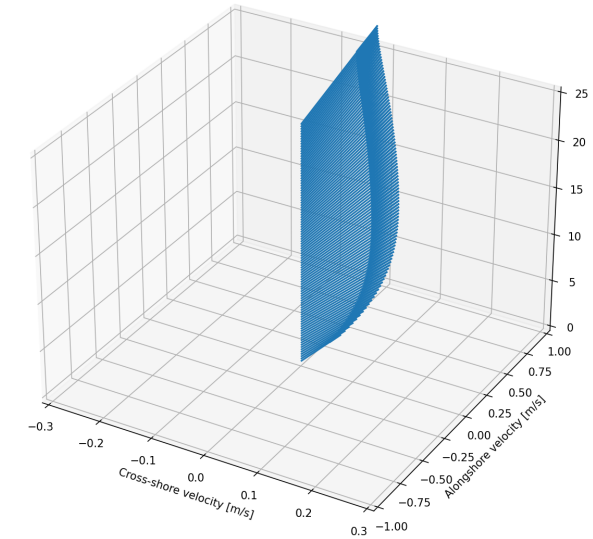

(a) $t = 0$

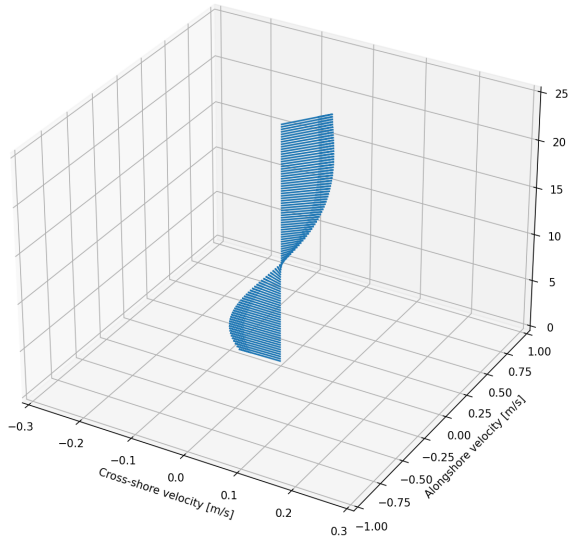

(b) $t = \frac{1}{4}T$

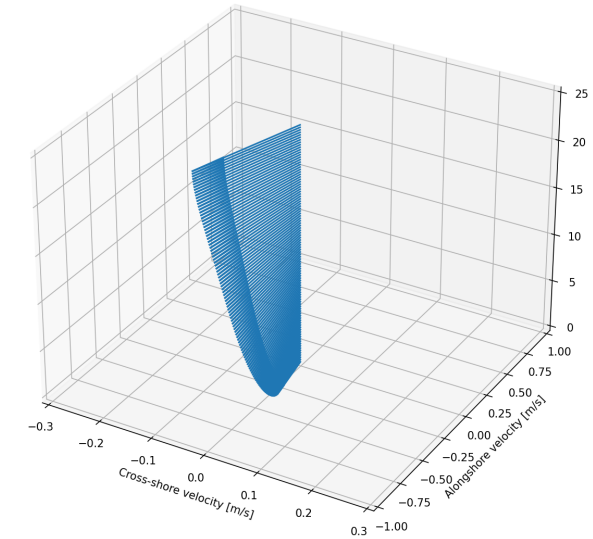

(c) $t = \frac{1}{2}T$

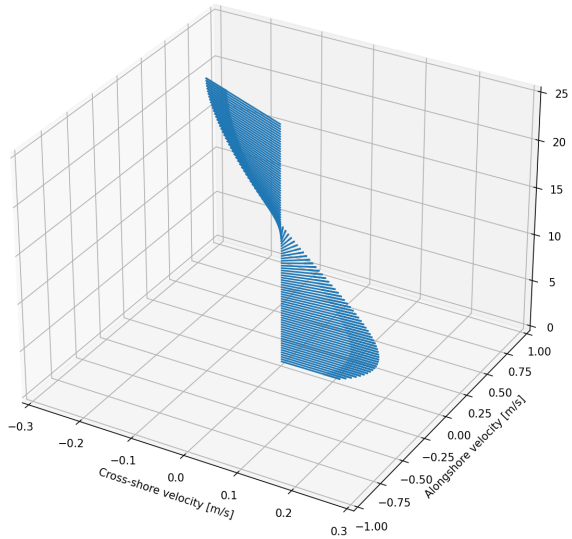

(d) $t = \frac{3}{4}T$

Figure 2.5: Evolution of 3D velocity structure over a tidal period for Prandle and Heaps

Chapter 3

Model development

3.1 introduction

In this chapter the model development will be discussed. It is important to have a model that can be applied for general cases with varying boundary conditions and dredging vessel types, it should not only be suitable for a sand nourishment project in the North Sea. Therefore it is chosen to create a python-based model based on object oriented programming, this allows for the creation of a class in which an object can be created by the user. The class functions as a blueprint for the energy consumption calculation, while the object is customizable by the user to represent a certain project. The model will be based on the Holtrop and Mennen method as previously mentioned, this allows for customization of the desired user case while simultaneously providing insight into the various parameters and the significance of their effect on the energy consumption of a vessel.

First, the basics of the Holtrop and Mennen method will be explained in section 3.2, forming the foundation of the python-based model. Hereafter, the modification on Holtrop and Mennen to calculate the resistance when sailing through a stratified flow field is given in section 3.3. After discussing the theory of the model, the actual model will be presented in section 3.4. The model is based on object-oriented programming in which an object, with the parameters for a desired user case, can be defined in a class.

3.2 Holtrop and Mennen

3.2.1 Basic principles

This section provides an expanded explanation of the Holtrop and Mennen method, which was previously introduced in subsection 2.1.7. For the sake of convenience, the basic principle are repeated in this subsection. The basic principle are considered to be the calculation of the energy consumption when the effective power of the engine is known. The comprehensive empirical formulae to calculate the different resistance components, as provided by Holtrop and Mennen, will be discussed in subsequent subsections.

Figure 3.1 depicts a schematic representation that illustrates how the brake horse power (BHP), delivered horse power (DHP) and effective (horse) power (EHP) are related to each other. In the remainder of this section these will respectively be denoted as P_b, P_d and P_e.

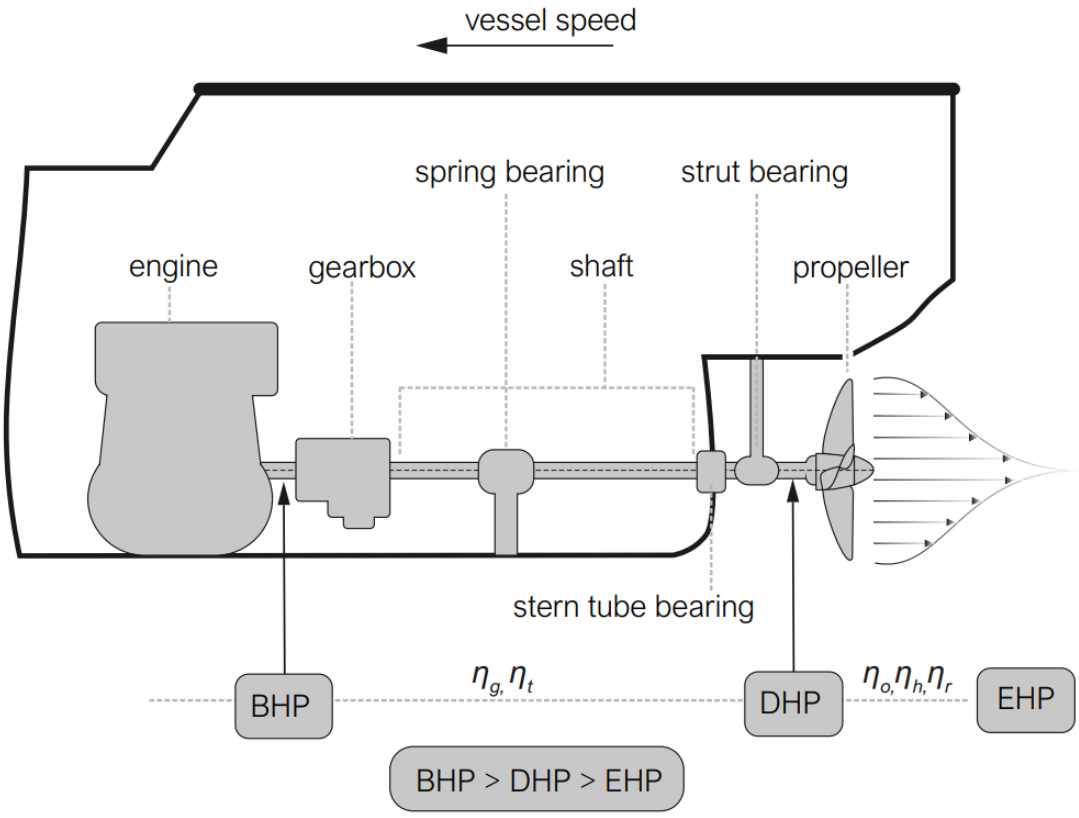

Figure 3.1: Schematization of relation between brake horse power, delivered horse power and effective horse power. (Koningsveld et al., 2021)

The foundation of Holtrop and Mennen (1982) method is the relationship between the effective power, the speed through water and the resistance:

$$P_e = R_{tot} * V \tag{3.1}$$

where:

P_e = Effective engine power $[kW]$

R_{tot} = Total resistance for a specific sailing speed $[kN]$

V = STW (speed through water) $[m/s]$

Note that the sailing speed is defined as the STW (speed through water), this is important because the resistance is induced by a sailing speed relative to the water and not relative to the ground. The resistance can be calculated with the empirically formulated formulae provided by Holtrop and Mennen. In this subsection the relationship between the effective power P_e and the energy consumption E is explained. First of all, the total energy consumption of a dredging vessel during a certain time duration is calculated as follows:

$$E = P_{tot} * \Delta t \tag{3.2}$$

where:

E = Energy consumption $[kWh]$

P_{tot} = Total required power on vessel $[kW]$

Δt = time duration $[hours]$

The total required power P_{tot} of a vessel determines the energy consumption, this total power is composed of two components: The power required for the engine, i.e. the brake horse power (P_b), and the power required to operate other utilities, such as the hotel facilities onboard the vessel:

$$P_{tot} = P_{transient} + P_{utilities} \tag{3.3}$$

The main interest for this thesis is the effect of the currents on the required engine power, i.e. $P_{transient}$, to reach a desired sailing speed, however, the remaining power requirements for other utilities become important when exploring different dredging strategies in chapter 4.

When the effective power for a certain sailing speed is determined, by utilizing the Holtrop and Mennen formulae to calculate the total resistance, the actual engine power can be calculated by means of empirically defined efficiency losses. These were previously mentioned in subsection 2.1.7:

$$P_d = \frac{P_e}{\eta_0 \eta_r \eta_h} \tag{3.4}$$

where:

P_d = Delivered horse power $[kW]$

η_0 = open water efficiency of propeller $[-]$

η_r = relative rotative efficiency $[-]$

η_h = hull efficiency $[-]$

$$P_b = \frac{P_d}{\eta_t \eta_g} (= P_{transient}) \tag{3.5}$$

where:

P_b = Brake horse power $[kW]$

η_t = shaft efficiency $[-]$

η_g = gearbox efficiency $[-]$

Equation 3.1, Equation 3.4 and Equation 3.5 can be combined to obtain obtain the relationship between the effective power and the brake horse power:

$$P_b = \frac{P_e}{\eta_0 \eta_r \eta_h \eta_t \eta_g} = \frac{R_{tot} * V}{\eta_0 \eta_r \eta_h \eta_t \eta_g} \tag{3.6}$$

Table 3.1 present the values for the different efficiency factors used in this thesis, based on the research done by Segers (2021). The hull efficiency factor is defined with an upper and lower limit for the user case of this thesis because it depends on the Froude number, which varies in time and space.

Parameter	Value	Unit
η_0	0.6	–
η_r	0.98	–
η_h	$0.97 - 1.03$	–
η_t	0.98	–
η_g	0.96	–

Table 3.1: Values for different efficiency factors

3.2.2 Resistance

This section presents a comprehensive explanation of the various resistance terms. The determination of each constituent part is based on the empirical formulas provided by Holtrop and Mennen, which, in turn, are based on model experiments. The total resistance is composed as follows:

$$R_{total} = R_F(1 + k_1) + R_{APP} + R_W + R_B + R_{TR} + R_A \tag{3.7}$$

where:

R_F = Frictional resistance $[N]$

$(1 + k_1)$ = The form factor describing the relationship between the frictional resistance and the viscous resistance $[-]$

R_{APP} = Appendage induced resistance $[N]$

R_W = Wave-making and wave-breaking resistance, not to be confused with the (wind) wave resistance $[N]$

R_B = Pressure induced resistance caused by a bulbous bow $[N]$

R_{TR} = Pressure resistance of immersed transom stern $[N]$

R_A = Model-ship correlation resistance $[N]$

Frictional resistance R_f

The first resistance component in the Holtrop and Mennen method is the frictional resistance. Frictional resistance is caused by the friction between the hull of the vessel and the water it is moving through, this resistance creates a net force in the adverse sailing direction. The frictional resistance is proportional to the wetted surface area of the hull, which is the surface area of the hull that is in contact with the water. The frictional resistance is expressed as a

function of the STW, the roughness of the hull surface, measured in a dimensionless friction coefficient, and the density of water (Bolt, 2003):

$$R_F = \frac{1}{2} C_f \rho V^2 S_T \tag{3.8}$$

where:

C_f = dimensionless friction coefficient $[-]$

ρ = density of water $[kg/m^3]$

V = sailing speed with respect to water (STW) $[m/s]$

S_T = wetted surface area $[m^2]$

The Holtrop and Mennen method employs empirical formulas for both the wetted surface area and the dimensionless friction coefficient to estimate the frictional resistance of a ship. The wetted surface area is calculated using a formula proposed by Holtrop and Mennen (1982), which takes into account various geometric characteristics of the hull. Similarly, Holtrop and Mennen (1982) provided a formula to calculate the dimensionless friction coefficient based on the ITTC57 friction line (ITTC, 2002) (International Towing Tank Conference). However, for the present research, the formula modified by Zeng et al. (2019) is used, which considers the effects of shallow water on the dimensionless friction coefficient.

The wetted surface area is defined as:

$$\begin{aligned} S_T = L_{WL}(2T + B)\sqrt{C_M}(0.453 + 0.4425 C_B - 0.2862 C_M \\ - 0.003467 \frac{B}{T} + 0.3696 C_{WP}) + 2.38 \frac{A_{BT}}{C_B} \end{aligned} \tag{3.9}$$

where:

L = Vessel length at waterline $[m]$

T = Draught $[m]$

B = Vessel width $[m]$

C_M = midship section coefficient $[-]$

C_B = block coefficient $[-]$

C_{WP} = water plane area coefficient $[-]$

A_{BT} = wet transverse sectional area of the bulbous bow $[m^2]$

The length, draught and width of the vessel are known, the various coefficients are based on these dimensions. The block coefficient C_B is the ratio of the underwater volume of the vessel's hull and the underwater volume of the rectangular underwater block. This is visualized in Figure 3.2. The block coefficient for dredging vessels is approximately 0.85 according to Vlasblom (2007).

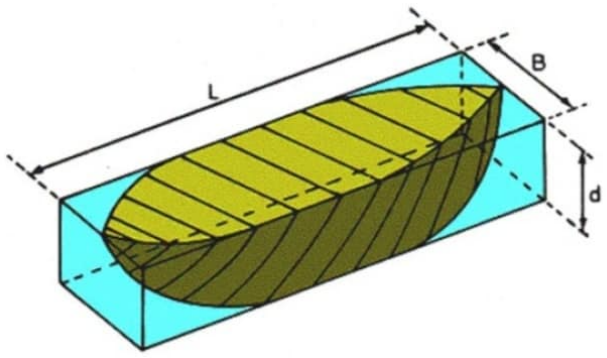

Figure 3.2: Underwater volume of hull in yellow, rectangular underwater block volume in blue (Maritmeculture, 2020)

The midship section coefficient and the water plane area coefficient depend on the block coefficient, Schneekluth and Bertram (1998) conducted research on this relationship. They provided the following empirical relationship that can be adopted in the present research:

$$C_M = 1.006 - 0.0056 C_B^{-3.56} \tag{3.10}$$

$$C_{WP} = \frac{1 + 2C_B}{3} \tag{3.11}$$

A_{BT} is the wet transverse sectional area of the bulbous bow. The bulbous bow is a circular extension located at the ship's stern. Its purpose is to decrease drag by influencing the flow around the hull, which ultimately reduces the resistance on the vessel (Chakraborty, 2021). Ventura (2022) has provided a formula for calculating A_{BT}:

$$A_{BT} = C_{BB} \cdot B \cdot T \cdot C_M \tag{3.12}$$

The value for C_{BB} is approximately 0.2 (Lamers, 2022). With the mentioned formulae, the wetted surface area S_T can be calculated.

The second parameter that needs to be determined in the Holtrop and Mennen method is the dimensionless friction coefficient, which is obtained from empirical research. Since the North Sea is a coastal area, the water can be considered as shallow. The original Holtrop and Mennen (1982) method employed the ITTC57 friction line, which assumes that the vessel is not limited by a shallow water depth. The present research adopts the formula proposed by

Zeng et al. (2019), which considers the shallow water effects. This modification is preferred as it provides a more accurate estimation of the dimensionless friction coefficient in shallow water conditions. The dimensionless friction coefficient, according to the ITTC (2002), is defined as follows:

$$C_F = \frac{0.075}{(\log(R_e) - 2)^2} = \frac{0.075}{(\log(\frac{VL}{\nu}) - 2)^2} \tag{3.13}$$

where:

R_e = Reynolds number $[-]$

ν = kinematic viscotiy $[m^2/s]$ $(\approx 10^{-6})$

Zeng et al. (2019) modified this equation to account for the shallow water depth and the vessel's dimensions. The formula that is used for the modified dimensionless friction coefficient depends on the ratio of the vertical length of the water column underneath the vessel and the vessel's length, i.e. $(D - T)/L_{WL}$.
In the scenario where this value is larger than one ($(D - T)/L_{WL} > 1$), the following equation is used:

$$C_f = C_F + (C_{deep} - C_{katsui})\frac{S_B}{S_T} \tag{3.14}$$

Additionaly, for $(D - T)/L_{WL} \leq 1$:

$$C_f = C_F + (C_{shallow} - C_{katsui})\frac{S_B}{S_T}\left(\frac{V_B}{V}\right)^2 \tag{3.15}$$

where:

S_B : Area of vessel's flat bottom $[m^2]$

C_{katsui} : Katsui friction coefficient $[-]$

$C_{shallow}$: Shallow water friction coefficient $[-]$

C_{deep} : Deep water friction coefficient $[-]$

V_B : Water velocity under vessel due to shallow water effects $[m/s]$

The area of the vessel's flat bottom can be approximated with the length at the waterline and width of the vessel as follows (Segers, 2021):

$$S_B = L_{WL} \cdot B \tag{3.16}$$

The averaged water velocity under the sailing vessel is approximated by fitting a regression line through data, this resulted in the equation 3.17 (Zeng et al., 2019). This is valid for $D/T \leq 4$, otherwise the initial speed through water V is used for V_B. Figure 3.3 illustrates a simplification of this increased water velocity.

$$V_B = V + \Delta V = 0.4277V \exp\left\{\left(\frac{D}{T}\right)^{-0.07634}\right\} \tag{3.17}$$

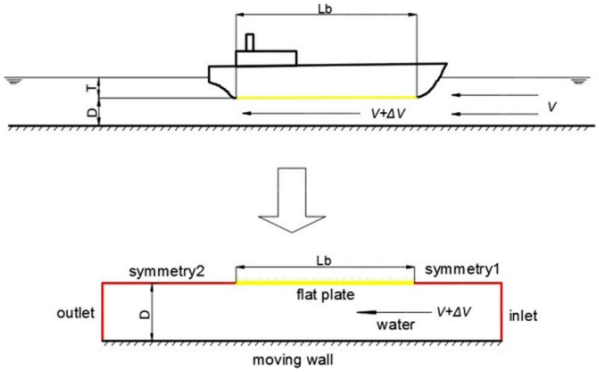

Figure 3.3: Simplification of a vessel in shallow water illustrating the sailing speed V and increased water velocity V_B $(=V + \Delta V)$ (Zeng et al., 2019)

The different components to calculate the dimensionless friction coefficient, namely C_{katsui}, C_{deep} and $C_{shallow}$, are defined as follows (Zeng et al., 2019):

$$C_{katsui} = \frac{0.0066577}{(\log R_e - 4.3762)^a}; a = 0.042612 \log R_e + 0.56725 \tag{3.18}$$

$$C_{deep} = \frac{0.08169}{(\log R_e - 1.717)^2} \tag{3.19}$$

$$C_{shallow} = \frac{0.08169}{(\log R_e - 1.717)^2} \cdot \left(1 + \left(\frac{0.003998}{(\log R_e - 4.393) \cdot ((D-T)/L)^{-1.083}}\right)\right) \tag{3.20}$$

Form factor $(1 + k_1)$

The second term in the total resistance as described in equation 3.8 is the form factor $(1 + k_1)$. This form factor accounts for the relationship between the frictional resistance and the viscous resistance. When a ship moves through water, it creates a boundary layer of water around its hull. This boundary layer experiences frictional forces due to the viscosity of water, resulting in

a resistance known as viscous resistance. This form factor is therefore a measure of the viscous resistance induced by the shape of the hull.

The form factor is expressed with the prismatic coefficient (C_P), which depends of the length at the waterline (L_{WL}) and the length of the run (L_R). The length of the run is the measurement of the vessel from the forwardmost point to the aftmost point. The formula to calculate the form factor is as follows (Roh and Lee, 2018):

$$\begin{aligned} 1 + k_1 = 0.93 + 0.487118 \cdot C_{14}(B/L_{WL})^{1.06806} \cdot (T/L_{WL})^{0.46106} \\ \cdot (L_{WL}/L_R)^{0.121563} \cdot (L_{WL}^3/\Delta)^{0.36486} \cdot (1 - C_P)^{-0.60247} \end{aligned} \tag{3.21}$$

where:

L_R : Length of the run $[m]$

C_P : Prismatic coefficient $[-]$

Δ : Water displacement $[m^3]$

C_{14} : Coefficient based on the shape of the stern $[-]$

The prismatic coefficient depends on the block coefficient C_B and the midship coefficient section coefficient C_M, it is defined according to Holtrop and Mennen (1982) as follows:

$$C_P = \frac{C_B}{C_M} \tag{3.22}$$

After determining the prismatic coefficient, the length of the run can be calculated with the following equation (Roh and Lee, 2018):

$$L_R = L_{WL}\left(1 - C_P + \frac{0.06 C_P lcb}{4C_P - 1}\right) \tag{3.23}$$

where lcb is the longitudinal position of the center of buoyancy forward (+) or aft (-) of halfway the length at the waterline ($0.5L_{WL}$), it is expressed as a percentage (%) (Segers, 2021):

$$lcb = -13.5 + 19.4C_P \tag{3.24}$$

The prismatic coefficient and length of the run L_R can now be determined. In order to calculate the form factor, the displacement of water Δ and the coefficient C_{14} have to be determined as well. The water displacement can be calculated using the block coefficient (Segers, 2021):

$$\Delta = C_B \cdot L_{WL} \cdot B \cdot T \tag{3.25}$$

Lastly, the coefficient C_{14} is defined as follows (Roh and Lee, 2018):

$$C_{14} = 1 + 0.011 C_{stern} \tag{3.26}$$

where C_{stern} is a coefficient that depends on the shape of the stern of the vessel, this parameter take the following values for varying shape (Segers, 2021):

$$C_{stern} = \begin{cases} -25 & \text{for barge-shaped forms} \\ -10 & \text{for V-shaped section stern} \\ 0 & \text{for normal section stern} \\ 10 & \text{for U-shaped section stern} \end{cases} \tag{3.27}$$

The value for C_{stern} is assumed to be 0 for simplicity, resulting in a value for C_{14} of 1. The form factor $(1 + k_1)$, i.e. the resistance the sailing vessel experiences due to the fluid viscosity, can now be determined.

Appendage resistance R_{app}

The third component in the total resistance as defined by Holtrop and Mennen (1982) is the frictional resistance caused by the appendages. These appendages, e.g. rudder, shafts, skeg, induce a frictional resistance experienced by the sailing vessel. The formula to calculate this appendage resistance is proposed by Holtrop and Mennen (1982):

$$R_{APP} = 0.5 \rho V^2 S_{APP} (1 + k_2) C_f \tag{3.28}$$

where:

V : Speed through water $[m/s]$

S_{APP} : Wetted area of the appendages $[m^2]$

$(1 + k_2)$: Coefficient based on the type of appendages $[-]$

C_f : Dimensionless friction coefficient $[-]$

The estimated wetted area of the appendages on inland ships is approximately 5% of the total wetted area S_T (Segers, 2021). The factor $(1 + k2)$ for appendage resistance varies depending on the type of appendage. To simplify calculations, a constant value of $(1 + k2) = 2.5$ is commonly utilized (Holtrop and Mennen, 1982).

Wave resistance R_W

The wave resistance, or wave-making resistance, is the resistance a vessel experiences due to the waves that are produced by the vessel sailing through the water. This resistance results from the wave energy that has to be produced in order to create waves, the source of energy for this production is the kinetic energy of the vessel, i.e. the sailing speed through water. The wave resistance increases significantly when a certain critical speed through water is achieved (van Koningsveld et al., 2021). Similarly to the frictional resistance, where the increased sailing speed addresses the effects of shallow water (Zeng et al., 2019), the water depth also has a significant influence on the wave resistance. The increased water velocity underneath the vessel is calculated by utilizing the Karpov modification defined as follows (van Terwisga, 1989) (Segers, 2021):

$$V_2 = \frac{V}{\alpha^{**}} \tag{3.29}$$

It can be seen that the altered water velocity depends on the coefficient α^{**}, which, in turn, depends on the Froude number Fr_h based on the ship's speed through water and water depth (van Terwisga, 1989):

$$Fr_h = \frac{V}{\sqrt{gh}} \tag{3.30}$$

a^{**} is expressed by means of 6^{th} order polynomials, where the chosen polynomial depends on the Froude number in combination with the ratio of the water depth h and the draught of the vessel T. The various 6^{th} order polynomials, for different intervals of the Froude number and ratio h/T, can be found in Appendix B. The water velocity underneath the sailing vessel can now be calculated. Note that this modified water velocity underneath the vessel V_2 is used in the wave resistance, pressure resistance of immersed transom stern and model-ship correlation resistance (Segers, 2021).

The formula for the wave resistance depends on different ranges of Froude numbers Fr_{V_2}, which depends on the modified water velocity and the vessel's length at the waterline (Segers, 2021):

$$Fr_{V_2} = \frac{V_2}{\sqrt{gL_{WL}}} \tag{3.31}$$

Three distinct formulae for the wave resistance exist for Froude numbers either below 0.4, above 0.55, and between 0.4 and 0.55. These wave resistance calculation methods are described by Sarris (2023) and are derived from the Holtrop and Mennen method. The formulae below present the different expressions for the wave resistance.

$Fr_{V_2} < 0.4$

$$R_{W1} = c_1 c_2 c_5 \Delta \rho g \exp\left(m_1 Fr_{V_2}^{-0.9} + m_4 \cos\left(\lambda Fr_{V_2}^{-2}\right)\right) \tag{3.32}$$

$Fr_{V_2} > 0.55$

$$R_{W2} = c_{17} c_2 c_5 \Delta \rho g \exp\left(m_3 Fr_{V_2}^{-0.9} + m_4 \cos\left(\lambda Fr_{V_2}^{-2}\right)\right) \tag{3.33}$$

$0.4 \leq Fr_{V_2} \leq 0.55$

$$R_{W3} = R_{W1} + \frac{(10 Fr_{V_2} - 4)(R_{W2} - R_{W1})}{1.5} \tag{3.34}$$

Pressure resistance caused by bulbous bow R_B

The presence of a bulbous bow at the stern of the sailing vessel induces an additional resistance due to pressure at the bulbous bow. The pressure due to the bulbous bow term in Holtrop and Mennen's method accounts for the additional pressure exerted on the bow of the ship due to the presence of the bulb. This term takes into consideration the shape and dimensions of the bulb, as well as the sailing speed through water (V). The formula to calculate this resistance is (Roh and Lee, 2018) (Lamers, 2022):

$$R_B = \frac{0.11 \exp\left(-3 P_B^{-2}\right) \cdot F_{ni}^3 A_{BT}^{1.5} \rho g}{1 + F_{ni}^2} \tag{3.35}$$

where:

P_B : Measure of the immersion of the bulbous bow $[-]$

F_{ni} : Froude number based on the immersion of the bulbous bow $[-]$

The coefficient P_B and Froude number F_{ni} are calculated as follows (Roh and Lee, 2018):

$$P_B = \frac{0.56\sqrt{A_{BT}}}{T_F - 1.5 h_B} \tag{3.36}$$

$$F_{ni} = \frac{V}{\sqrt{g(T_F - h_B - 0.25\sqrt{A_{BT}}) + 0.15 V^2}} \tag{3.37}$$

where:

T_F : Forward draught of the vessel $[m]$

h_B : Position of the centre of the transverse area $[m]$

Pressure resistance of immersed transom stern R_{TR}

Similarly to the pressure resistance of the bulbous bow, the presence of a transom stern can also induce an additional pressure resistance. This resistance should also be taken into account and it is included in the Holtrop and Mennen formulae (1982). As previously mentioned, the Karpov modified water velocity V_2 will be used, following the same procedure as Segers (2021). The pressure resistance of the immersed transom stern is calculated as:

$$R_{TR} = 0.5\rho V_2^2 A_T c_6 \tag{3.38}$$

where A_T is the immersed part of the transverse area of the transom, this is calculated as follows (Segers, 2021):

$$A_T = 0.2 \cdot B \cdot T \tag{3.39}$$

the coefficient c_6 depends on the transom immersion Froude number Fr_T. The transom immersion Froude number and, subsequently, coefficient c_6 are calculated according to the following equations (Segers, 2021):

$$c_6 = 0.2(1 - 0.2Fr_T) \tag{3.40}$$

$$Fr_T = \frac{V_2}{\sqrt{2gA_T/(B + BC_{WP})}} \tag{3.41}$$

Model-ship correlation resistance R_A

The model-ship correlation resistance was also introduced in the originial Holtrop and Mennen method (1982). This resistance accounts for the differences between the measured resistance based on model experiments and the resistance a sailing vessel experiences in reality. It primarily descibres the effect of the hull roughness and the still-air resistance (Roh and Lee, 2018). The formula to calculate this resistance according to Segers (2021) is:

$$R_A = 0.5\rho V_2^2 S_T C_A \tag{3.42}$$

where C_A is a model-ship correlation allowance coefficient, which is calculated as follows (Holtrop and Mennen, 1982):

$$C_A = 0.006(L + 100)^{-0.16} - 0.00205 + 0.003\sqrt{L/7.5}C_B^4 c_2(0.04 - C_4) \tag{3.43}$$

with:

$$c_4 = \begin{cases} T_F/L_{WL} & \text{for } T_F/L_{WL} \leq 0.04 \\ 0.04 & \text{for } T_F/L_{WL} > 0.04 \end{cases} \tag{3.44}$$

3.3 Modification to include stratified flow field

To account for the stratified coastal currents on the energy usage of a dredging vessel, three additional factors should be accounted for in the Holtrop and Mennen method:

1. Drag and lift force on rudder
2. Dead-water resistance
3. Altered sailing time

These factors should be taken into account to get an estimate of the effect of oblique stratified currents on resistance and the energy consumption of the vessel. Neglecting these factors will result in the resistance for a dredging vessel sailing through non-stratified still water, this can also be seen as the part that differentiates the presented research with the research done by Lamers (2022). Subsection 3.3.1 outlines the effect of the drag and lift force generated at the rudder of the vessel. Subsection 3.3.2 explains the dead-water phenomenon and why its additional resistance is assumed to be negligible.

3.3.1 Drag and lift force on rudder

It is important to note that for a small rotation of the vessel with respect to the relative water direction, it can be assumed that the vessel is sailing parallel to the streamlines of the water. The pressure resistance components of the Holtrop and Mennen model considers the drag caused by the whole geometry of the vessel when it is sailing straight through the water, i.e. parallel to the streamlines. Because this research addresses the energy consumption when the vessel is free sailing, the sailing speed through water (STW) is of a significant larger magnitude than the currents. Therefore, these additional hydrodynamic forces at the bow and stern of the vessel can be neglected.

However, the rudder of a vessel can have a significant impact on the drag and overall resistance experienced by the vessel. When the rudder's centerline is not parallel to the vessel's centerline, the streamlines of the flow are not parallel to the rudder's centerline, creating a zone of separation or recirculation behind the rudder due to an adverse pressure gradient. The turbulent characteristics of this problem are not part of the scope of the current research, but a simplification of the hydrodynamics is illustrated in Figure 3.4. This disturbance of the flow, and generation of turbulence, creates an additional drag and lift force at the rudder of the vessel, leading to an increased total resistance.

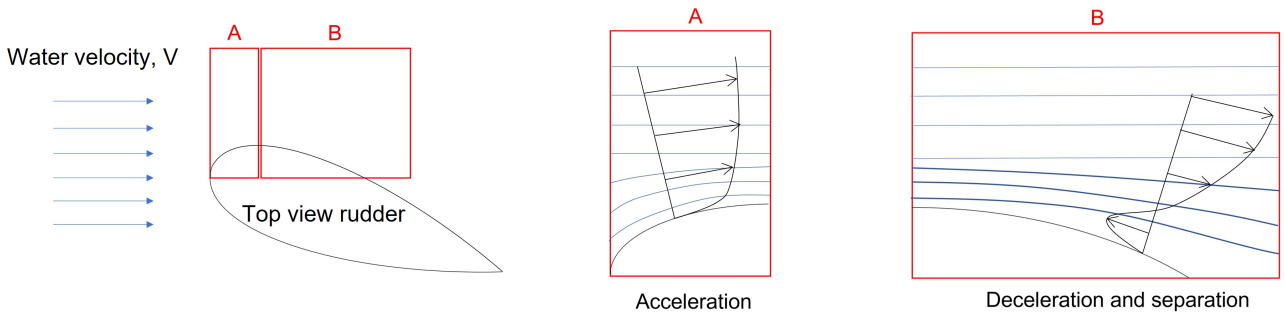

Figure 3.4: Top view of rudder, highlighting the acceleration zone (A) and decelerating or separation zone (B)

The angle between the rudder's centerline and the direction of the water velocity with respect to the rudder is called the drift angle. Note that the the direction of water with respect to the rudder is antiparallel to that of the sailing direction through water. The resulting drag and lift forces on the rudder depend on the drift angle, water velocity with respect to the rudder, the lateral area of the rudder, and the drag or lift coefficient (Lübke, 2016). The schematization in Figure 3.5 depicts a top view of the rudder including the corresponding forces when the rudder is under an angle with the sailing direction through water.

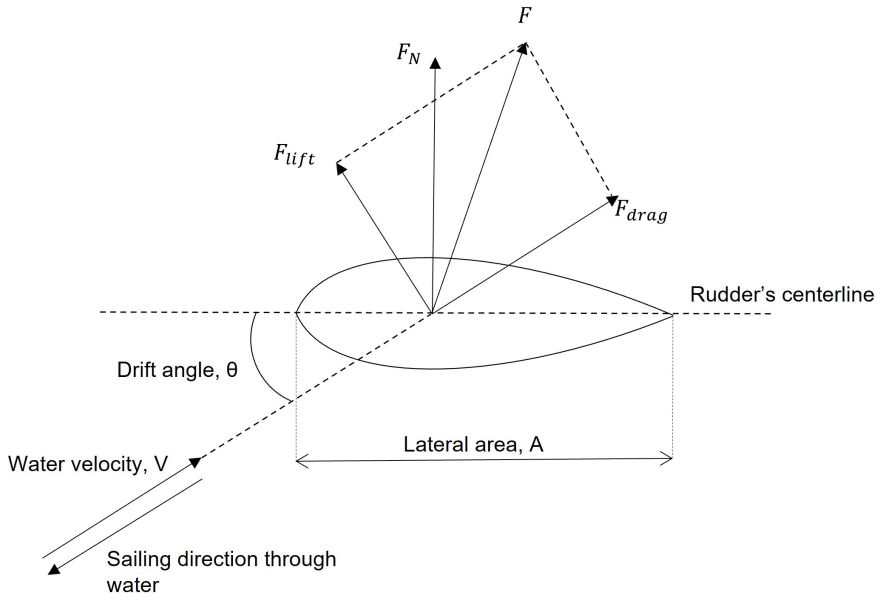

Figure 3.5: Top view of rudder with corresponding forces when the rudder is not aligned with the sailing direction

The lift force is perpendicular to the sailing direction, making it unable to simply be added to the total resistance. Instead, the lift force causes a sideways force which attempts to rotate the vessel around its center of gravity, which is the very function of the rudder. The actual rotating of the vessel is caused by the hydrodynamic forces at the bow and stern of the vessel. A hull is designed to create a larger moment due to bow forces than an opposite rotating moment due to stern forces (Chakraborty, 2021), causing the vessel to rotate. Figure 3.6 shows the moments on the vessel caused by the drift angle and hydrodynamic forces.

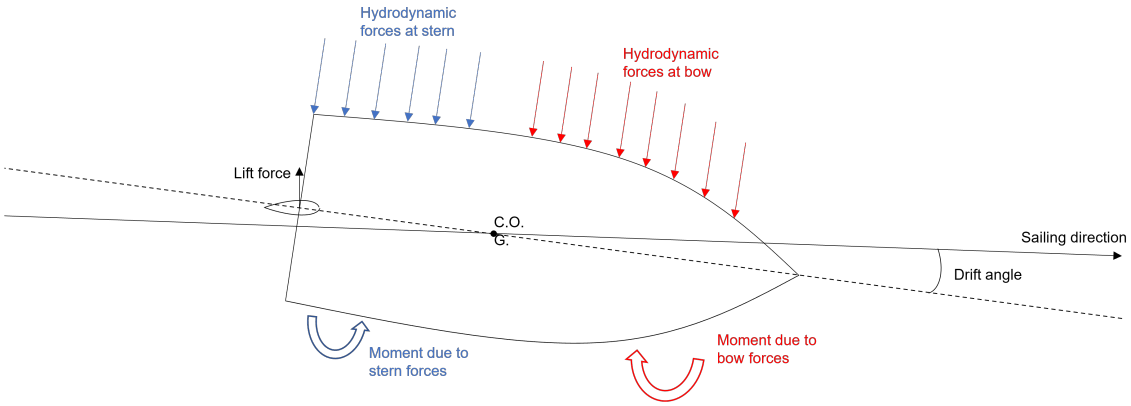

Figure 3.6: Top view of a sailing vessel, including bow and stern moments caused by hydrodynamic forces along the vessel

Because the lift force is perpendicular to the sailing direction and only initiates the rotation of the vessel, it is assumed that its additional resistance can be neglected in the calculation of energy consumption.

The modification of the Holtrop and Mennen method will therefore only consider the drag force in the total resistance. The formula to calculate the drag resistance is the generic formula to calculate a drag force, note that the increased velocity V_2 as explained in subsection 3.2.2 is used:

$$R_{drag} = \frac{1}{2}\rho C_D V_2^2 A \tag{3.45}$$

where:

ρ = density of water $[kg/m^3]$

C_D = drag coefficient $[-]$

V_2 = Increased water velocity underneath vessel $[m/s]$

A = Surface area of the rudder, characteristic of a specific vessel $[m^2]$

The value of the drag coefficient varies based on the drift angle of the vessel. Figure 3.7 displays the corresponding values of C_D for drift angles ranging from 0 to 35 degrees.

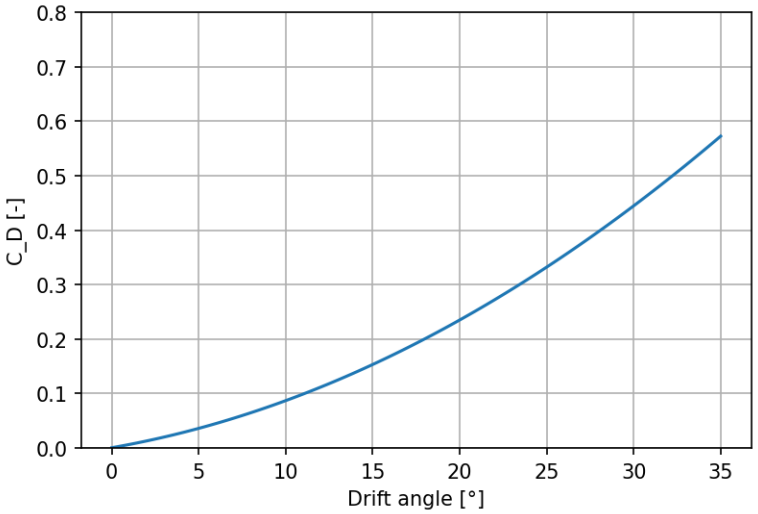

Figure 3.7: Drag coefficient for increasing drift angle, based on research from Lübke (2016)

To calculate the drift angle, the STW magnitude and direction are added vectorially to the currents magnitude and direction. As a result of this vector addition, a new vector is generated that represents the SOG (speed over ground) magnitude and direction. This can intuitively be interpreted as the currents that cause the vessel to deviate from its intended sailing path. The rudder is then adjusted to correct for this "deviation angle". The difference between the STW direction and the deviation angle is known as the drift angle, which can be determined by taking the absolute value of this difference. Figure 3.8 on the next page provides a top view that illustrates the angles in a Cartesian coordinate system and the deviation angle and magnitude by means of vector addition.
When the sailing speed through water angle and deviation angle are known, the drift angle is calculated as follows:

$$\theta_{drift} = |\theta_S - \theta_D| \tag{3.46}$$

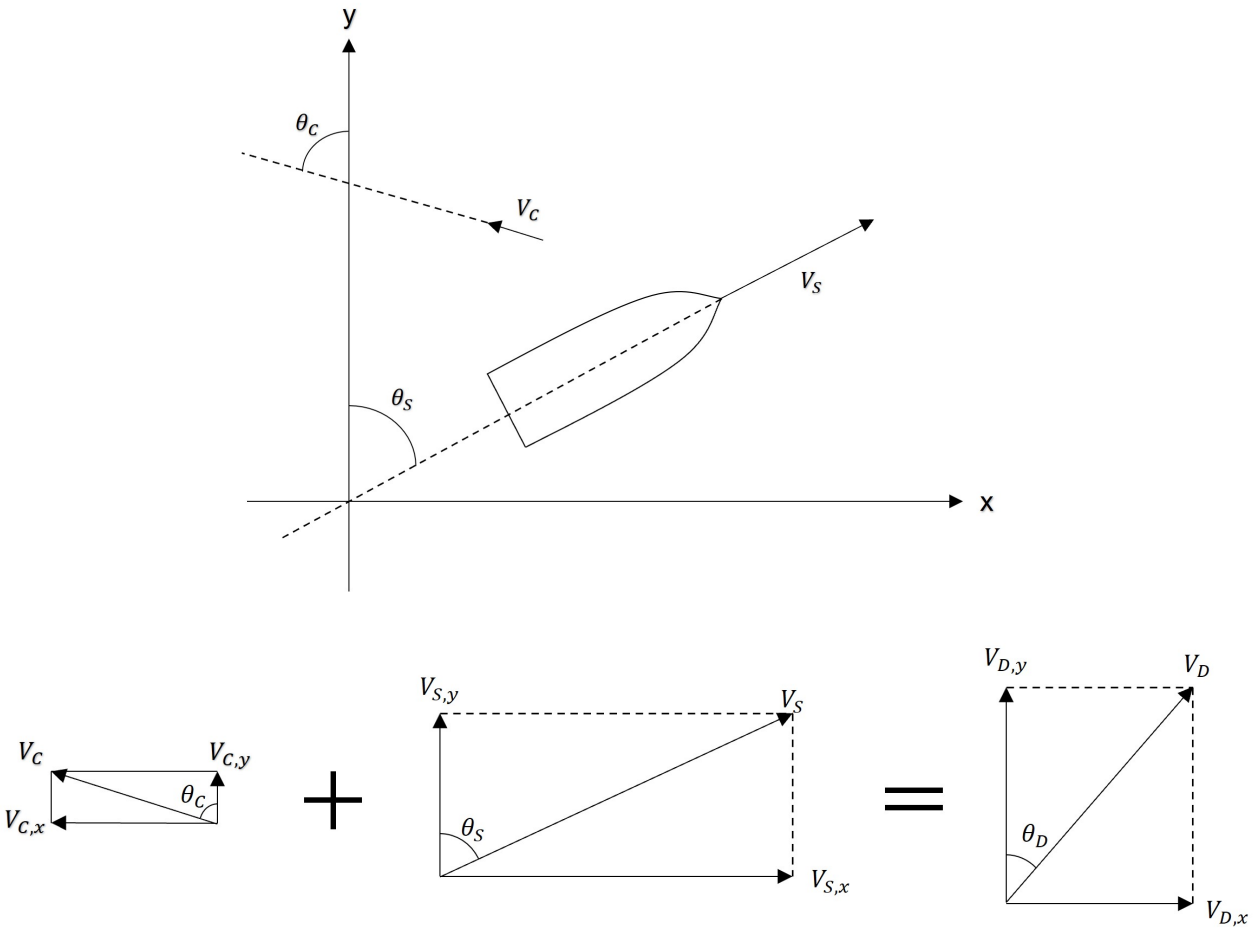

Figure 3.8: Top view of STW magnitude and angle and current magnitude and angle (upper), vector addition (lower). Where V_S = STW $[m/s]$, θ_S = STW angle [°], V_C = current magnitude $[m/s]$, θ_C = current angle [°], V_D = Deviation sailing speed, i.e. SOG $[m/s]$, θ_D = Deviation angle, i.e. SOG angle [°].

3.3.2 Dead-water resistance

In addition to stratified flows, stratification in oceans can also lead to the formation of internal waves. The generation of internal waves in oceans can be explained by considering the interface between water and air, where surface waves are generated due to external forces such as wind and gravity. Analogously, when the water column is viewed as a two-layer system, with a significant jump in density at the internal interface between the two layers, internal waves can be generated at this interface due to forcing. A vessel sailing through a stratified water column can act as the external forcing that generates these internal waves. Similarly to the

wave-making resistance, this internal wave can cause a significant resistance on a sailing vessel also known as the dead-water resistance (Esmaeilpour et al., 2018).

The buoyancy frequency N, also known as the Brunt-Vaisala frequency, is an important parameter that affects the stability of stratification in the ocean and the formation of internal waves. The buoyancy frequency is a measure of the rate at which a parcel of fluid oscillates when displaced from its equilibrium position (Pietrzak, 2021). It is determined by the vertical gradient of density, the gravitational acceleration and reference density as follows:

$$N^2 = -\frac{g}{\rho_0}\frac{\partial \rho}{\partial z} \tag{3.47}$$

When the buoyancy frequency is high, the stratification is more stable, making it more difficult for internal waves to form. Conversely, when the buoyancy frequency is low, the stratification is more unstable, leading to a greater likelihood of internal wave formation.

Another important parameter that is assesses the stability of a stratified fluid is the Richardson number Ri, this parameter is defined as the square of the buoyancy frequency divided by the velocity shear over the vertical squared (Pietrzak, 2021):

$$Ri = \frac{N^2}{\left|\frac{\partial u}{\partial z}\right|^2} = -\frac{\frac{g}{\rho_0}\frac{\partial \rho}{\partial z}}{\left|\frac{\partial u}{\partial z}\right|^2} \tag{3.48}$$

where the commonly used criterion for stability of a stratified fluid states that $Ri > \frac{1}{4}$. The Richardson number can also be expressed as the density difference from the free surface to a reference depth in which density changes during the evolution of the flow are negligible (Esmaeilpour et al., 2016):

$$Ri = \frac{\Delta \rho}{\rho_0}\frac{g L_0}{U_0^2} \tag{3.49}$$

where:

$\Delta \rho$ = density difference from surface to reference depth $[kg/m^3]$

ρ_0 = reference density $[kg/m^3]$

L_0 = vertical length scale from surface to reference depth $[m]$

U_0 = velocity at reference depth $[m/s]$

To determine the dead-water resistance, the Richardson number is related to the densimetric Froude number Fr_h (Esmaeilpour et al., 2016):

$$Ri = \frac{1}{Fr_h^2} \tag{3.50}$$

which can be rewritten as follows:

$$Fr_h = \frac{1}{\sqrt{Ri}} = \frac{U_0}{\sqrt{gL_0\frac{\Delta\rho}{\rho_0}}} = \frac{U_0}{c^*} \tag{3.51}$$

where c^* is the internal wave celerity, which is lower than the celerity of surface waves, as the restoring forces responsible for internal waves are weaker due to reduced gravity. The value of Fr_h indicates the relative importance of internal waves to fluid dynamics. Low values indicate strong influence from the density stratification and internal waves, whereas high values indicate dominance of fluid inertia.

Esmaeilpour et al. (2018) conducted a study using computational fluid dynamics (CFD) to investigate the impact of densimetric Froude number on the total resistance experienced by a vessel traveling through a stratified fluid. Figure 3.9 illustrates the total resistance when sailing through a stratified fluid and compares it to the non-stratified case.

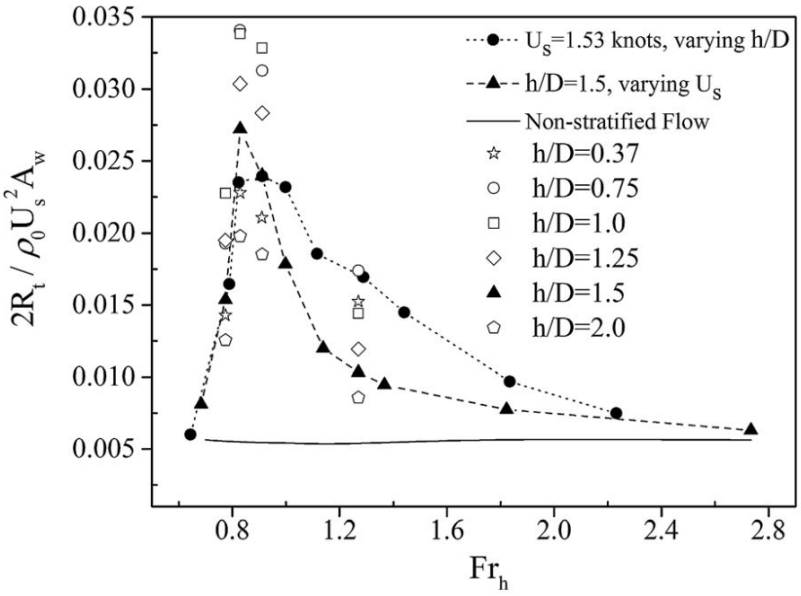

Figure 3.9: Dimensionless total resistance for an increasing densimetric Froude number and different ratios of draught to total water depth (h/D) (Esmaeilpour et al., 2018)

As can be seen on the graph, the dead-water resistance has a peak at a Fr_h of approximately 0.9, which lies in the region of the subcritical Fr_h. When the densimetric Froude number is subcritical, the strong stratification conditions dominate over other effects. It also shows that for supercritical Fr_h, as inertia dominates, the dead-water resistance converges to the non-stratified case.

This graph is used to obtain a first order estimate of the significance of the effect of the internal waves on a dredging vessel during free sailing in the North Sea. Because the free sailing part generally corresponds to a large STW, the velocity at reference depth U_0 is assumed to be 5 m/s. Moreover, the water column is assumed to be a two-layer system with a freshwater density at the surface of 1000 kg/m^3 and a saline water density at the reference depth of 1020 kg/m^3. The reference water depth L_0, i.e. draught, is assumed to be 5 m. Plugging these values into Equation 3.51 results in:

$$Fr_h = \frac{5}{\sqrt{9.81 * 5 * \frac{20}{1000}}} = 5.05$$

As the water column in the North Sea differs from the idealized two-layer system used in the calculation, the densimetric Froude number is expected to be higher in reality. Hence, the present study assumes that the dead-water resistance can be disregarded. It is important to note that the sailing speed can be significantly lower when the vessel is not free sailing, for instance during accelerating, decelerating, or dredging. In that case a new evaluation of the densimetric Froude number must be conducted. However, this is not part of the scope of the current research.

3.4 Model Set-Up

This section will explain the python-based model that is developed to determine the energy consumption when sailing through a flow field, i.e. the effect of currents on the energy consumption of a dredging vessel. In subsection 3.4.1, the implementation of the modified Holtrop and Mennen method in the model will be explained. In addition to the increased resistance experienced by a vessel sailing through a flow field, the vessel experiences an altered sailing time when sailing through a flow field. This is taken into account in the model and will be explained in subsection 3.4.2. Following that, an NSD (Nassi–Shneiderman diagram) will be presented in subsection 3.4.3, providing an overview of the Python class and its methods. Lastly, the section will go into the technical details of each of the class methods in subsection 3.4.4, providing a more comprehensive understanding of the model.

3.4.1 Holtrop and Mennen implementation

The modified Holtrop and Mennen method requires both dynamic and static parameters as inputs. Dynamic parameters include the STW (speed through water), water depth, draught, and drift angle, while static parameters include ship characteristics such as dimensions and total installed engine power. With these parameters known, the Holtrop and Mennen function can return values such as the various resistance components, the effective engine power and the brake horse power. The following equation illustrates the relation between the input values and output values.

$$R_{tot}, R_i, P_e, P_b = f(STW, d, T, \theta_{drift}) \tag{3.52}$$

where:

R_i = Individual resistance components $[kN]$

d = Water depth $[m]$

T = Draught of vessel $[m]$

This version of the modified Holtrop and Mennen method works in theory, but the standard form of the Holtrop and Mennen method is not practical for real-world applications. This is because a dredging vessel typically maintains a constant engine power rather than a constant STW. This requires the Holtrop and Mennen method to be rewritten such that it takes the engine power as an input variable and returns the STW instead. However, due the the complex nature of the defined empirical formulae, this option is not feasible. Therefore it is chosen to use the bisection method to calculate the STW with as input the engine power.

The bisection method approach involves setting a tolerance level and defining an upper and lower limit for the STW, respectively V_{upper} and V_{lower}. The first iteration, the STW used as the input variable, V_{input} is calculated as follows:

$$V_{input} = \frac{V_{upper} - V_{lower}}{2} \tag{3.53}$$

The method then calculates the brake horse power using the modified Holtrop and Mennen formula and compares it to the target engine power, i.e. the set constant power, using Equation 3.52. If the calculated engine power is larger than the set constant power, the new upper limit is replaced by V_{input}. Vice versa, if the calculated engine power is smaller than the set constant power, the lower limit value is replaced by V_{input}. This algorithm remains iterating until the difference between the sailing speed's upper and lower limit is smaller than a certain set tolerance. Using this approach, Equation 3.52 can be rewritten as follows:

$$STW = g(P_b, V_{upper}, V_{lower}, tol, f(STW, d, T, \theta_{drift})) \tag{3.54}$$

Where g can be interpreted as the bisection method. tol is the tolerance set for the allowable difference in the upper and lower limit for the sailing speed. Note that decreasing this tolerance increases the computational time required to meet the tolerance, while increasing the tolerance makes the STW, corresponding to the power used as input, less accurate. It can be seen that the function is implicit, the bisection is found as a suitable solution to this problem.

3.4.2 Altered sailing time

This subsection explains the altered sailing time due to the presence of a flow field. a distinction is made between the speed through water (STW) and the speed over ground (SOG), as well as the course through water (CTW) and the course over ground (COG). An understanding of these concepts is crucial to clarify the mechanism underlying the altered sailing time. To make this more intuitive, consider a scenario in which a vessel with a captain and a GPS tracking device is sailing. While the captain on board experiences the STW and the CTW, the GPS tracking device measures the STG and COG as it tracks the vessel's movement relative to a fixed Cartesian framework, i.e. the Earth's surface. To explain how the python-based model determines the altered sailing time, four different scenarios are illustrated by means of kinematic diagrams.

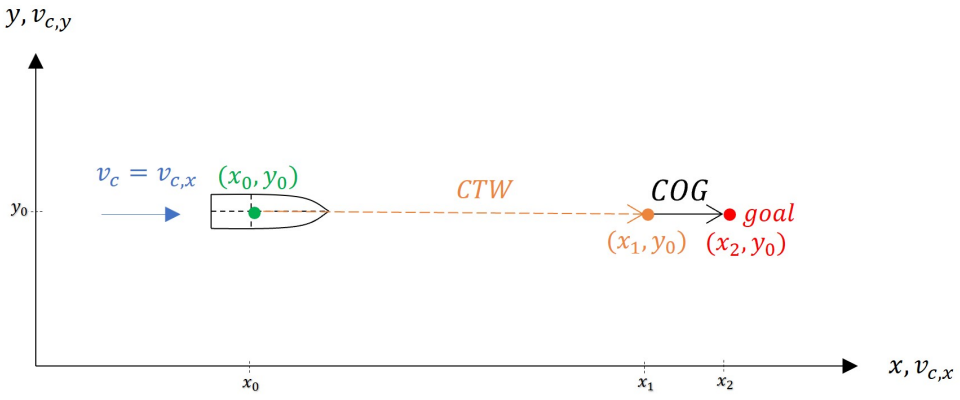

Figure 3.10: Scenario 1: sailing in x-direction, parallel current

The first scenario can be seen on Figure 3.10, both the vessel's sailing direction and the current direction v_c are in x-direction. As previously explained, the drift angle is induced by

a deviation of the intended sailing direction, this does not happen in this scenario. The total resistance R_{tot} will in this case be identical to the original Holtrop and Mennen resistance, there will be no drag resistance R_{drag} on the rudder. However, because the current is in the sailing direction, the sailing time will change. The sailing time is calculated by dividing the CTW by the STW as calculated with the bisection method. Note that this calculation is identical in all the scenarios, and also the python-based model, it can be seen as the foundational theory on which the sailing time calculation is based.

$$t_{sailing} = \frac{CTW}{STW} \left(= \frac{COG}{SOG} \right) \tag{3.55}$$

where the CTW is based on the distance to the end goal, i.e. course over ground (COG), and the ratio of the STW and the SOG:

$$CTW_{(x_0,y_0)\to(x_1,y_0)} = COG_{(x_0,y_0)\to(x_2,y_0)} * \frac{STW}{STW + v_{c,x}} \tag{3.56}$$

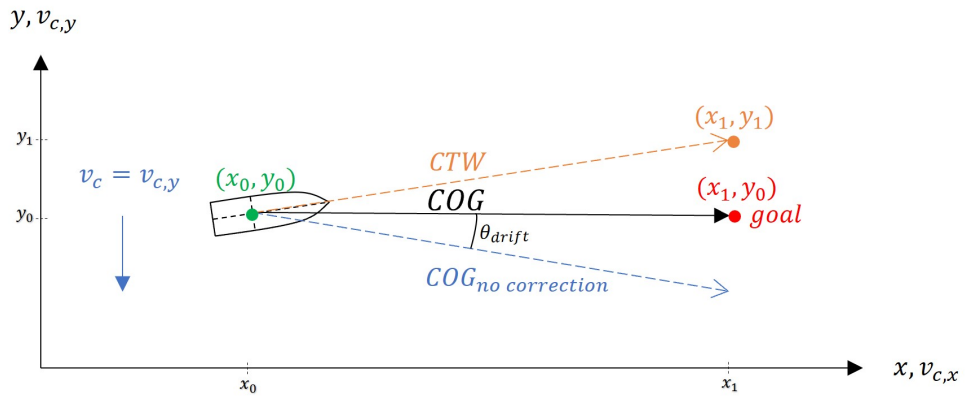

Figure 3.11: Scenario 2: sailing in x-direction, perpendicular current

the second scenario can be seen in Figure 3.11, in this case the current is solely perpendicular to the sailing direction. Because this results in a drift angle for which the rudder has to compensate, the drag resistance R_{drag} is larger than zero and therefore the total resistance R_{drag} increases and the STW decreases. In order to maintain the same COG, the CTW has to compensate for the ambient flow. Figure 3.11 illustrates the vessel's CTW to end up at the desired goal. Based on this CTW and the STW, the alter sailing time can now be calculated again. However, this time the CTW is based on the drift angle, which is calculated as follows:

$$\theta_{drift} = \tan^{-1}\left(\frac{v_{c,y}}{STW}\right) \tag{3.57}$$

Subsequently, the CTW can be determined:

$$CTW_{(x_0,y_0)\to(x_1,y_1)} = \frac{COG_{(x_0,y_0)\to(x_1,y_0)}}{\cos\theta_{drift}} \tag{3.58}$$

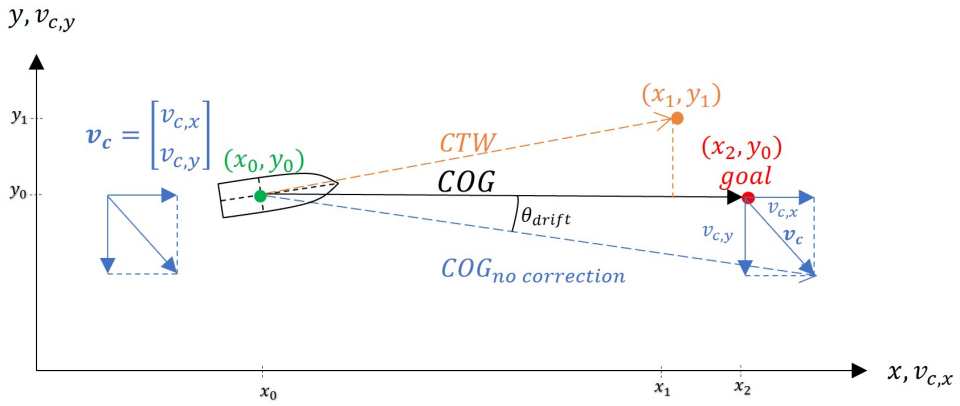

Figure 3.12: Scenario 3: sailing in x-direction, current has a perpendicular and parallel component

The third scenario can be seen in Figure 3.12, this time the vessel experiences a current with a parallel and perpendicular component with respect to the sailing direction. If the vessel sails with the STW and the initial sailing direction, ignoring the currents, it would follow to blue line and end up at a location which is not the desired goal. The drift angle to compensate for this deviation from the sailing direction is calculated as follows in this scenario:

$$\theta_{drift} = \tan^{-1}\left(\frac{v_{c,y}}{STW + v_{c,x}}\right) \tag{3.59}$$

the calculation for the CTW can be seen as a combination of scenario 1 and 2, and is determined with the following formula:

$$CTW_{(x_0,y_0)\to(x_1,y_1)} = \frac{COG_{(x_0,y_0)\to(x_2,y_0)}}{\cos\theta_{drift}} * \frac{STW}{STW + v_{c,x}} \tag{3.60}$$

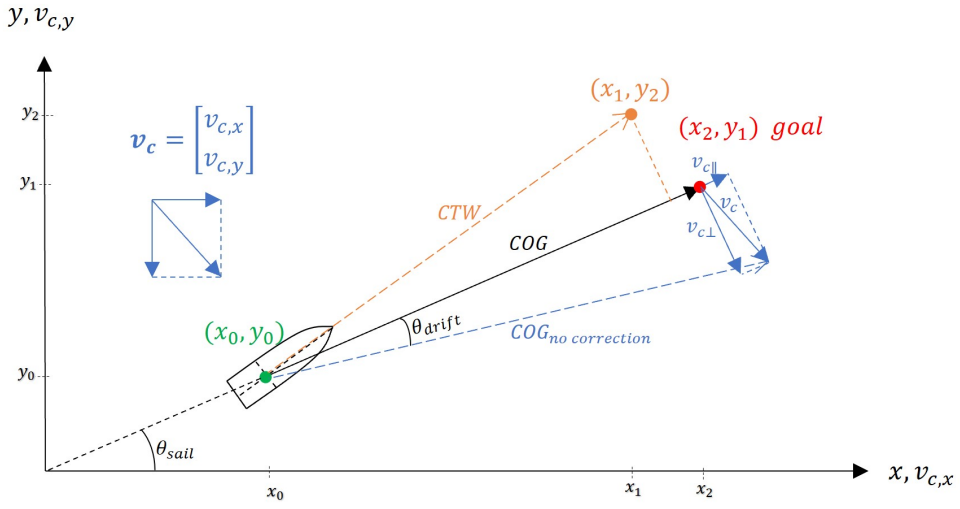

Figure 3.13: Scenario 4: Both the sailing direction and the current have a x- and y-component

The last scenario is depicted on Figure 3.13, where both the sailing direction and the current direction have a x- and y-component. This is the decomposition of components that is implemented in the python-based model, the energy consumption calculations are based on this kinematic diagram. This last scenario does not differ significantly from the third scenario, the main difference is that the current has to be projected on the sailing direction, i.e. the COG. This is done with the following formulae:

$$v_{c\perp} = v_{c,x} \cos\theta_{sail} + v_{c,y} \sin\theta_{sail} \tag{3.61}$$

$$v_{c\parallel} = -v_{c,x} \sin\theta_{sail} + v_{c,y} \cos\theta_{sail} \tag{3.62}$$

The formulae to calculate the drift angle and sailing time are derived by replacing $v_{c,x}$ and $v_{c,x}$ in equations 3.59 and 3.60 by $v_{c\parallel}$ and $v_{c\perp}$ respectively. This results in the equations that are utilized in the python-based model:

$$\theta_{drift} = \tan^{-1}\left(\frac{v_{c\perp}}{STW + v_{c\parallel}}\right) \tag{3.63}$$

$$CTW_{(x_0,y_0)\to(x_1,y_2)} = \frac{COG_{(x_0,y_0)\to(x_2,y_1)}}{\cos\theta_{drift}} * \frac{STW}{STW + v_{c\parallel}} \tag{3.64}$$

3.4.3 NSD diagram

On the following page, there is a diagram called NSD (Nassi-Schneiderman Diagram) which illustrates a Python class along with its different components. In subsection 3.4.4, a description of each individual component can be found.

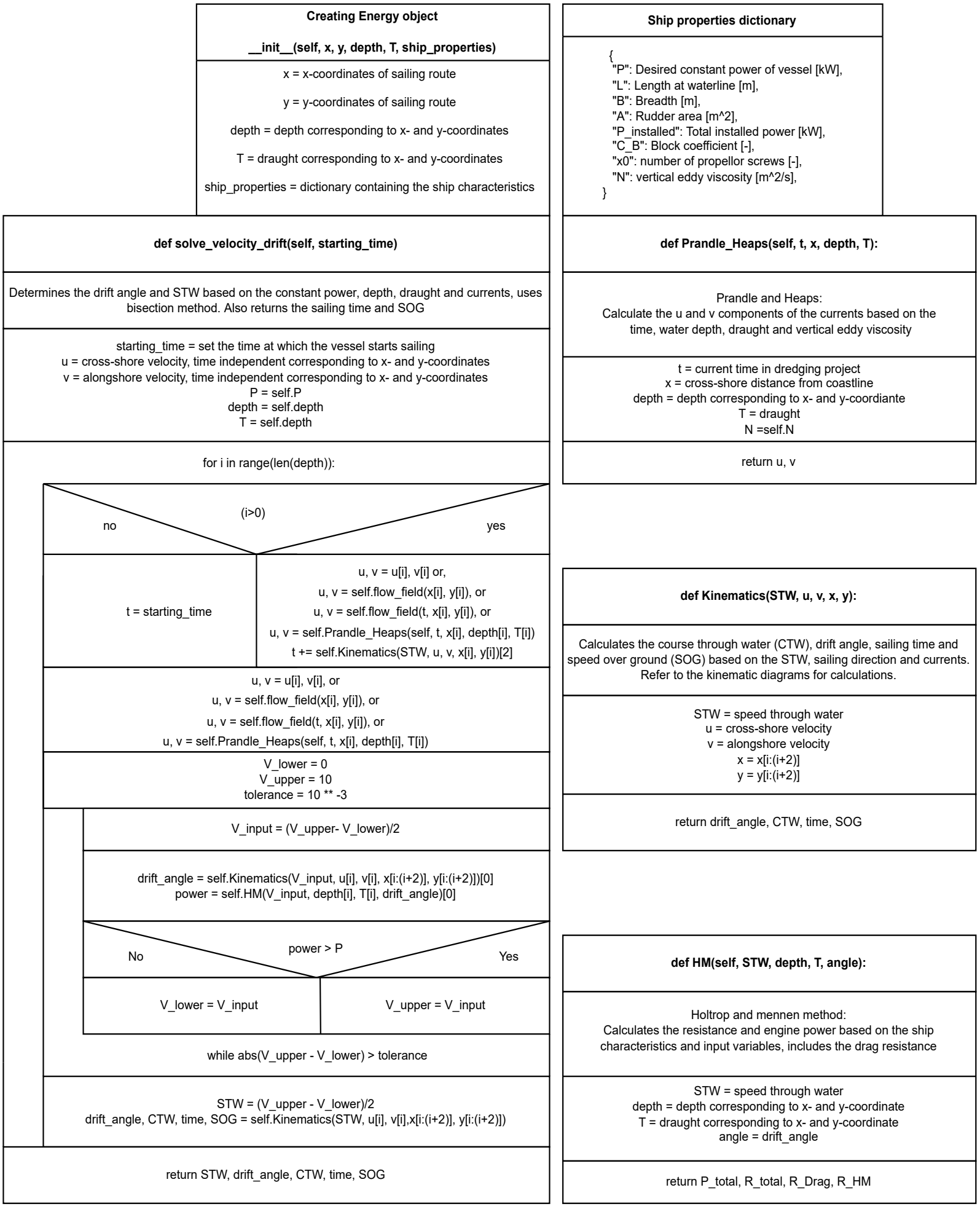

Figure 3.14: NSD: Python Class of energy calculation model

3.4.4 Class Methods

Initialize method

The initialize method, *__init__*, creates the class instance or object as desired by the user. The sailing path is defined with x- and y-coordinates with a corresponding depth and draught at those x- and y-coordinates. Additionally to the depth varying along the sailing route, the draught also varies depending on the dredging status. A dredging vessel has a larger draught when it is filled with dredged material, referred to as "sailing full", as opposed to when it is empty, referred to as "sailing empty". Moreover, the constant variables, which are inherent to the vessels characteristics, are defined in the "ship_properties" dictionary. The following parameters can be defined in this dictionary:

P = Desired constant power used to calculate the corresponding sailing speed $[kW]$

L = Length of the vessel at the waterline $[m]$

B = Breadth, or width, of vessel $[m]$

A = Area of the rudder $[m^2]$

$P_{installed}$ = The total installed engine power $[kW]$

C_B = Block coefficient of vessel $[-]$

$x0$ = Amount of propellers $[-]$

N = vertical eddy viscosity $[m^2/s]$

It is important to note, that the input arguments x, y, water depth and T (draught) have the same length, otherwise the model does not work. After defining all the mentioned parameters, an instance or object of the class is created. The other methods of the class can now be used to calculate the desired parameters.

Bisection method

The bisection method, defined as $solve\_velocity\_drift$, is the most important method in the class, it uses the other class methods to return the speed through water (STW), drift angle, time (sailing duration), speed over ground (SOG). The input arguments are the instance variables ($self$) and the time that the vessel starts sailing, i.e. sailing time. The bisection approach, as described in subsection 3.4.1, is implemented using a while loop that continues iterating until the tolerance is reached. This while loop is enclosed within a for loop that iterates over all the coordinates along the sailing path.

This for loop provides the flexibility for the user to customize the cross-shore and alongshore velocities, represented as u and v respectively, as per their preference. The user has the option

to choose from four types of current fields: constant, varying in space, varying in space and time, or the Prandle and Heaps flow field. To incorporate the first three options, the user should define and include them in the class using a class method called $flow\_field()$. In case the user does not specify the flow field, the model will automatically utilize the Prandle and Heaps velocities.

Subsequently, these velocities, in combination with the sailing direction and the first guess for the STW V_{input}, determine the first guess for the drift angle. Hereafter, the brake horse power P_b is determined with this calculated drift angle in combination with the estimated STW, depth and draught. The calculated brake horse power is then compared to the desired engine power as defined in the *ship_properties* dictionary, and the while loop keeps iterating until the absolute difference of V_{lower} and V_{upper} is smaller than the set tolerance. When this criterion is met, the STW is determined and used to calculate the drift angle, course through water (CTW), sailing time and speed over ground (SOG). This is done by means of the class methods $self.Kinematics()$, which is explained in the following subsection.

Kinematics method

The basis of this method is the kinematic diagrams presented in subsection 3.4.2. The input parameters required for this method are the ship's speed through water (STW), along with the coastal current's cross-shore and alongshore components denoted by u and v, respectively. Additionally, the method also requires the coordinates of the current position and the next position. To obtain a complete understanding of the equations utilized in this method, refer to subsection 3.4.2. The full set of equations in this class method are defined as follows:

$$COG = \sqrt{(x_1 - x_0)^2 + (y_1 - y_0)^2} \tag{3.65}$$

$$\theta_{sail} = \tan^{-1}\left(\frac{y_1 - y_0}{x_1 - x_0}\right) \tag{3.66}$$

$$v_{c\perp} = v_{c,x}\cos\theta_{sail} + v_{c,y}\sin\theta_{sail} \tag{3.67}$$

$$v_{c\parallel} = -v_{c,x}\sin\theta_{sail} + v_{c,y}\cos\theta_{sail} \tag{3.68}$$

$$\theta_{drift} = \tan^{-1}\left(\frac{v_{c\perp}}{STW + v_{c\parallel}}\right) \tag{3.69}$$

$$CTW_{(x_0,y_0)\to(x_1,y_2)} = \frac{COG_{(x_0,y_0)\to(x_2,y_1)}}{\cos\theta_{drift}} * \frac{STW}{STW + v_{c\parallel}} \tag{3.70}$$

$$t_{sailing} = \frac{CTW}{STW}\left(= \frac{COG}{SOG}\right) \tag{3.71}$$

$$SOG = \frac{COG}{t_{sailing}} \tag{3.72}$$

Holtrop and Mennen method

The principles of the Holtrop and Mennen method are already thoroughly explained in section 3.2, only the implementation in the energy calculation model will be explained here. As can be seen on the NSD diagram, it is chosen to use the Holtrop and Mennen method to return the total engine power, total resistance, drag resistance, and Holtrop and Mennen resistance. The Holtrop and Mennen resistance is defined as the total resistance without the modification for currents as explained in section 3.3. By comparing the Holtrop and Mennen resistance with the drag resistance on the rudder, the influence of currents on the total resistance can be determined. Furthermore, the drag resistance is calculated based on the rudder area A from the *ship_characteristics*, STW and drift angle as explained in subsection 3.3.1.

Prandle and Heaps method

The prandle and heaps method contains the elaborate and complex derivations for the vertical structure of the tidal-induced currents and residual density-driven flow. The model automatically utilizes this class method if a flow field is not defined, it is a built-in method in the class. The time that is calculated, based on the STW and CTW, is used to determine the phase of the velocity structure. As explained in chapter 2, the magnitudes of the cross-shore and alongshore components of the coastal currents oscillates with the tidal period. Furthermore, the marine currents reduce in magnitude towards the offshore direction due to spatial dependency of a Kelvin wave. This is implemented by multiplying the cross-shore and alongshore velocities with an exponential depending on the cross-shore distance x:

$$u_x = U * e^{x/50} \tag{3.73}$$

$$v_x = V * e^{x/50} \tag{3.74}$$

where:

U = absolute cross-shore velocity, space-independent$[m/s]$

V = absolute alongshore velocity, space-independent $[m/s]$

u_x = cross-shore velocity adjusted due to offshore distance $[m/s]$

v_x = alongshore velocity adjusted due to offshore distance $[m/s]$

x = cross-shore distance $[km]$

Note that the origin of the chosen Cartesian coordinate system is set at the coastline, the x value therefore is negative and decreasing in offshore direction.

Because the only part affecting the dredging vessel is from the bottom of the vessel up until the water surface, the marine current components u_x and v_x should only be considered on this vertical length scale. It is chosen to integrate the cross-shore and alongshore velocities over this length scale, this is done as follows:

$$u = \int_{-T}^{\eta} u_x dz \tag{3.75}$$

$$v = \int_{-T}^{\eta} v_x dz \tag{3.76}$$

where:

T = draught of the vessel $[m]$

η = elevation of the water surface above its undisturbed level $[m]$

These are the cross-shore and alongshore marine current components that will be used in the calculation of the of the bisection method, note that every new coordinate contains new values for u and v due to the time- and space dependency of this continuous flow field and the varying draught and surface water level.

Chapter 4

Model Implementation and Results

This chapter presents the results obtained with the model explained in chapter 3, it is divided in three parts, namely the verification, validation and the sustainable dredging strategy. Various test cases are presented in section 4.1 aiming to verify expected results. The purpose of these test cases is to gain insight into the effect of the various parameters, such as the currents, water depth and draught, on the energy consumption of the dredging vessel. The model is validated using in-house databases of Van Oord in combination with coastal currents data from Rijkswaterstaat, this is presented in section 4.2. Lastly, this chapter presents the sustainable dredging strategy that is explored in section 4.3, namely harnessing the cross-shore currents to reduce energy consumption for a fictitious sand nourishment project.

4.1 Model Verification

This subsection consists of the various test cases that are done to verify the model, these are summarized in the test case matrix in Table 4.1. Note that the water depth, draught, engine power and flow field are denoted as D, T, P and V respectively. The first test case serves as the reference case, whereas the vessel is sailing through a water column with a constant water depth and draught. Test case 2 until 4 do not include the currents, they aim to verify the model for the original Holtrop and Mennen method. in Test case 5 the water depth, draught and engine power are kept constant, but this time a flow field is added in the form of a constant current. Different simulations are conducted in which the current is allowed to rotate, this is done to study the effect of the direction of the current on the different parameters such as the resistance, SOG (speed over ground) and energy consumption. Lastly, test case 6 uses the Prandle and Heaps flow field to study the results of the model when using a space and time varying vertical velocity structure. For this test case the starting time of when the dredging vessel starts sailing is varied, corresponding to different vertical velocity structures as the shape depends on the time.

Table 4.1: Test case matrix

Test case	Varying Variables	Constant Variables	Not Included
1	-	D, T, P	V
2	D	T, P	V
3	T	D, P	V
4	P	D, T	V
5	-	D, T, V, P, V	-
6	V (PH)	D, T, P	-

Figure 4.1 illustrates the plan view of the test cases and its corresponding Cartesian coordinate system. The cross-shore direction corresponds with the x-coordinates, with positive direction indicating onshore and negative direction indicating offshore. The cross-shore current is defined as u $[m/s]$. Moreover, the alongshore direction corresponds with the y-coordinates, with positive direction indicating northward and negative direction indicating southward. The alongshore current is defined as v [m/s].

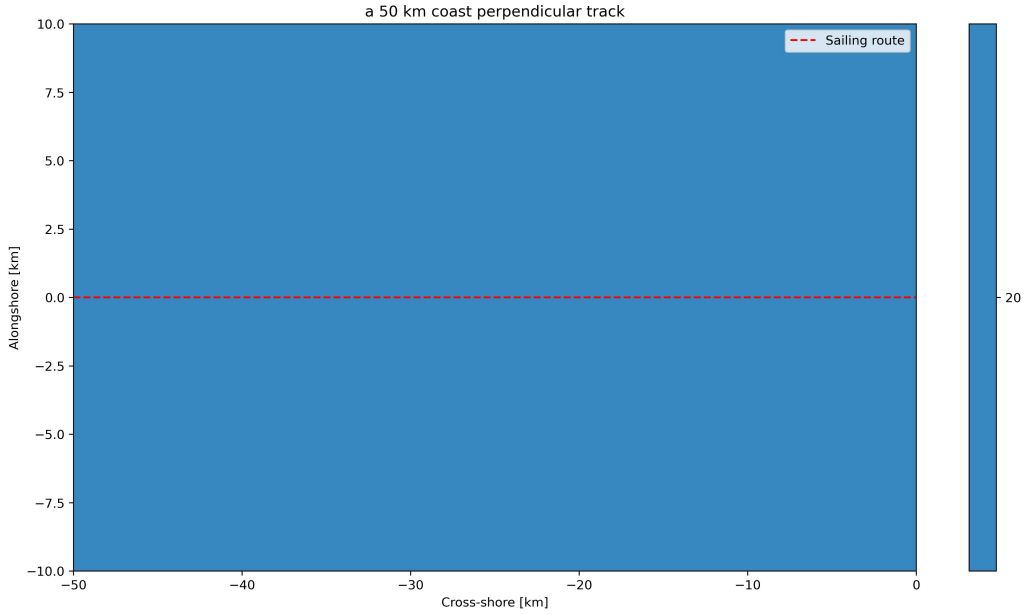

Figure 4.1: Plan view of reference case

Table 4.2 shows the values that are used in the ship characteristics dictionary during the verification by means of the various test cases. The values for the various parameters are based on the Vox Olympia, which is a dredging vessel owned by Van Oord. This is done because this vessel also made it possible to validate the model with actual on-board data measurements which is presented in section 4.2.

Parameter	**Value**	**Unit**
P_b	3000	$[kW]$
L	95.57	$[m]$
B	19.93	$[m]$
A	10	$[m^2]$
$P_{installed}$	6542	$[kW]$
C_B	0.85	[-]
x_0	1	[-]
N	0.0028	$[m^2/s]$

Table 4.2: Values used in the ship characteristics dictionary, based on the Vox Olympia

4.1.1 Test Case 1-4

The different input values for the water depth, draught and engine power for these test cases are summarized in Table 4.3. The total energy consumption and sailing duration for the different simulations are presented in Table 4.4. In Figure 4.2 the results for the first four test cases can be seen, the main outcomes are discussed.

Test Case	D	T	P_b
1	20 m	5 m	3000 kW
2	Linear decrease: 20 m till 8 m	5 m	3000 kW
3.1	20 m	Linear decrease: 5 m till 1 m	3000 kW
3.1	20 m	Linear increase: 5 m till 9 m	3000 kW
4.1	20 m	5 m	2500 kW
4.2	20 m	5 m	3500 kW

Table 4.3: Input values for test cases 1-4

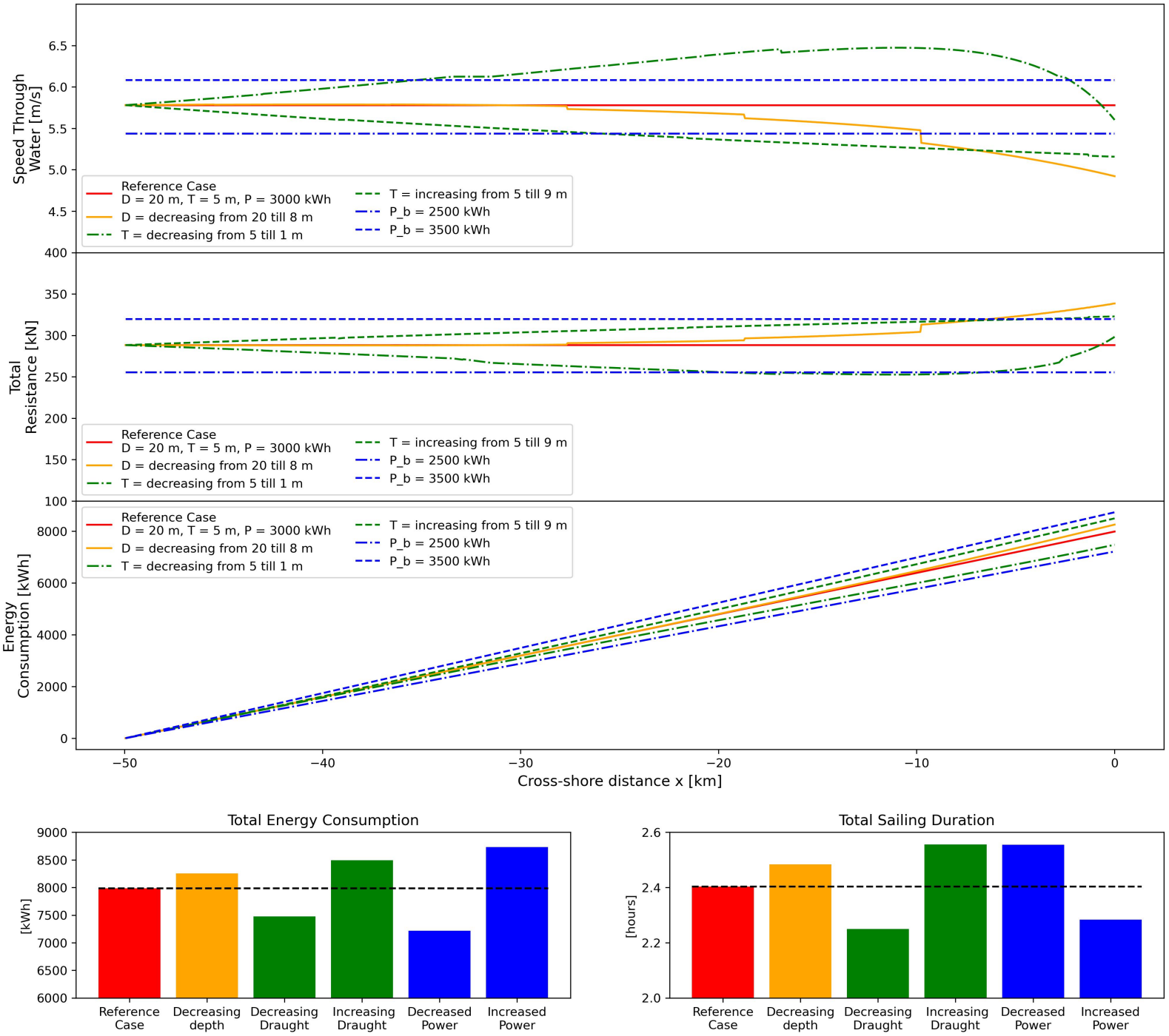

Figure 4.2: Test cases 1-4: respectively the reference case, varying the water depth D, varying the draught T and varying the engine power P_b

Test Case	Total Energy Consumption	Total Sailing Duration
1	7987.14 kWh	2.40 hours
2	8255.54 kWh	2.48 hours
3.1	7476.88 kWh	2.25 hours
3.2	8495.79 kWh	2.56 hours
4.1	7215.02 kWh	2.56 hours
4.2	8731.06 kWh	2.28 hours

Table 4.4: Total energy consumption and sailing duration for test case 1-4

Test case 1: Reference case

The first test case is the reference case, the water D, draught T and engine power P_b are constant, currents are not concluded. The results are plotted on the graphs in Figure 4.2, depicting the STW (speed through water), total resistance and total cumulative energy consumption during the sailing path. It can be seen that for the reference case, the STW and corresponding total resistance are constant. This is expected because the input arguments for the python-based model are also kept constant.

Test case 2: Varying water depth D

The results of the second test case are presented in Figure 4.2, in this scenario the water depth D decreases linearly from 20 m to 8 meter as the vessel sails through the water column. As expected, the total resistance increases when the vessel approaches shallower water, this corresponds to a decrease in STW over water. When compared to test case 1, the total sailing duration and therefore total energy consumption are slightly higher due to the influence of the bottom. What is important to note, is the discontinuity in the solution which is caused by the Karpov (Rotteveel, 2013) modification. Karpov made a modification that takes into account the shallow water effect on the wave-making resistance, which is based on the ratio of D/T and the Froude number. This alters the wave-making resistance with a factor that is determined with a sixth order polynomial, depending on the combination of the D/T ratio and Froude number (see Appendix B). It is chosen to not include a simulation in which the water depth is increased, this is left out because the outcomes were identical to the reference case. This is because the bottom only starts affecting the total resistance when the vessels enter the shallow water region. In the current simulation for test case 2 this region is reached at $x \approx -28$ km, where the STW and resistance start to deviate from the reference case.

Test case 3: Varying draught T

In the third test case, the effect of a varying draught T is studied. This is done for two simulations, one simulation in which the draught increases compared to the reference case draught, and a second simulation in which the draught decreases compared to the reference case draught. The results are plotted in graphs and can be seen in Figure 4.2.

The first simulation in which the draught is reduced initially leads to a decrease in the total resistance, primarily due to the decrease in wetted surface area, which results in a decrease in the frictional resistance. However, as the draught continues to decrease and reaches a very small value, the total resistance starts increasing again. Although this might seem counter-intuitive, it can be explained by examining the various components of the resistance obtained using the Holtrop and Mennen (1982) method. Generally, a decrease in draught results in an increase in wave-making resistance and a decrease in frictional resistance. However, for a very small draught, the wave-making resistance increases exponentially, leading to an overall increase in the total resistance. In this case, the decrease in the frictional resistance is not sufficient to offset the significant increase in wave-making resistance. Overall, the decreasing draught results in an increased speed through water when compared to the reference case, and thus has a lower total energy consumption and sailing duration.

The second simulation addresses an increasing draught during the sailing activity. The results show that as the draught increases, the total resistance also increases and the corresponding STW water decreases. This is expected because an increasing draught results in an increase of the wetted surface area and therefore frictional resistance component in the Holtrop and Mennen (1982) method. The total energy consumption and sailing duration are larger than the reference case due to this increased draught.

Test case 4: Varying engine power P_b

The fourth test case investigates the effect of varying the engine power P_b, while keeping the draught T and water depth D constant. The results are displayed in Figure 4.2. The first simulation decreases the engine power to 2500 kW during the whole sailing route, it can be seen that the both corresponding total resistance experienced by the vessel and the STW are decreased in this scenario. When studying the absolute difference in the bar diagram, the total sailing duration is increased but the total energy consumption is decreased quite significantly.

The second simulation shows the opposite, a higher engine power results in an increase in the STW, which leads to a reduced total sailing duration. However, the increased engine power also results in a larger total energy consumption during the entire sailing activity. Apparently, for this scenario and the specific used values for the draught and water depth, the increased energy consumption due to the increased engine power outweighs the decrease of the total energy consumption due to the decreased total sailing duration.

4.1.2 Test Case 5

The fifth test case includes a constant flow field in which the dredging vessel sails, aiming to verify the theory explained in subsection 3.4.2. The fictitious sailing route is identical to the one presented in Figure 4.1. Various simulation are conducted in which the direction of the current is varied, while the magnitude is kept constant at 1 m/s. The direction of the current rotates from 0°, which aligns with the offshore direction, towards 180°, which is in the onshore direction. This corresponds respectively with an adverse current and a favourable current. The intervals in which the current is allowed to rotate is 30°. The results are illustrated in Figure 4.3, the primary findings are discussed here. Table 4.5 presents the total energy consumption and total sailing duration for the different directions of the current.

Current angle	Total Energy Consumption	Total Sailing Duration
No currents	7987.14 kWh	2.40 hours
0°	9658.19 kWh	2.91 hours
30°	9540.34 kWh	2.87 hours
60°	9019.84 kWh	2.71 hours
90°	8248.36 kWh	2.48 hours
120°	7509.25 kWh	2.26 hours
150°	7002.81 kWh	2.11 hours
180°	6809.04 kWh	2.05 hours

Table 4.5: Total energy consumption and sailing duration for test case 5

Current parallel to sailing direction

The results obtained with the python-based model agree with the theory explained in subsection 3.4.2, which stated that a current parallel to the sailing direction solely effects the sailing time and not the resistance experienced by the vessel. The vessel sails in onshore direction (see plan view on Figure 4.1), a current parallel to this direction is therefore cross-shore. The magnitude of the current that is solely parallel to the sailing direction has the values of -1 m/s and 1 m/s, respectively corresponding to an angle of 0° and 180°. The results show that the drift angle is zero, this is of course because the vessel does not have to compensate for a deviation direction. Because the drift angle is zero, the drag resistance is also zero and the total resistance is equal to the resistance for the case without currents. The STW (speed through water) is therefore also equal to the STW for the case without currents. However, what can be seen is the difference between the STW and the SOG. As the currents corresponding to 0° and 180° have the largest parallel component, the deviation between the STW and SOG is the largest and exactly 1 m/s. This results in the largest deviation of the total energy consumption when compared to the reference case without currents.

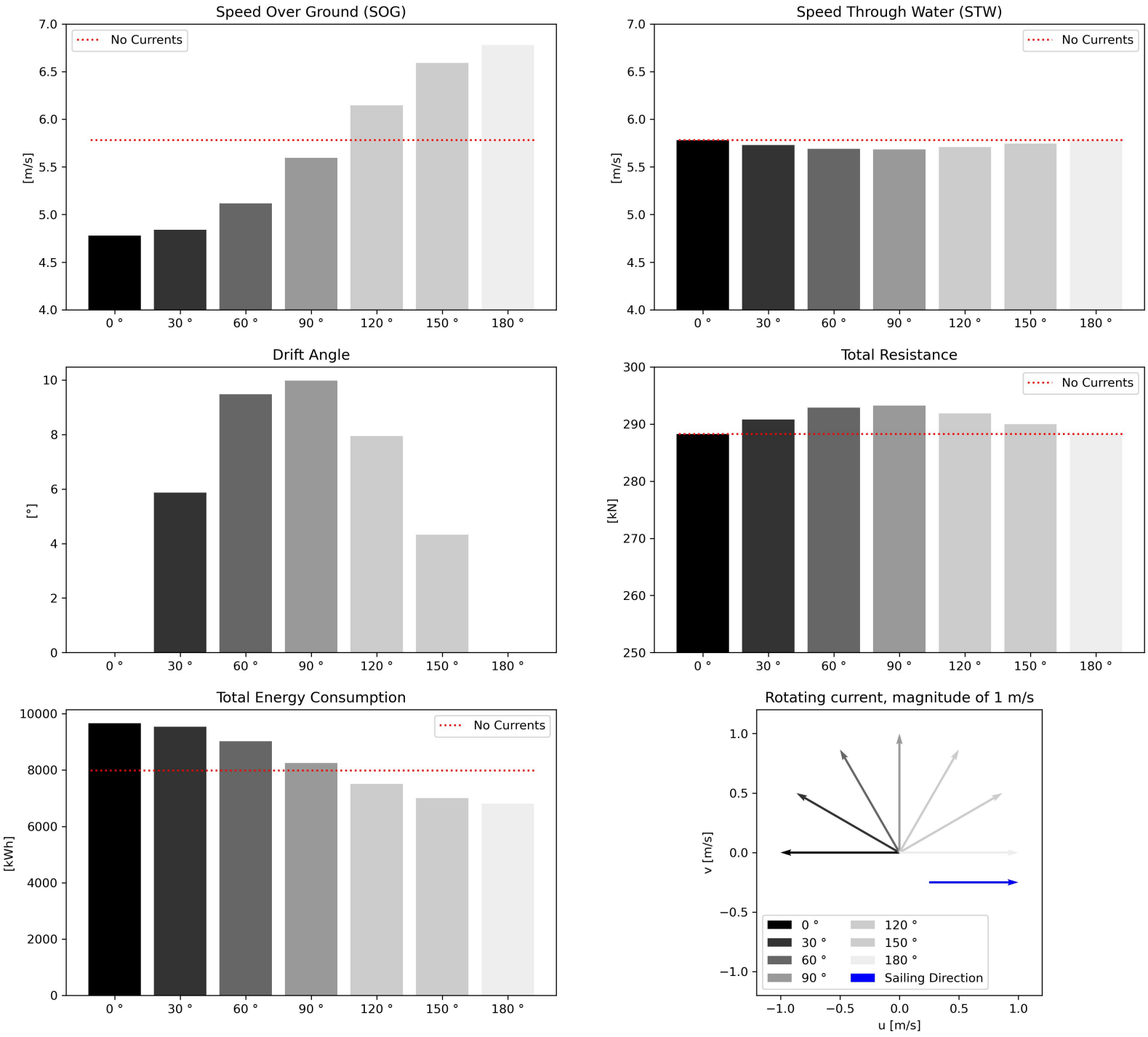

Figure 4.3: Test case 5: varying space- and time independent currents

Current perpendicular to sailing direction

The simulation in which the current has an angle of 90° aims to verify the effects of a current that is perpendicular to the sailing direction. A perpendicular current attempts to push the vessel of its intended path, the rudder is used to adjust the vessel's heading to compensate for this deviation. Figure 4.3 shows that the drift angle is the largest for this current direction, this is because the perpendicular component of the current is the largest in this scenario. This results in an additional drag resistance on the rudder and therefore an increased total resistance when compared to the case without currents. This added resistance results in a lower STW. Because the course through water (CTW) is longer than the course over ground (COG) in this scenario, the SOG corresponding to this shorter COG should be lower than the STW as well (see Equation 3.71). Moreover, the total energy consumption is larger than the total energy consumption of the case without currents due to the increased total sailing duration and constant engine power P_b.

Current with a parallel and perpendicular component

The simulations where the currents have angles of 30°, 60°, 120° and 150° consist of both a perpendicular and parallel component with respect to the sailing direction. According to the theory explained in subsection 3.4.2, the combination of the parallel and perpendicular component determines the magnitude of the drift angle and therefore the increased drag resistance. In general, as the perpendicular component of the current increases, the drift angle increases as well. The influence of the parallel component on the drift angle can be seen when for instance comparing the results of a current of 30° and 150°. Both simulations have the same magnitude for the perpendicular component, however, the drift angle is smaller for a current that has a favourable parallel component. The influence of the parallel component, if a perpendicular component exists, can be seen in Equation 3.69. For identical perpendicular magnitudes, an increasing favourable parallel component decreases the drift angle.

4.1.3 Test Case 6

The last test case includes the Prandle and Heaps stratified coastal currents utilizing the class method previously explained in 3.4.4. It is chosen to keep the vertical velocity structure independent of space during this verification, this is done in order to enhance the comprehensibility of the outcomes. However, keep in mind that in reality the currents magnitudes decay in offshore direction. This test case is split up in four simulations, where the vessel starts sailing at $t_0 = 0$, $t_0 = 0.25\text{T}$, $t_0 = 0.50\text{T}$ and $t_0 = 0.75\text{T}$. The total energy consumption and sailing duration for these simulations are presented in Table 4.6. The results for the four simulations are presented in Figure 4.4. Note that SOG (speed over ground) and total resistance are plotted along with its corresponding cross-shore distance x on the x-axis, while the current magnitudes are plotted against time expressed in the tidal period T on the y-axis. The colored arrows in the graph with the surface current components correspond to experienced currents during the sailing route of the different starting times. Additionally, a time-distance diagram is included for a clearer visual representation of the varying starting times.

Starting time	Total Energy Consumption	Total Sailing Duration
$t_0 = 0$	7896.24 kWh	2.38 hours
$t_0 = 0.25\text{T}$	7736.08 kWh	2.33 hours
$t_0 = 0.50\text{T}$	8348.65 kWh	2.51 hours
$t_0 = 0.75\text{T}$	8431.31 kWh	2.53 hours

Table 4.6: Total energy consumption and sailing duration for test case 5

Simulation 1: $t_0 = 0$

At the initial time point $t_0 = 0$, the cross-shore component of the velocity is zero, while the alongshore component reaches its peak value of approximately $0.7\ m/s$. These values correspond respectively to the components parallel and perpendicular to the direction of sailing. Then as the vessel starts sailing and time progresses, the cross-shore component of the current grows more favourable and the alongshore component decreases. As the alongshore, or perpendicular, component decreases, the total resistance experienced by the sailing vessel decreases. The combination of the decreasing total resistance and increasing favourable current causes the speed over ground to increase as the vessel is sailing. These effects can both be seen in the top two graphs.

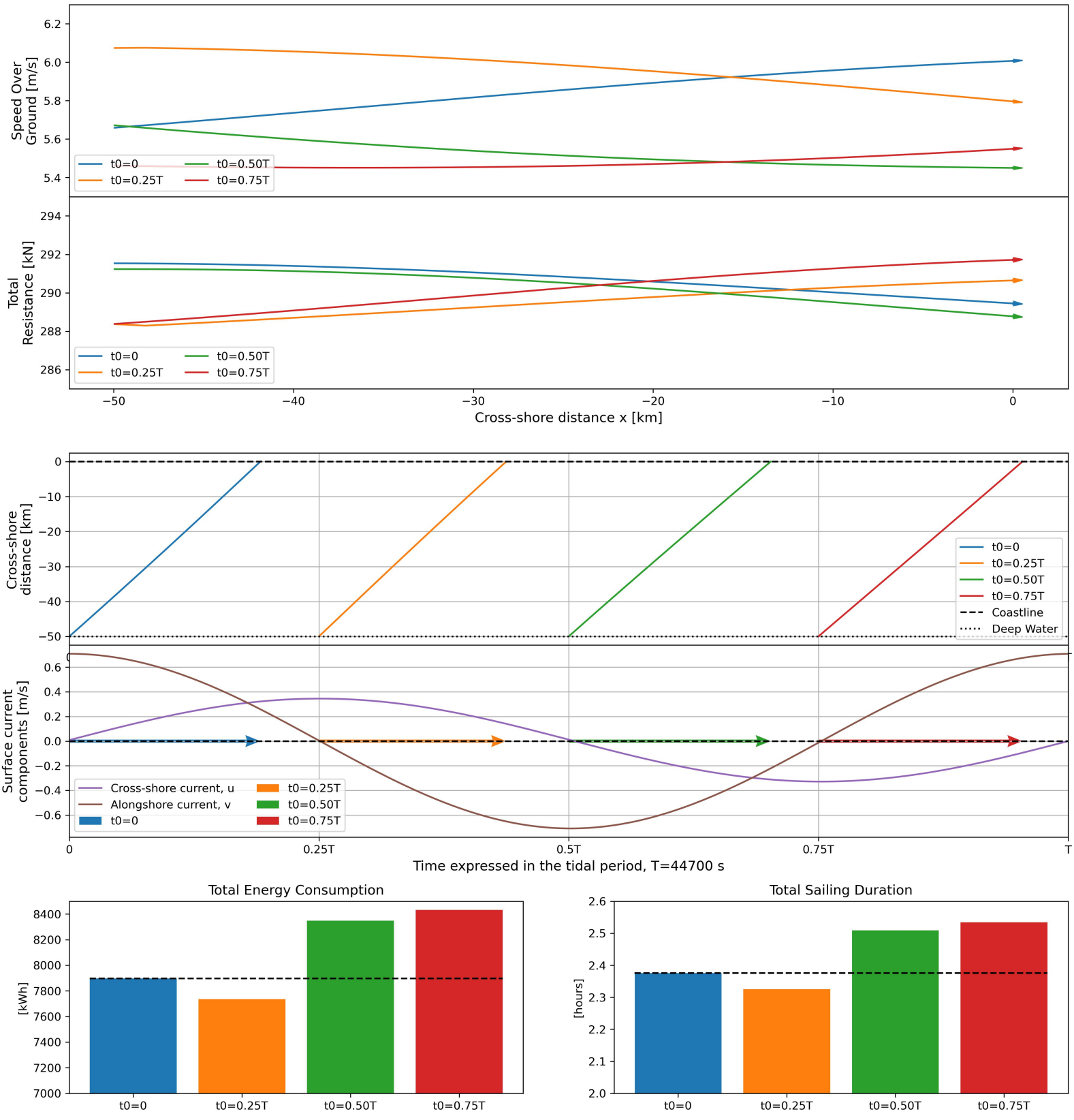

Figure 4.4: Test case 6: Prandle and Heaps flow field, varying the starting time

Simulation 2: $t_0 = 0.25T$

In the scenario that the vessel starts sailing at t_0 = 025T, the total energy consumption and total sailing duration are decreased when compared to the scenario in which the vessel starts sailing at $t_0 = 0$. This can be seen in the bar diagrams in Figure 4.4. It will again be explained by studying the currents experienced by the dredging vessel during sailing. Precisely at t_0 = 0.25T, an optimal combination of surface current components arises, characterized by a highly favourable maximum parallel component and the absence of a perpendicular component that would otherwise increase the total resistance. Consequently, at a cross-shore distance of x = -50 km, Simulation 2 exhibits a noticeably higher speed over ground (SOG) and reduced total resistance in comparison to Simulation 1. As the vessel sails and time progresses, the cross-shore current becomes less favourable and the alongshore component increases again. This causes that, towards the shore, the SOG decreases and the total resistance increases.

Simulation 3: $t_0 = 0.50T$

In simulation 3, the vessel starts sailing half a tidal period later than simulation 1, at t_0 = 0.50T. Upon examination of the surface current components, it can be seen that the initial cross-shore component exactly at t_0 = 0.50T is the same as at $t_0 = 0$. The initial magnitude of the alongshore component is also approximately the same, however southwards as opposed to northwards in simulation 1. Because only the magnitude of the alongshore component determines the additional drag resistance on the rudder, and the cross-shore component is identical, the initial SOG and total resistance of simulation 1 and 3 are similar. This time, however, the cross-shore component grows in the adverse direction as the vessel starts sailing. As the total resistance decreases during sailing, due to the decreasing magnitude of the alongshore component, the SOG actually decreases as well due to the parallel current growing larger in adverse direction. This results in a significantly larger total energy consumption and sailing duration when compared to simulation 1.

Simulation 4: $t_0 = 0.75T$

The last simulation is when the dredging vessel starts sailing at t_0 = 0.75T. In this scenario the cross-shore component of the current, i.e. parallel component, is at its maximum in adverse direction. This causes the speed over ground at the moment the vessel starts sailing to be the lowest. The initial alongshore component is zero, which results in a lower total resistance when compared to simulation 1 and 3. The effect of the lower total resistance on the SOG is outweighed by the adverse cross-shore current which decreases the SOG. As the vessel sails and time progresses, the alongshore current and therefore total resistance increases and the cross-shore current grows towards the favourable direction. The SOG can be seen to increase slightly during sailing, the parallel component apparently has a larger influence on the SOG than the alongshore component in this scenario.

4.2 Model Validation

The model is validated using actual measurements from the Vessellog database, which is owned by Van Oord and contains data on various ship parameters such as engine power, sailing speed, water depth, location and time. These measurements are obtained using on-board sensors and GPS tracking. However, the vessel does not measure information on the coastal currents, which is why additional measurements from Rijkswaterstaat are also used. Rijkswaterstaat has installed current measuring poles in the North Sea, this data is publicly accessible and is utilized for the validation. A combination of the Vessellog and Rijkswaterstaat data is used to conduct ten simulations, consisting of ten free sailing activities, to evaluate the model's performance and accuracy.

The focus of this research is on the free sailing part, with acceleration and deceleration being excluded from the scope. To ensure accurate validation of the Python-based model, it is essential to identify the part where the vessel is free sailing. The free sailing part is defined as the period during which the vessel maintains a stationary condition, and this criterion is crucial for the effective use of data in validating the Python-based model. The following criteria are used to identify the free sailing part:

1. Constant sailing speed
2. Constant Engine Power
3. Constant Pitch
4. Constant Thrust

The constant sailing speed is used to confirm that the vessel is not accelerating or decelerating. The python-based model is developed to take as input the constant engine power, therefore a constant engine power should be visible in the Vessellog data. Additionally, two more checks are performed to ensure the stationary condition. The first check is for thrust, which measures the force induced by the rotating propeller. If the thrust is not constant, it indicates that the ship is accelerating or decelerating, as the fluctuation in force is related to changes in sailing speed. The final check is for the pitch, which is the angle of the blades on the propeller. For the thrust to remain constant, the pitch must be maintained at a constant angle. An additional check is done by comparing the effective power and the engine power, where the effective power is generally around $60 - 70\%$ of the engine power.

5. $P_{\text{effective}} \approx$ (0.6-0.7) P_{engine}

An example of how the validation criteria are checked is given in Figure 4.5. The grey shaded area depicts the time interval in which the vessel is considered to be free sailing, the corresponding Vessellog and Rijkswaterstaat data during this interval is utilized in the validation.

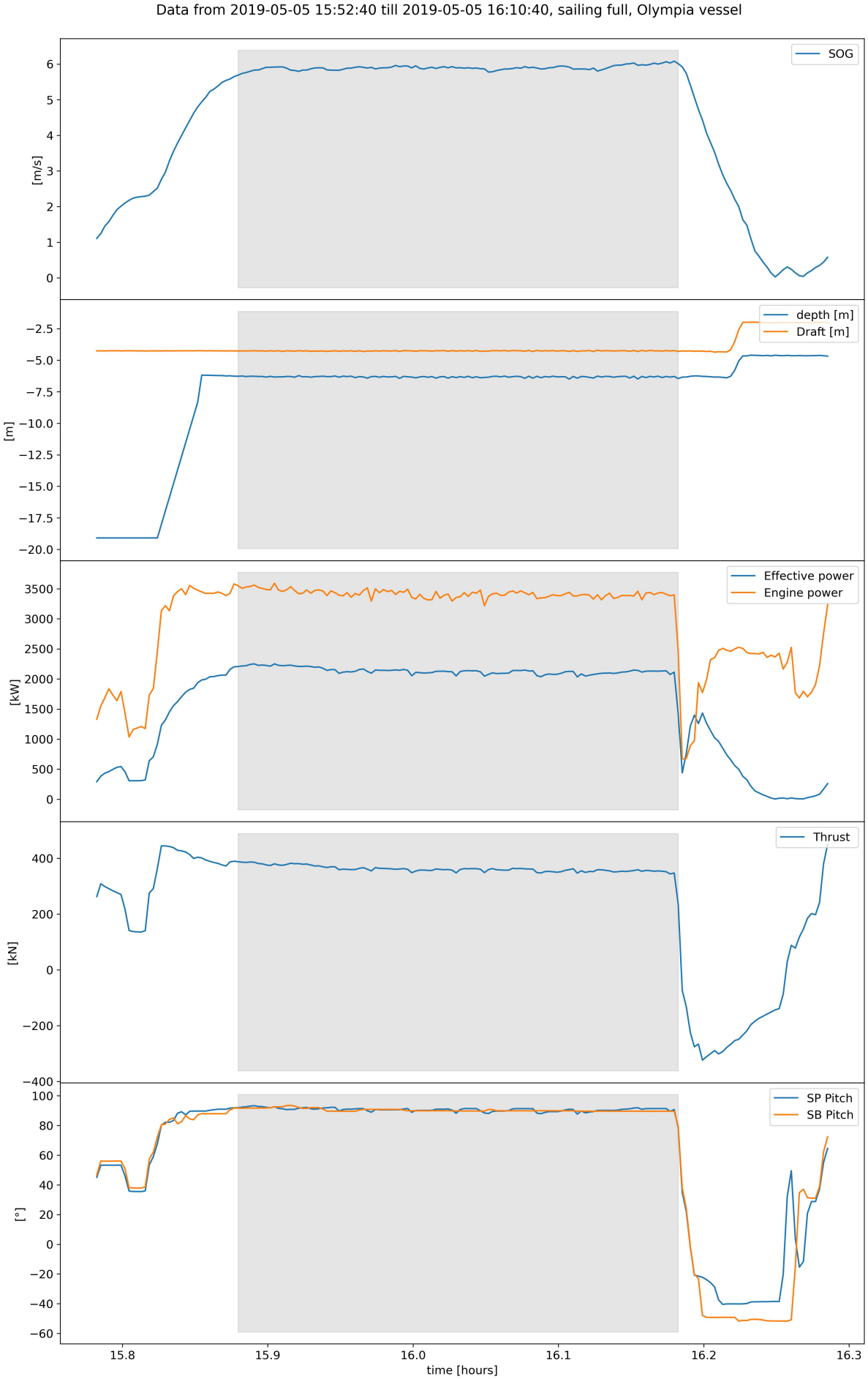

Figure 4.5: Validation criteria check for Vessellog data. The dredging vessel sails from the deep dredged channel to shallows next to the channel.

Project IJgeul

Due to the fact that the validation process uses data from a current measuring pole owned by Rijkswaterstaat, the number of projects that can be used to validate the model is limited to those that are in close proximity to the measuring pole. The only project that has been identified with both proximity to the measuring pole and valid on-board data, is a dredging project in the Ijgeul (sea access) that was carried out in 2019 by the vessel named Volvox Olympia. This project had a total duration of 5 days. The location of the Rijkswaterstaat measuring pole and the approximate route taken by the Volvox Olympia during the project are shown in Figure 4.6. The white part of the line represents the sailing path for which the Volvox Olympia is accelerating or decelerating, whereas the red segment is the free sailing path. The vessel traveled back and forth in the sea access, transporting the dredged material from the sea access to deeper water. It should be noted that the exact sailing path as measured with the GPS tracking system will be utilized in the validation process, not the approximate sailing path as shown here.

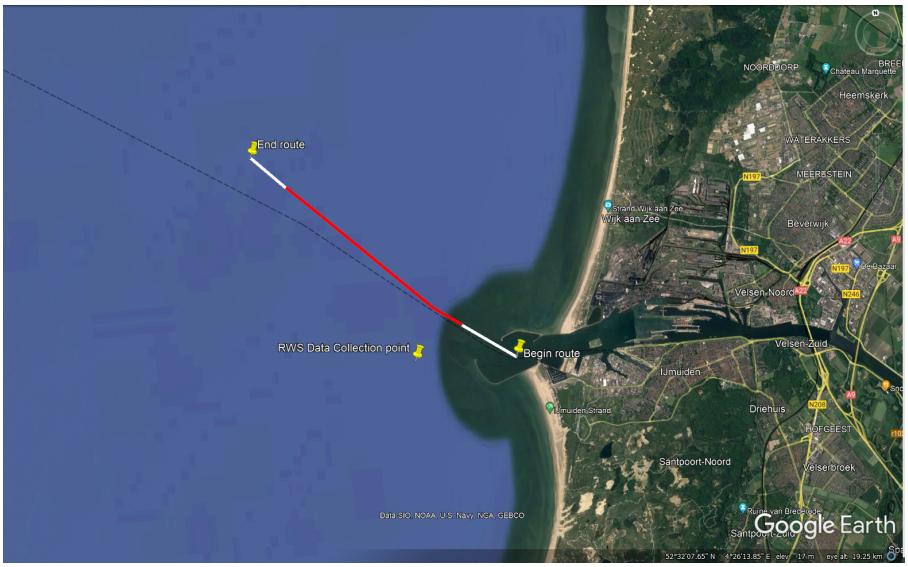

Figure 4.6: Ijmuiden sea access, RWS measuring pole and the Volvox Olympia sailing route. The white segment of the path indicates the acceleration/decelaration part, the red segment of the path indicates the free sailing part. (Source: Google Earth Pro. [Screenshots]. Retrieved from https://www.google.com/earth/versions/earth-pro, 06-05-2023)

Data

The data measured by Rijkswaterstaat consists of the direction (with respect to true North) and the magnitude which can be used to obtain the longitudinal and latitudinal components of the current, respectively the x- and y components. The Vessellog database contains numerous parameters that can be utilized in the validation. Table 4.7 shows an overview of the data that is used to validate the model.

Table 4.7: Validation parameters

Parameter	Unit	Database
Current direction	[°]	RWS
Current magnitude	$[m/s]$	RWS
Time	[Timestamp]	RWS and Vessellog
Easting	[cm]	Vessellog
Northing	[cm]	Vessellog
Engine power	[kW]	Vessellog
Vessel SOG	$[m/s]$	Vessellog
Water depth	[m]	Vessellog
Draught	[m]	Vessellog
Thrust	[kN]	Vessellog
Pitch	[°]	Vessellog

It is important to note that the measuring frequency of Rijkswaterstaat is 10 minutes, while Vessellog has a much higher frequency. To reduce the file size of the measured data, Vessellog uses the Ramer-Douglas-Peucker algorithm for data reduction. However, the filtered data frequency is still of the order of 10 seconds. It is therefore chosen to utilize a linear interpolation on the data of Rijkswaterstaat to get a first order estimate of the current magnitudes during the time intervals between the measuring points.

Validation procedure

The validation process is done by comparing the SOG (speed over ground) calculated with the python-based model, and the SOG as measured by the GPS tracking system on-board of the Volvox Olympia. The input parameters for the python-based model are the measured x- and y-coordinates with their corresponding water depth and draught, in combination with the measured engine power delivered during the free sailing activity. To include the coastal currents, the data from the Rijkwaterstaat current measuring pole are used. Note that in this validation, the currents are considered to have the measured magnitude and direction along the sailing route, whereas in reality they are measured in a constant point in space (see Figure 4.6).

To emphasize the impact of currents on the model, a differentiation is made between two simulations: one that includes the currents, and one that does not include the currents.

Ten simulations are carried out in which the SOG from the GPS tracking system, SOG from model excluding currents and SOG from model including currents are compared. These simulations address sailing activities where the stationary condition requirements are met and the required data for the python-based model is available in both Vessellog and Rijkswaterstaat. Vessellog contains a parameter in which the sailing activities are logged, these activities define the state of the vessel. These states are; unknown, sailing empty, dredging, sailing full, dumping and reclaim. A typical dredging cycle is presented in Figure 4.7.

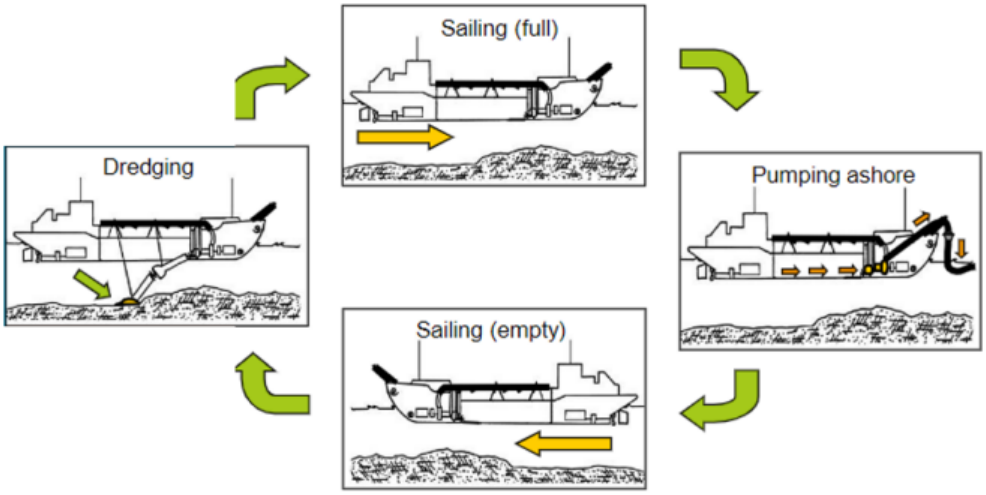

Figure 4.7: Four stages of a typical dredging cycle; dredging, sailing full, dumping (pumping ashore) and sailing empty. (Lamers, 2022)

Because the validation is done for a free sailing dredging vessel, only the sailing empty and sailing full states are relevant. The energy consumption during dredging, dumping and reclaiming are outside of the scope of the present study. After analysing the Vessellog data, it has been concluded that the data during the sailing empty state is not suitable for validation of the python-based model. Both the sailing speed over ground (SOG) and the engine power, obtained from Vessellog, illustrate fluctuations. The stationary condition criteria are not met for the sailing empty state during the total project duration. The validation is therefore only done for the sailing full state. The total project duration consists of approximately 50 cycles during its five days, of which 10 cycles contain a sailing full activity that meets the stationary condition criteria and has data available from both Vessellog and Rijkswaterstaat to validate the python-based model. These 10 sailing full activities are validated with the python-based model.

4.2.1 Results

The initial model calculations revealed that the estimated speed over ground (SOG) was consistently lower than the measured values obtained from Vessellogs. This applies to both the model calculations, where one includes the coastal currents and one does not include the coastal currents. To address this underestimation, a correction factor was introduced to minimize the margin of error between the calculated and measured SOG. Due to the consistent underestimation, the correction factor simply raises the model's results by 6%. By implementing this correction factor, the error in the SOG calculations when accounting for the coastal currents are reduced to less than 5.5%. The results of the model are compared by means of the relative root mean square error ($RMSE_{rel}$). This is done for both the case where the currents are included and excluded, and for including and excluding the correction factor. The $RMSE$ and $RMSE_{rel}$ are calculated as follows:

$$RMSE_{rel} = \frac{RMSE}{V_{avg}} \cdot 100\% \tag{4.1}$$

$$RMSE = \sqrt{\frac{\sum_{i=1}^{N} \left(\text{Model}_i - \text{Actual}_i\right)^2}{N}} \tag{4.2}$$

where:

$RMSE$: root mean square error $[-]$

V_{avg} : Average measured SOG, Vessellog $[m/s]$

$Actual$: SOG, obtained from Vessellog $[m/s]$

$Model$: SOG, calculated by python-based model $[m/s]$

N : Amount of timesteps in Vessellog data $[-]$

Figure 4.8: (on the following page) 1 out of 10 validations, consisting of 1 sailing full activity. Comparison of the SOG (speed over ground) resulting from the python-based model, including and excluding currents, and the measured SOG from Vessellog (a), the measured water depth D and draught T (b) and the measured effective power P_e and brake horse power P_b (c). The grey shaded areas in (a), (b) and (c) depict the region in which the criteria for free sailing is met. The model outcomes for each increment along the sailing route are presented in a scatter plot, along with the ideal fit (d). The path of the sailing route with the corresponding interpolated time-varying currents (e).

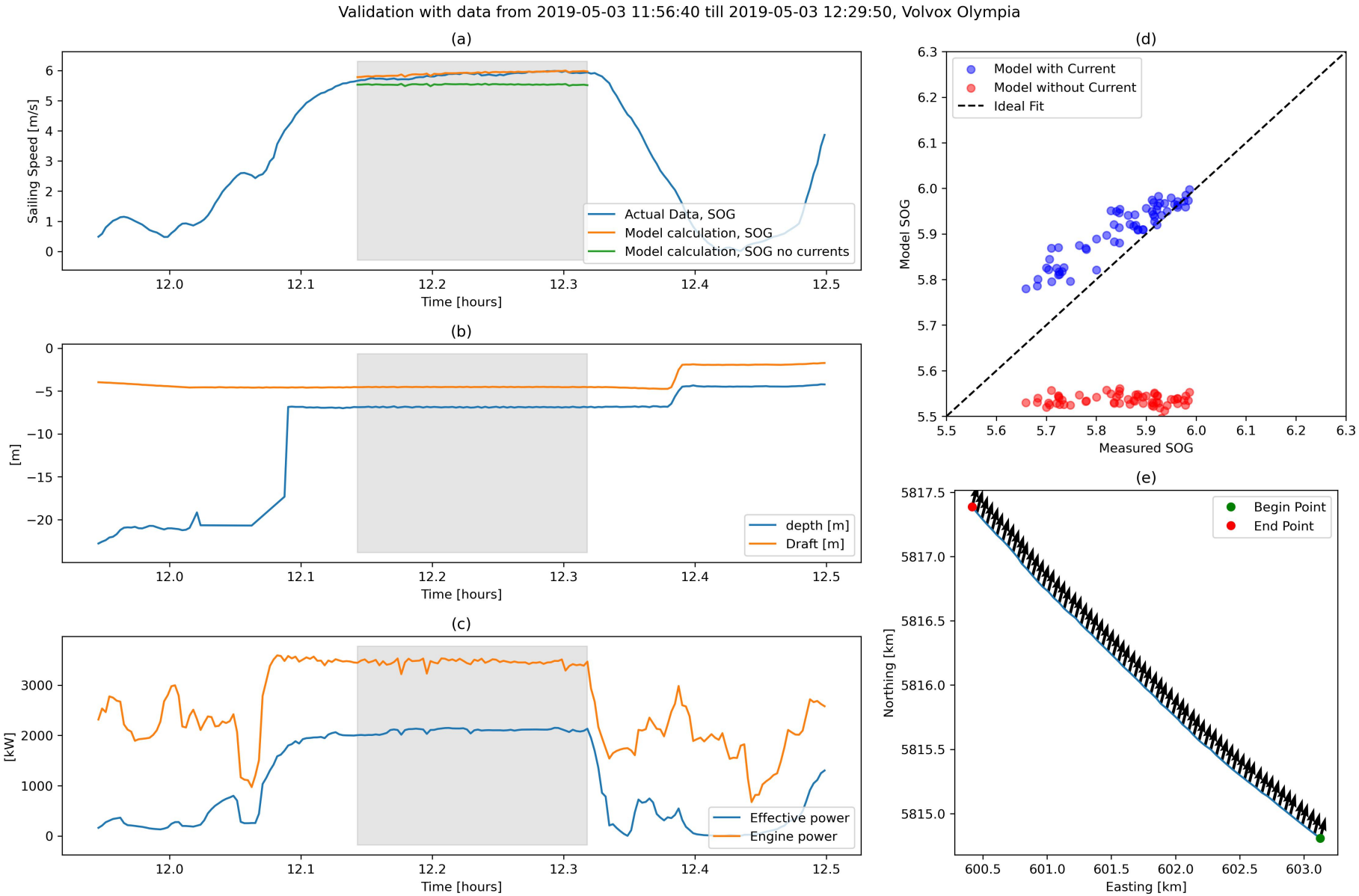
Validation with data from 2019-05-03 11:56:40 till 2019-05-03 12:29:50, Volvox Olympia
(a)
Sailing Speed [m/s]
Time [hours]
Actual Data, SOG
Model calculation, SOG
Model calculation, SOG no currents
(b)
[m]
Time [hours]
depth [m]
Draft [m]
(c)
[kW]
Time [hours]
Effective power
Engine power
(d)
Model SOG
Measured SOG
Model with Current
Model without Current
Ideal Fit
(e)
Northing [km]
Easting [km]
Begin Point
End Point

Figure 4.8 presents the results from the first validation, which is one sailing full activity. The remaining 9 validations can be seen in Appendix C. It can be seen that the model outcomes when excluding the currents are horizontal in the scatter plot, this is as expected as the input arguments in the python-based model are approximately constant. The model outcomes in which the currents, as measured by the current measuring pole, are added as a flow field seem to be more spread in the scatter plot. The result in the first validation seems to follow the ideal fit, however this is not always the case for the other validations (see Appendix C). The SOG as measured by the GPS tracking system on-board the Volvox Olympia, still shows a slight increase within the grey shaded area that depicts the region of free sailing. It can be concluded that other external factors influence the sailing speed in reality, this can for instance be caused by forcing from wind and waves. Moreover, the data for the currents are constant in space, whereas the sailing route is varying in space. Lastly, Vessellog can also contain inaccurate data. This can for instance be caused by the data reduction method or non-calibrated on-board sensors.

Table 4.8 below shows relative root mean square error $RMSE_{rel}$ for the different scenarios. It can be seen that generally, with a few exceptions, the model outcome including the currents seem to have a smaller error with respect to the measured SOG when compared to the results when excluding the currents. Keep in mind that this validation only addresses the sailing full activity. Although the results seem to have a small error when compared to the actual measured data, more simulations are necessary to validate the python-based model.

Table 4.8: Relative root mean square errors [%] for the ten validation cases

	Without correction factor		With correction factor	
Validation	No currents	Including currents	No currents	Including currents
1	10.85	4.79	5.60	1.25
2	2.71	9.37	4.52	4.19
3	5.40	9.12	1.32	3.80
4	3.44	3.44	2.73	3.79
5	6.90	3.87	13.26	2.42
6	13.00	9.65	7.81	4.35
7	6.29	5.16	2.25	2.37
8	13.99	10.33	8.94	5.33
9	4.94	5.48	1.79	1.32
10	9.69	5.20	4.30	0.87

4.3 Dredging Strategy

The sustainable dredging strategy focuses on a sand nourishment of the Dutch Coastline, it is a fictitious project in the proximity of the Rhine ROFI (region of freshwater influence). The movement of the dredging vessel is solely cross-shore, dredging sediment from deeper waters and depositing it in shallow waters near the coast. To maintain consistency with the model verification and validation, the Volvox Olympia has been selected as the designated vessel for carrying out the dredging operations. The simulations that are made all use the Prandle (1982) and Heaps (1972) flow field. The sustainable dredging strategy proposed in this study is as follows: upon returning from deep water to the coast or vice versa, the dredging vessel is allowed to wait for the cross-shore component of the flow field to grow more favourable before sailing. The python-based model is extended by means of a new class method called *waiting_time*, which determines if the cross-shore current is more favourable in subsequent time steps. Figure 4.9 depicts the plan view of the repetitive sailing route.

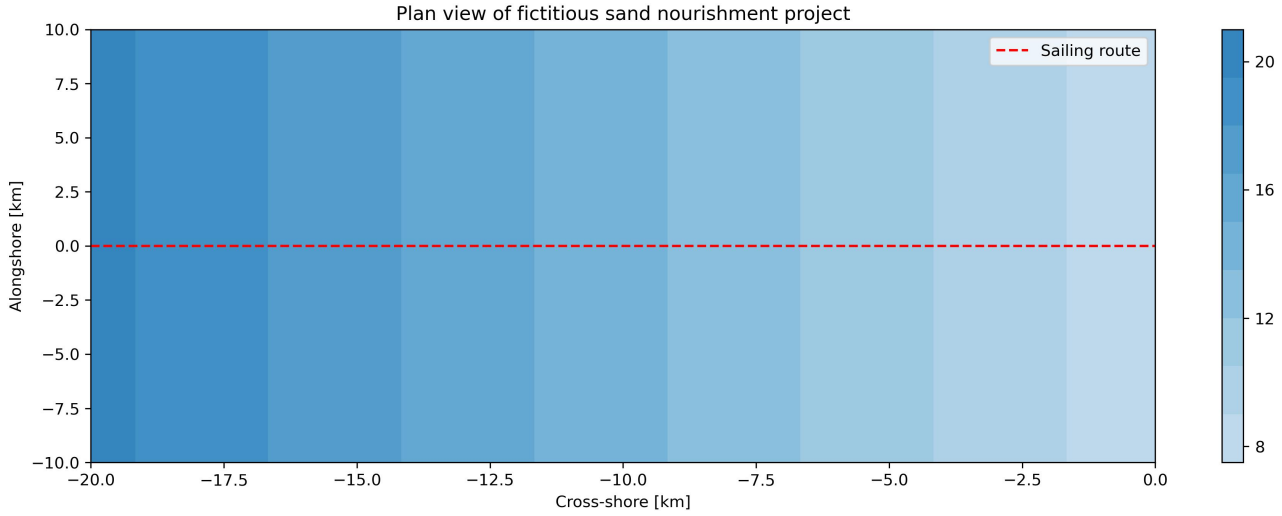

Figure 4.9: Plan view for the fictitious sand nourishment project

Hypothetical and Realistic case

Two cases will be studied, one hypothetical case in which the dredging vessel does not consume energy during waiting, and a realistic case where the dredging vessel consumes energy during waiting. The total required power of the dredging vessel, as given in section 3.2 equation 3.3, is repeated here:

$$P_{tot} = P_{transient} + P_{utilities} \tag{4.3}$$

Where $P_{transient}$ [kW] is the instantaneous power delivered by the engine, and $P_{utilities}$ [kW] is the instantaneous power delivered by the on-board power generator. The on-board utilities are for instance the lighting and heating of the hotel in which the crew resides. The power generator needs to deliver continuously, also when the vessel is not sailing, while the engine power is only required during sailing.

Neap Tide and Spring Tide

To asses the potential of harnessing the North Sea currents during a neap tide scenario compared to a spring tide scenario, different simulations are conducted in which the magnitudes and ellipticity of the currents are adjusted. The ellipticity is defined as follows (de Boer, 2009):

$$E = \frac{A_{minor}}{A_{major}} \tag{4.4}$$

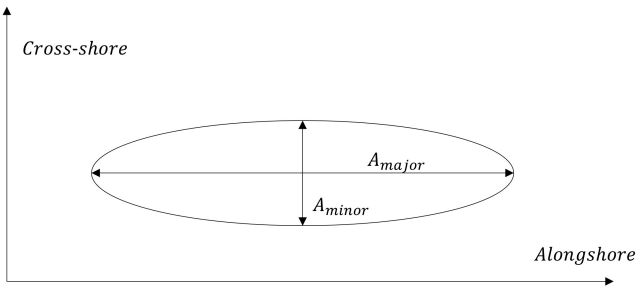

Figure 4.10: Ellips with the major axis in alongshore direction and the minor axis in cross-shore direction

The ellipticity during a neap tide compared to a spring tide scenario was assessed by Visser et al. (1994). He concluded that during well mixed conditions, which occurs during a spring tide, the tidal currents are rectilinear and parallel to the coast (see Figure 4.11). However, with highly stratified conditions, during a neap tide scenario, the cross-shore currents can reach up to 40% of the alongshore current (Visser et al., 1994). It is chosen to run simulations of the proposed dredging strategy for different vertical velocity profiles, ranging from a neap tide scenario to a spring tide scenario. The Prandle (1982) and Heaps (1972) flow field is adjusted to represent these scenarios, the magnitudes for the surface currents can be seen in Table 4.9. These input values are based on previous studies conducted on the currents in the area of the Rhine ROFI (Visser et al., 1994), (de Boer, 2009), (Flores et al., 2020), (Rijnsburger et al., 2021).

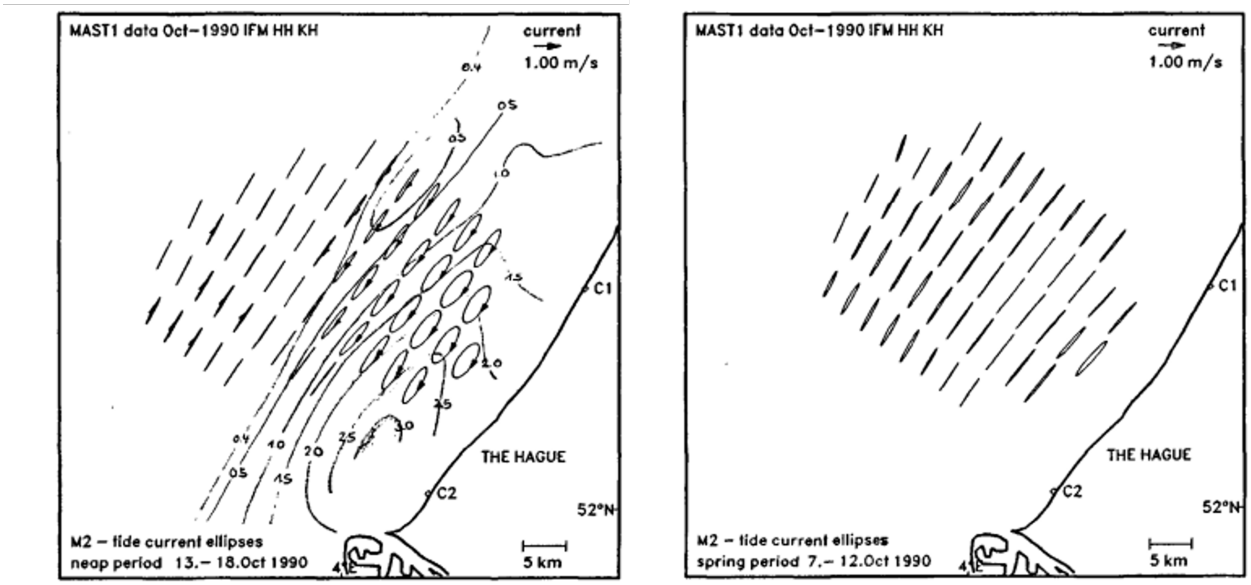

Figure 4.11: Surface tidal current ellipses calculated from CODAR data from records. A neap tide or stratified scenario (left) and a spring tide or well mixed scenario (right). (Visser et al., 1994)

Table 4.9: Ellipticity and corresponding alongshore and cross-shore current magnitudes ranging from a neap tide scenario (top) till a spring tide scenario (bottom)

Ellipticity [-]	Alongshore current $[m/s]$	Cross-shore current $[m/s]$
$\frac{1}{2}$	0.7	0.35
$\frac{1}{4}$	0.8	0.2
$\frac{1}{8}$	0.9	0.1125
$\frac{1}{16}$	1.0	0.0625

4.3.1 Hypothetical case

Two simulations are conducted for the hypothetical case. The first simulation addresses a one way trip from deep water to the coast (i.e. onshore direction). The second simulation consists of five sailing cycles, where one cycle is considered as the sailing path from deep water to the coast and back to deep water. Because the scope of this research adresses the potential of harnessing the cross-shore currents, and these current have the largest magnitude during a neap tide, only the neap tide scenario ($E = \frac{1}{2}$) is presented here. The results for the spring tide scenario ($E = \frac{1}{16}$) and the scenario in between neap and spring ($E = \frac{1}{4}$ and $E = \frac{1}{8}$) can be found in Appendix D. Table 4.10 presents the different parameters and their corresponding values used in the hypothetical case simulations.

Table 4.10: Parameters hypothetical case

Parameter	Deep water	Coast
Engine Power [kW]	3000	3000
Generator power [kW]	0	0
Water depth [m]	20	8
Draught full [m]	5	5
Draught empty [m]	2	2
x-coordinate [km]	-20	0
y-coordinate [km]	0	0

The water depth decreases linearly from deep water towards the coast. During the dredging process at the offshore location, as the vessel collects sediment and increases its total weight, the draught of the vessel also increases. To differentiate between the draught when the vessel is filled with sediment ("Draught full") and when there is no sediment in the dredging vessel ("Draught empty"), specific conditions are considered. The "Draught full" condition applies when sailing from deep water to the coast, while the "Draught empty" condition applies when sailing from the coast back to deep water. Additionally, the engine power is set to 3000 [kW] and the generator power is set to 0 [kW].

The simulations are conducted for a varying allowable waiting time and a varying starting time. Because the cross-shore and alongshore components of the Prandle (1982) and Heaps (1972) flow field exhibit a sinusoidal oscillation, the maximum allowable waiting time and starting time is set to one complete tidal period T. The sinusoidal oscillation is that of an M2-tide, which corresponds to a tidal period of 44700 seconds.

4.3.2 Hypothetical case: One way trip

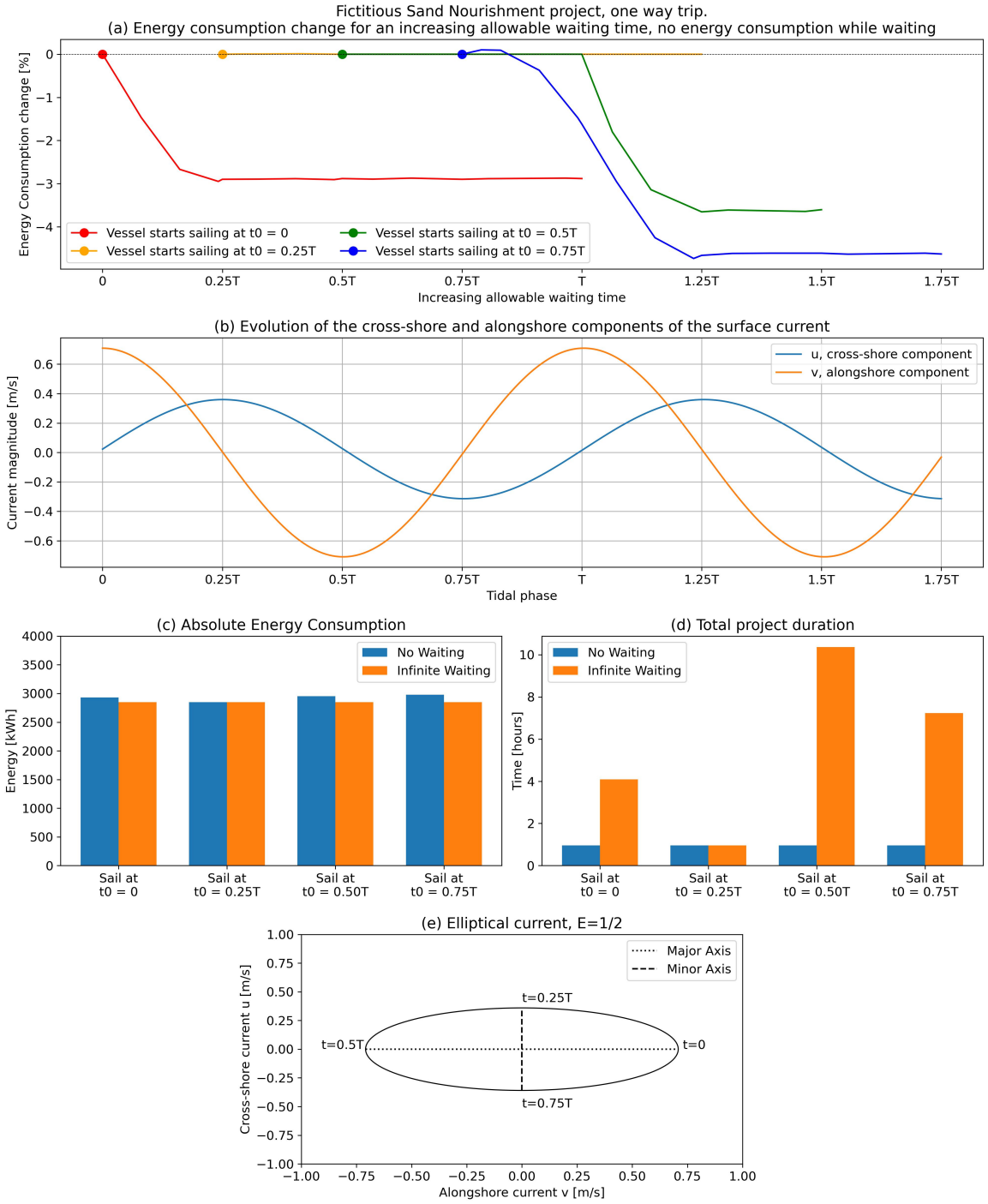

Figure 4.12: Results for sailing a one way trip. Relative energy consumption change compared to no allowable waiting time for four different starting times (a), cross-shore and alongshore components at x = -20km (b), absolute energy consumption change (c) and total project duration (d). Ellipticity E = 1/2 (e).

Figure 4.12 illustrates the results for the one way trip, from deep water to the coast, for a varying starting time and increasing allowable waiting time. The relative energy consumption is calculated by determining the change for a certain starting time and an increasing allowable waiting time. For instance, the energy consumption for the starting time $t_0 = 0$ with no allowable waiting time functions as the reference case for the same starting time ($t_0 = 0$) and an increasing allowable waiting time until T. As a result, the different starting times start at an energy consumption change of zero.

When studying the graphs for different starting times, several observations stand out. When the starting time is set to $t_0 = 0$, there is an immediate reduction in energy consumption, even for a very short allowable waiting time. for starting times of $t_0 = 0.25T$ and $t_0 = 0.5T$, there is no noticeable change in energy consumption for small allowable waiting times. the starting time of $t_0 = 0.25T$ does not show a change in energy consumption, even for an allowable waiting time of a full tidal period. The starting time of $t_0 = 0.5T$ shows an energy consumption reduction start exactly at an allowable waiting time of $0.5T$. The graph for $t_0 = 0.75T$ actually shows an increase of the energy consumption when allowing for a waiting time, up until approximately a quarter tidal period $0.25T$. Moreover, the maximum achievable energy reduction for the one way trip in this scenario is approximately 4.5%. Although this reduction is quite substantial, the total project duration increases significantly as well in order to achieve this reduction.

These observations are explained by analysing the oscillations of the cross-shore component u and alongshore component v, as presented in Figure 4.12. Note that these are solely the surface currents of the flow field at the offshore location, the actual flow field is 3D and varies in space. Keep in mind that a current perpendicular to the sailing direction, which in this case is the alongshore current v, increases the total resistance and course through water (CTW). This subsequently increases the energy consumption. A current parallel to the sailing direction, in this case u, increases the energy consumption when adverse, and decreases the energy consumption when favourable.

Starting time $t_0 = 0$

As the starting time is set to $t_0 = 0$, allowing for a waiting before sailing initially increases the cross-shore component u in the sailing direction while the alongshore component v decreases. Both result in a decreased energy consumption. The maximum decrease in energy consumption is achieved for an allowable waiting time of 0.25T, this is due to the maximum favourable parallel (cross-shore) current and a small perpendicular (alongshore) component.

Starting time $t_0 = 0.25T$

In the scenario that the dredging vessel starts sailing at $t_0 = 0.25T$, the optimal combination of the cross-shore and alongshore components is already achieved. Hence, allowing for a waiting time does not reduce the energy consumption.

Starting time $t_0 = 0.50T$

For the starting time $t_0 = 0.5T$, a small waiting time does not reduce the energy consumption as the cross-shore component grows towards the adverse direction. Half a tidal period later, the cross-shore component starts growing more favourable when compared to the current at the starting time. The optimal combination is then achieved a quarter tidal period later again, hence, the largest energy reduction occurs at an allowable waiting time of 0.75T.

Starting time $t_0 = 0.75T$

The last scenario, where the dredging vessel starts sailing at $t_0 = 0.75T$, first has an increase in energy consumption when allowing for a waiting time. This can again be explained with the graph containing the cross-shore and alongshore components of the surface currents. After the starting time at 0.75T, the cross-shore component u grows towards the favourable direction, which causes the python-based model to let the dredging vessel wait. However, the alongshore component also grows in magnitude, which increases the total resistance and the CTW (course through water). The increase in energy consumption due to the alongshore component outweighs the decrease in energy consumption due to an increasing cross-shore current in the sailing direction. The total energy consumption is therefore larger than the reference case, this occurs for a waiting time up until approximately 0.1T. After this, the energy consumption starts to decrease and reaches the optimal combination of alongshore current and cross-shore current at an allowable waiting time of 0.5T.

Decreasing ellipticity

The simulations exploring decreasing ellipticity values of $E = \frac{1}{4}$, $E = \frac{1}{8}$, and $E = \frac{1}{16}$ can be found in Appendix D. the main observations derived from these simulations are discussed here. As the ellipticity becomes smaller, the potential for energy consumption reduction decreases, since the magnitude of the cross-shore current, which can be harnessed for energy, decreases. Moreover, when the alongshore current becomes more significant compared to the cross-shore current, the impact of additional rudder-induced drag resistance on total energy consumption becomes more pronounced. The algorithm used in the *waiting_time* class method only considers the cross-shore current in subsequent time steps to make decisions regarding waiting. Consequently, it does not account for the alongshore current, which can contribute to increased resistance experienced by the vessel during sailing. The increasing influence of the additional drag resistance on the energy consumption can be seen in the simulation in which the starting time is set to $t_0 = 0.75T$. The results for this starting time show an initial increase of energy consumption compared to the reference case that grows larger for a decreasing ellipticity.

4.3.3 Hypothetical case: Five cycles

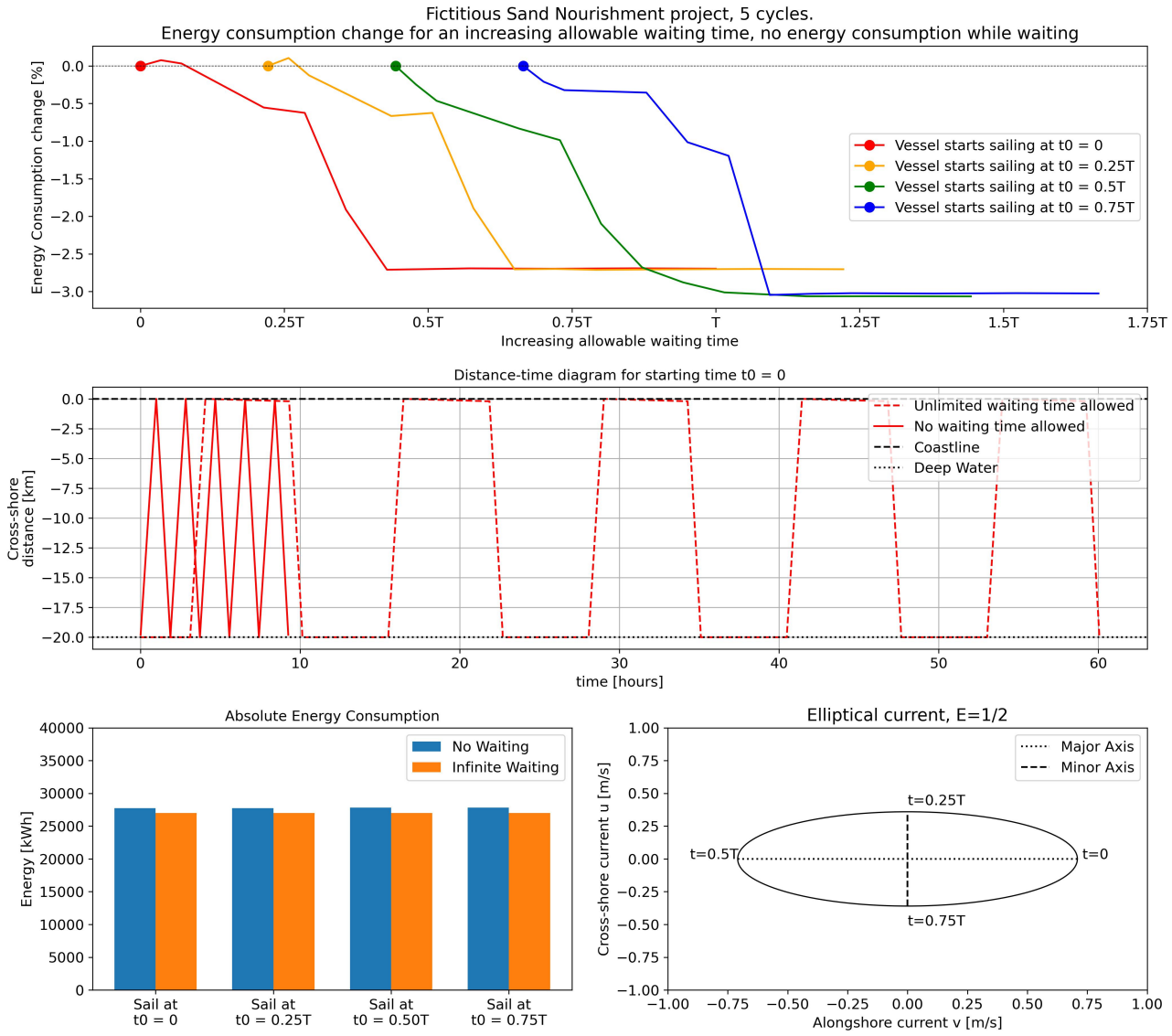

Figure 4.13: Results for sailing 5 cycles. Relative energy consumption change compared to no allowable waiting time for four different starting times (top), time-distance diagram for starting time $t_0 = 0$ (middle), absolute energy consumption change (bottom left) and ellipticity E = 1/2 (bottom right).

Figure 4.13 presents the results for 5 cycles, where each cycle is considered as the movement from deep water to the coast and then back to deep water. The results are for the Prandle (1982) and Heaps (1972) flow field representing a neap tide scenario ($E = \frac{1}{2}$), in which the cross-shore currents are largest. The simulation is again conducted for four different starting times, namely $t_0 = 0$, $t_0 = 0.25T$, $t_0 = 0.50T$ and $t_0 = 0.75T$. The total energy consumption of the 5 cycles for these four starting times, excluding an allowable waiting time, are used as the reference case to calculate the relative energy consumption reduction. The relative energy consumption reduction is determined by comparing the total energy consumption of the 5 cycles for increasing allowable waiting times with the total energy consumption of the reference case for each respective starting time.

The distance-time diagram focuses on the scenario with a starting time of $t_0 = 0$. This is done for the case that the dredging vessel is not allowed a waiting time upon returning and the case that an infinite waiting time upon returning is allowed. The *waiting_time* algorithm is configured such that, for an infinite allowable waiting time, it constantly starts sailing at the optimal combination of the cross-shore and alongshore current upon returning. This optimal combination is a maximum favourable cross-shore current and a minimum alongshore current. It can be seen that achieving an energy consumption reduction of approximately 2.6% (for $t_0 = 0$) comes at the cost of significantly increasing the total project duration from 10 hours to around 60 hours. unless the overall project duration is not considered in the decision-making process during the design phase, this can be considered as an inefficient method to reduce energy consumption. The difference in time scales between the M2 tidal period and the duration of a single trip from deep water to the coast (or vice versa) is the main factor contributing to this issue. The M2 tidal period lasts approximately 12 hours and 25 minutes, whereas a single trip takes around 1 hour.

The maximum achievable reduction in energy consumption, when harnessing the cross-shore currents, is approximately 3% ($t_0 = 0.5T$ and $t_0 = 0.75T$). This shows the absolute potential of harnessing the cross-shore currents for a repetitive sailing route. The results for an increasing ellipticity ($E = \frac{1}{4}$, $E = \frac{1}{8}$ and $E = \frac{1}{16}$) can be found in Appendix D.

4.3.4 Realistic case

The realistic case studies the potential of harnessing the cross-shore current by allowing for a waiting time upon returning from deep water to the coast, or vice versa. However, this time the dredging vessel remains consuming energy while waiting, which reflects the real-life scenario. In addition to the energy consumed by the engine power necessary for operation, the vessel also has a constant energy requirement for its generator, which powers various utilities such as lighting and heating for the on-board accommodations. A realistic estimate for the generator power $P_{utilities}$ is approximately 5% of the total installed power $P_{installed}$ on-board of the vessel (Lamers, 2022), (Segers, 2021). For the Volvox Olympia, which has a total installed power of 6542 kW, this would indicate a required generator power of:

$$P_{utilities} = P_{installed} \cdot 0.05 = 6542 \cdot 0.05 = 327.1kW \tag{4.5}$$

This is confirmed by analysing the Vessellog data, which measures the actual generator power during the different dredging activities, this can be seen in Figure 4.14. The generator power showcased peaks during the actual dredging activity. These peaks are filtered out as no dredging operations are being performed while the vessel is waiting. The average filtered generator power during the 24 hour period as depicted in Figure 4.14 is 323.1 kW, further supporting the validity of the 5% estimation rule.

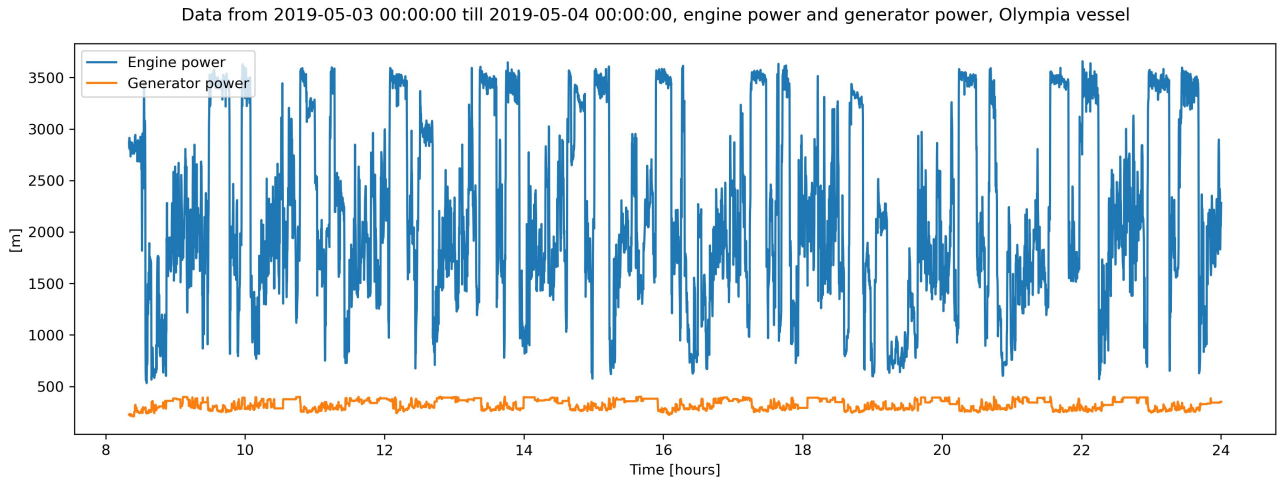

Figure 4.14: Engine power and generator power of the Volvox Olympia for a time period of 24 hours during the IJgeul sea access project.

The fictitious sand nourishment project consisting of 5 cycles is simulated again with the python-based model, however, this time the generator power $P_{utilities}$ of 327.1 kW is switched on. The results are presented in subsection 4.3.5.

4.3.5 Realistic case: Five cycles

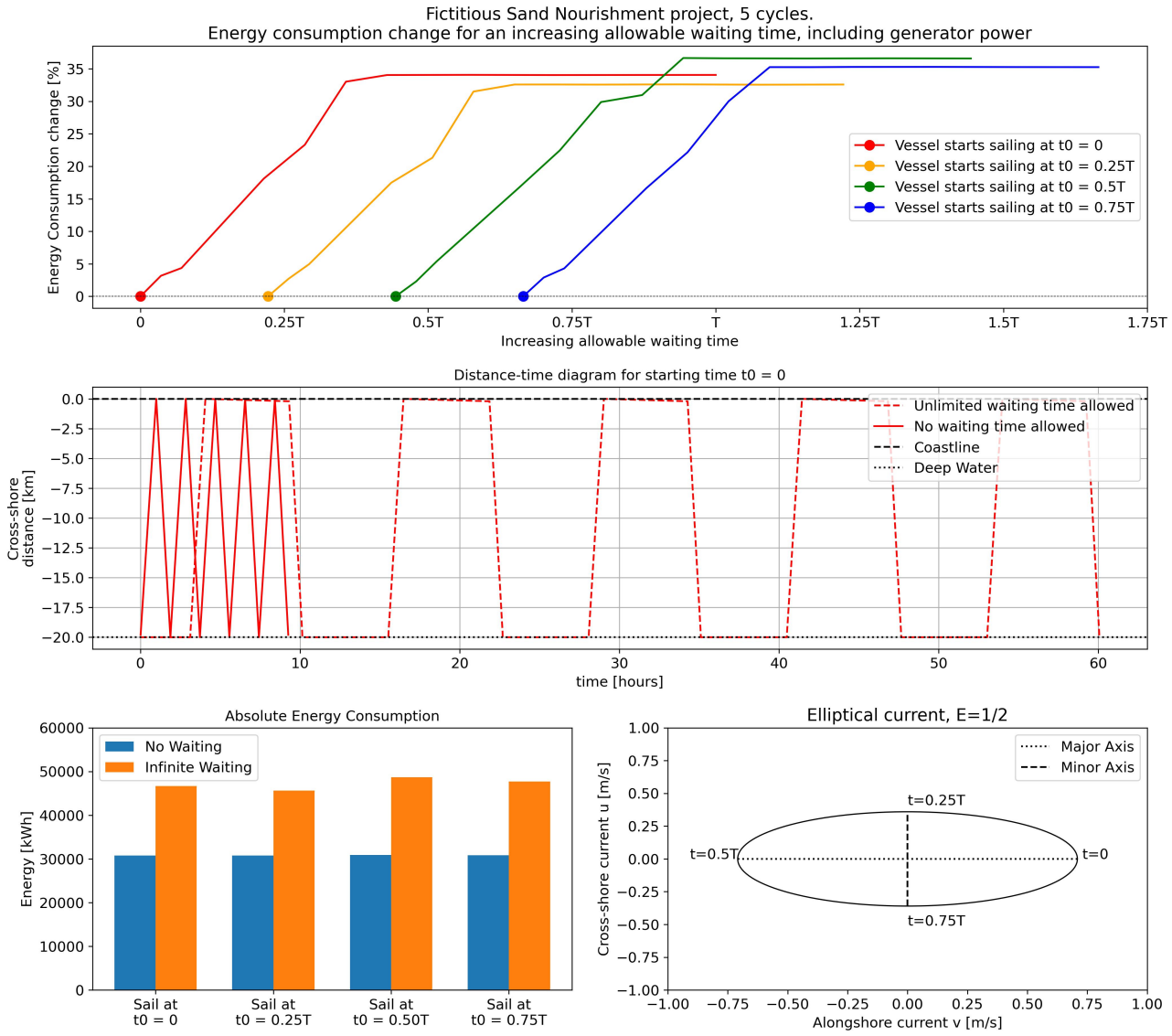

Figure 4.15: Results for sailing 5 cycles, including generator power ($P_{generator}$ = 327.1 kW). Relative energy consumption change compared to no allowable waiting time for four different starting times (top), time-distance diagram for starting time $t_0 = 0$ (middle), absolute energy consumption change (bottom left) and ellipticity E = 1/2 (bottom right).

The results of the realistic case for 5 cycles, depicted in Figure 4.15, reveal that the total energy consumption increases for all four different starting times and increasing allowable waiting times. This occurs because the constant energy consumption resulting from the power generator outweighs the reduction achieved by harnessing the currents. The large time scale of the M2-tide requires a substantial waiting time for the currents to become more favourable, this causes a large increase in energy consumption as the power generator consumes energy during waiting. The rate of energy consumption reduction due to waiting is not large enough to compensate for the generator induced energy consumption during waiting. Because this simulation addresses the neap tide scenario, in which the to be harnessed cross-shore currents are largest, it is chosen to exclude simulations for decreasing ellipticities.

Decreasing the generator power

Because the conventional dredging vessels include on-board accommodations for the crew, the proposed dredging strategy is unable to achieve energy consumption reduction by waiting for more favourable cross-shore currents upon returning. To evaluate the potential of new innovative dredging vessels, which have reduced energy consumption attributed to the power generator, an additional simulation is conducted. This simulation aims to determine the generator power magnitude at which energy consumption can be effectively reduced. Specifically, the simulation involves decreasing the generator power for a one-way trip from deep water to the coast. The selected generator power values used in the simulation are 5%, 10%, 25%, and 50% of the original generator power, as indicated in Table 4.11. The starting time is kept constant at $t_0 = 0$ for this simulation.

Table 4.11: Values for decreased generator power simulation

Scenario [-]	Generator power [%]	Value [kW]
0	100	327.1
1	50	163.55
2	25	81.775
3	10	32.71
4	5	16.355
5	0	0

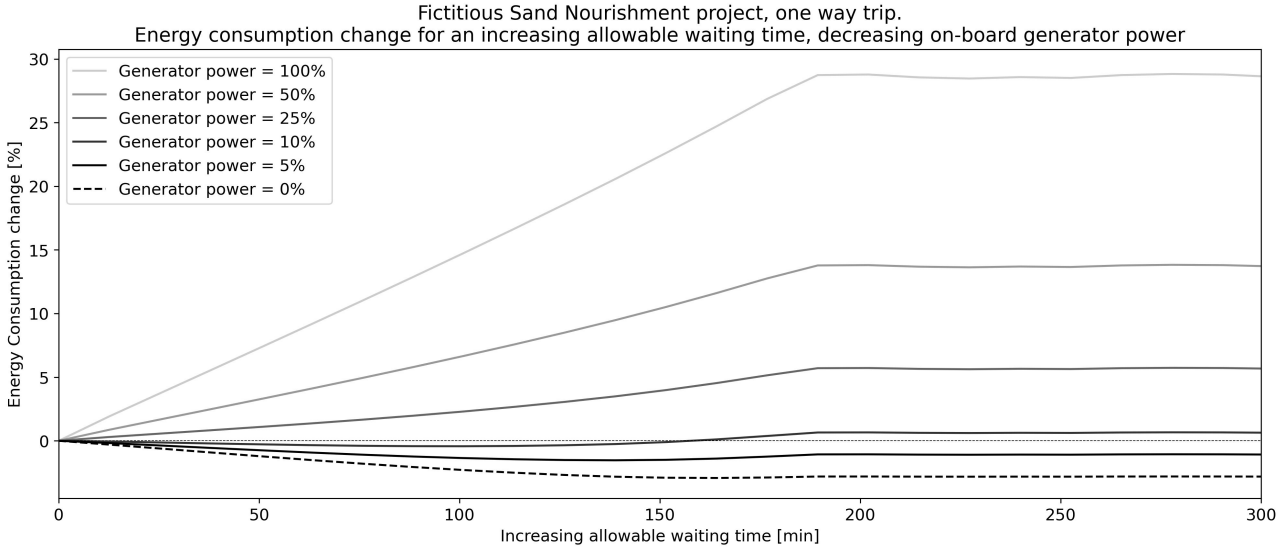

Figure 4.16: Results for a one way trip from deep water to the coast. Relative energy consumption reduction for a decreasing generator power.

Figure 4.16 shows the results of the simulation for a decreasing generator power $P_{utilities}$. It can be seen that only the scenarios in which the generator power is 5% or 10% of a conventional required generator power are able to reduce energy consumption. For these two scenarios, the total energy consumption initially reduces when the allowable waiting time is increased. However, as the allowable waiting time is increased further, the energy consumption during waiting gets larger and the energy consumption reduction reduces again. Note that at a waiting time of approximately 180 minutes, further increasing the waiting time does not further decrease the total energy consumption. This is because the optimal combination of the cross-shore and alongshore current components is reached 180 minutes (approximately 0.25T) after $t_0 = 0$. It can be concluded that, in order to utilize the proposed dredging strategy and reduce the total energy consumption by harnessing cross-shore North Sea currents, the conventional dredging vessels have to decrease their generator power by 90-100%.

Chapter 5

Discussion

This chapter provides an in-depth analysis and interpretation of the research findings. In section 5.1, a summary of the key findings of the energy calculation model and the sustainable dredging strategy are presented. This is then followed by the interpretation of these findings in section 5.2, the results from the energy calculation model are compared to existing literature. Hereafter, the discussion will present both the theoretical and practical implications in section 5.3. Additionally, the limitations of the study that were be identified during the research will be discussed in section 5.4.

5.1 Summary of findings

The main research objective was to study the impact of currents on the energy consumption and to find a way to harness these currents to reduce energy consumption. In order to do so, a python-based model was developed that utilizes the Holtrop and Mennen (1982) method with a modification to include currents in combination with a desired flow field. This section summarizes the results obtained with the python-based model, this includes the verification, the validation and the explored sustainable dredging strategy.

The verification was done with several test cases where different parameters were adjusted to study their impact on the resistance of the dredging vessel. These adjustable parameters were the draught, water depth, currents and engine power. In general, it was observed that a decreasing water depth and an increasing draught increases the total resistance of the sailing vessel. A decreased engine power increases the total sailing duration, but decreases the total energy consumption. Vice versa for an increased engine power. Furthermore, adding a constant current perpendicular to the sailing direction causes a decreased STW (speed through water) due to extra drag resistance on the rudder and an increased sailing duration due to a longer CTW (course through water) compared to COG (course over ground). Adding a constant current parallel to the sailing direction alters the sailing time: an opposed current decreases the SOG (speed over ground) with respect to the STW and a favourable current increases the

SOG with respect to the STW. When using the analytical solution of Prandle (1982) and Heaps (1972) for the dynamic and time-dependent North Sea currents, the altered speed over ground, and therefore the total energy consumption, depends on the phase of the tide and thus the starting time of the vessel's sailing. Generally, the SOG is governed by the component of the current parallel to the sailing direction and the extra drag resistance on the rudder is governed by the component of the current that is perpendicular to the sailing direction.

The validation was conducted with an existing sea access dredging project at IJmond, which was carried out in 2019 by the dredging vessel Volvox Olympia. The validation consisted of 10 simulations comparing the measured SOG (speed over ground) with the python-based model outcomes for the SOG, excluding and including the currents. Every individual simulation addressed one sailing full activity, in which the dredging vessel sails with dredged material. After validating the model with data obtained from on-board measuring sensors and current measuring poles, it was found that the model consistently underestimated the vessel's speed over ground. To improve the accuracy of the model's prediction, a correction factor that simply raises the output SOG was introduced which reduced the average error between the model prediction and the measurements to less than 5.5%.

The sustainable dredging strategy that was explored allows for the dredging vessel to wait for the currents to increase in the sailing direction, with the goal of reducing the total energy consumption during a dredging project. The chosen dredging project was a fictitious sand nourishment project at the Dutch coast, aiming to harness the cross-shore currents during a neap tide scenario. The dredging vessel travels back and forth in a cross-shore direction, and at the point of returning, it is allowed to wait until the currents become more favourable before sailing. This was done for a hypothetical case where there is no energy consumption during waiting and for the realistic case in which the vessel's energy consumption continues during waiting. This additional energy consumption during waiting is caused by an on-board power generator. The results showed that for the hypothetical case, a maximum energy consumption reduction of 3% for 5 cycles could be achieved when allowing for a infinite waiting time during a neap tide scenario. This energy consumption reduction was shown to decrease when the allowable waiting time was decreased. The spring tide scenario showed a decrease in total energy consumption of approximately 1.5% when sailing 5 cycles and allowing for an infinte waiting time. During a spring tide scenario the cross-shore component is negligible, hence this reveals the influence of the alongshore component (perpendicular to the sailing direction) on the energy consumption. However, when taking into account the additional components that consume energy, i.e. the realistic case, the energy consumption decrease due to allowing for a waiting time was outweighed by the energy consumed during waiting.

5.2 Interpretation of findings

This section presents the conclusions drawn from the results discussed in the previous section. The findings of the study revealed a positive correlation between the draught of the dredging vessel and its total resistance, as well as between water depth and total resistance. The correlation between water depth and resistance aligns with existing research done by Rotterveel (2013) and Lamers (2022), who demonstrated that a limited water depth increases the overall resistance. The positive correlation between the vessel's draught and total resistance is caused due to the fact that the frictional resistance increases when the dredging vessel has a larger draught. However, it has also been observed that when comparing two very small draughts, the smallest draught has a larger total resistance. After analysing the different resistance components, this can be explained by comparing the frictional resistance and the wave-making resistance. The frictional resistance decreases with a decreasing draught, while the wave-making resistance increases with a decreasing draught. When the draught is extremely small, decreasing it further means a larger increase in wave-making resistance than the decrease in frictional resistance, causing an increase of the total resistance.

The impact of currents on the dredging vessel was analyzed in two distinct factors: the extra drag resistance on the rudder and the potential change in sailing time. The test results indicated that there was a positive correlation between the additional drag resistance and the component of the current perpendicular to the vessel's sailing direction. This is because the perpendicular current component creates a force that pushes the vessel off its intended course, requiring the rudder to exert more effort to maintain the desired heading. This causes a larger angle of attack between the rudder and the water velocity with respect to the rudder, and thus an increased drag resistance and decreased STW. The drift angle, however, also depends on the current parallel to the sailing direction, whereas a favourable current decreases the drift angle and an adverse current increases the drift angle. The difference between the STW and SOG generally depends on the current component parallel to the sailing direction. A favourable current in the sailing direction increases the SOG and thus decreases the sailing time and energy consumption, and vice versa for an adverse current in the sailing direction.

The validation process revealed that the python-based model initially underestimated the SOG when compared to the real-world data. After addition of the correction factor, the error was reduced to below 5.5%. The validation involved running 10 simulations in which the dredging vessel navigated through shallow waters. Lamers (2022) observed that the results of the Holtrop and Mennen (1982) were accurate for shallow water, however, for deeper water the resistance was underestimated. Earlier studies on Holtrop and Mennen (1982) also observed that the energy consumption calculation estimates for deeper water are lower than measured (Rotteveel, 2013) (Zeng et al., 2019). This has not been validated because a deep water dredging project in the proximity of a current measuring pole and containing the required data in Vessellog was not available. The python-based model requires additional validations with various types of dredging projects and vessels to ensure its accuracy and reliability.

The sustainable dredging approach demonstrated that there is a quite significant reduction in energy consumption when harnessing the cross-shore currents during a neap tide. The reduction for an infinite waiting time is approximately 3% for 5 cycles of sailing from deep water to the coast and back. This falls between the range of the predicted energy consumption reduction due to voyage optimization of 1% - 10% (IMO, 2022). However, keep in mind that the proposed sustainable dredging strategy increases the total project duration significantly and requires innovative dredging vessel that do not consume energy when waiting. For conventional dredging vessel, the energy consumption of the hotel on-board the vessel outweighs the potential energy reduction that can be achieved by waiting for a more favourable current. The generator power of conventional dredging vessels should be decreased by 90-100% in order to achieve energy consumption reduction for the proposed sustainable dredging strategy.

5.3 Implications

The developed python-based model provides both practical and theoretical implications. The model has theoretical implications, as it allows for a more precise understanding of the energy consumption of dredging vessels and the impact of currents on energy consumption. This insight can help researchers and organizations develop more efficient and sustainable dredging practices. The model provides a fundamental base for future research, allowing for further refinement of the model and deeper exploration of the impact of currents on energy consumption. Moreover, to create a more accurate theoretical model that can quantify the different resistance terms for various vessel types, the modification to include the additional drag resistance of the rudder can be added to the original Holtrop and Mennen method.

The model has practical implications, as it can be applied in real-world settings to address emissions from dredging vessels. Dredging companies can use this model to better understand their energy consumption during dredging operations and develop strategies to reduce their emissions. Additionally, this model can be used in tenders, where companies can showcase alternative dredging strategies as opposed to conventional dredging strategies by including an analysis of their energy consumption during dredging operations. Existing open-source simulation software called OpenCLSim (Van Oord, 2022) allows for this model to be added in the form of an extension module, whereafter it can be used for the simulation of dredging projects and offshore wind farm projects. It is important to note that this model requires input on the coastal currents, which can be challenging to obtain for future dredging projects as they depend on the tidal phase and bi-weekly occurrence of neap-tide and spring-tide. Additionally, while this model can provide valuable insights into energy consumption during dredging operations, it is not entirely accurate. Therefore, a correction factor has been added to ensure that the results are as reliable as possible. This inaccuracy can be caused by model limitations such as neglecting acceleration and deceleration in the calculation, but also not taking into account weather conditions such as wind and waves. It can also be caused by the chosen databases, the on-board sensory measuring devices from Vesselog can possible be uncalibrated or the data can

be inaccurate due to the reduction method. Additionally, a simplification for the currents is made where in the model calculations they are assumed to move along with the sailing vessel, while in reality the currents are measured in one point in space.

5.4 Limitations

The study also consisted of various limitations that are addressed in this section. The limitations mentioned here are those that are inside of the scope of the research, they address the simplifications made while developing the model. The limitations are followed by recommendations to improve the current research. The recommendations presented in chapter 6 address possible follow-up research outside of the scope of the current research.

One of the simplifications is the flow field that is based on Prandle (1982) and Heaps (1972). Although this analytical solution provides a first order estimate of the vertical velocity structure during a tidal cycle, it is not a fully accurate model that takes into account all the physical processes that occur in the North Sea and influence the currents. To obtain a more accurate representation of the full hydrodynamics in the North Sea, a CFD (computational fluid dynamics) model should be used. A CFD model takes into account a wider range of physical processes that can influence the flow of water, such as the wind stress, wave-induced currents and a more detailed bathymetry. A CFD model is also more accurate in turbulence modelling, the analytical solution in the present study utilizes a constant eddy viscosity while CFD models are capable of modelling the turbulence with for instance the k-ϵ model.

Another limitation is caused by the assumption that the dead-water drag can be neglected, this is based on the high densimetric Froude number during free sailing where sailing speed is considered much larger than the internal wave celerity. In reality this densimetric Froude number might become critical at low sailing speed and large stratification, potentially causing a significant increase in the total resistance. This could either occur in a coastal area in the proximity of the region of freshwater influence (ROFI), but also as a dredging vessel approaches the river mouth. It is therefore recommended that a separate study is conducted that studies the impact of the dead-water resistance on the energy consumption during a neap tide in the North Sea, for a seagoing vessel sailing with a low STW.

Similar to the dead-water resistance, the hydrodynamic forces on the bow and stern are assumed to be negligible in the total resistance. This assumption is made based on the fact that for a large STW during free sailing, the currents impacting the vessel and therefore the drift angle are relatively small. It is therefore assumed that the centerline of the dredging vessel is parallel to the streamlines of the flow and thus the hydrodynamic forces are already accounted for in the Holtrop and Mennen method. However, it should be noted that as the STW decreases, the drift angle increases, and the hydrodynamic forces may become more significant in contributing to the total resistance. It is therefore also recommended that these hydrodynamic forces, during a low STW, and their impact on the total resistance are studied.

Chapter 6

Conclusion & Recommendations

This chapter presents the conclusion and recommendations of the conducted research. The conclusion provides answers to the sub-questions and main research question, based on the findings of the python-based model and the study on the sustainable dredging strategy. Furthermore, recommendations for future research are provided, presenting possibilities outside of the scope of the present study.

6.1 Conclusion

This section presents the conclusion of the conducted research. The sub-questions are addressed first, and then the main research question is answered.

The first sub-question is:

> *How can the essential physical features of the dynamic and time-dependent coastal currents in the North Sea be represented in a continuous three-dimensional space?*

As discussed in section 2.2, a first order estimate of the physical features of the North Sea currents can be represented by utilizing analytical solutions for the tidal-induced and residual density-driven flow. The general analytical solution for the tidal-induced current was derived by Prandle (1982), and the general analytical solution for the residual density-driven flow was derived by Heaps (1972). Because these are general solutions, the input variables have to be chosen such that they represent realistic values for the magnitude of the coastal currents in the North Sea. de Boer (2009) provided values for the input variables that result in a vertical velocity structure with realistic magnitudes for a neap tide and spring tide at the Rhine ROFI. Using the combination of the general analytical solutions in combination with these input values, results in a vertical velocity structure that represent the physical features of the dynamic and time-dependent coastal current in the North Sea in a continuous three-dimensional space.

The second sub-question is:

> *How can the energy consumption of sailing dredging vessels be quantified, taking into account the influence of dynamic and time-dependent coastal currents?*

This question was treated partially in section 2.1, where the suitable existing energy consumption methodologies were discussed. The section concluded that the Holtrop and Mennen (1982) method was the most appropriate, as it provides the most detailed bottom-up approach. Additionally, subsection 3.3.1 and subsection 3.4.2 discussed how to incorporate the effects of dynamic and time-dependent coastal currents on energy consumption. The former discusses how an additional drag resistance is induced on the rudder of the sailing vessel, and provides a means to quantify this resistance and add it to the total resistance of the original Holtrop and Mennen method. The latter discussed the altered sailing time that occurs when a vessel is sailing through a flow field, this is based on the CTW (course through water) and STW (speed through water). The CTW is calculated using the perpendicular and parallel components of the current with respect to the sailing direction. The STW is calculated using the Holtrop and Mennen method, which includes the modification for drag resistance. The energy consumption of sailing dredging vessels, sailing through dynamic and time-dependent coastal currents, can therefore be quantified by means of the Holtrop an Mennen method with a modification for the drag resistance and taking into account the altered sailing time.

The third sub-question is:

> *How can a practical and user-friendly model be developed to estimate the energy consumption of dredging vessels in project-specific conditions?*

This question was addressed in subsection 3.4.1, subsection 3.4.3 and subsection 3.4.4. The Holtrop and Mennen method in its original form takes as input the STW, amongst other parameters, to return the various resistance components, effective power and engine power. In practice, captains of dredging vessels sail with a constant engine power, as opposed to a constant STW, so the method first had to be modified. This was done by means of the bisection method, which proved to be a fast and accurate solution to calculate the STW for an engine power as input variable. To create a practical and user-friendly model, the method was implemented using Object Oriented Programming in Python. The resulting class can be customized for a specific vessel and project conditions, allowing users to define a sailing route with relevant water depth, draught and currents, as well as a desired vessel and constant engine power to estimate energy consumption during free sailing. However, the python-based model was found to underestimate SOG (speed over ground) when compared to on-board measurements and data on currents from Rijkswaterstaat. A calibration factor was therefore applied, reducing the average error in SOG to less than 5.5%. A practical and user-friendly model to estimate the energy consumption can therefore be developed by means of an importable Python class that only requires adjustments of the input variables.

The main research question is:

> *What is the effect of a dynamic and time-dependent stratified coastal current on the energy consumption of dredging vessels, and how can these currents be harnessed to reduce energy consumption?*

The main research question is a combination of the previously mentioned sub-questions with an addition on exploring alternative dredging strategies. As the python-based model utilizes a constant engine power, the energy consumption is primarily dependent on the altered sailing time caused by the currents. The current perpendicular to the sailing direction induces an increased resistance due to drag on the rudder, leading to a decreased STW and increased sailing time and energy consumption. The current parallel to the sailing direction can either increase or decrease the sailing time and therefore energy consumption, depending on whether it is in an adverse or favourable direction. Furthermore, the stratified water column can induce dead-water resistance, significantly increasing the total resistance when the densimetric Froude number approaches 0.9. This becomes important at large stratification in combination with a seagoing vessel sailing at a low STW.

To explore the sustainable dredging strategy, a fictitious sand nourishment project in the North Sea was simulated. The input variables of the Prandle (1982) and Heaps (1972) flow field were adjusted such that the solution represents a neap tide scenario, in which the cross-shore component of the stratified coastal currents are largest. A sand nourishment project was chosen because the primary movement is cross-shore, thus interacting with these cross-shore currents. The sustainable dredging strategy used to harness the currents, is allowing for a waiting time to let the stratified currents become more favourable and thus reducing sailing time and energy consumption. A hypothetical case was simulated where the dredging vessel does not consume energy while waiting, resulting in a maximum achievable reduction in energy consumption of 3% for 5 repetitive cycles from deep water to the coast and back. However, in reality, the dredging vessel continues to consume energy while waiting, negating the reduction in energy consumption achieved by waiting. Therefore, innovative new ships that do not consume energy while waiting could potentially harness the currents by the waiting strategy, but for existing dredging vessels, alternative sustainable dredging strategies must be investigated and developed. It has been assessed that harnessing the cross-shore currents using the waiting time strategy during a neap tide scenario, requires a generator power reduction of 90-100%. However, this would still increase the total project duration quite significantly.

The stratified coastal currents are elliptical, whereas the minor axis (cross-shore) can be of an order of magnitude smaller than the major axis (alongshore). The current research concludes that harnessing the cross-shore component of the stratified coastal current, for a repetitive sailing route (sand nourishment project), results in an inefficient energy reduction. However, harnessing the alongshore component of the stratified coastal current can have a more significant reduction in energy reduction as the magnitude of these currents are larger.

6.2 Recommendations

The recommendations presented in section 5.4 focussed on the possible improvements within the scope of the present study. This section presents recommendations outside of the scope of the current research.

Because the present study aimed to harness the cross-shore currents that arise during a neap tide scenario, i.e. large stratification, the model was solely used to explore a sustainable dredging strategy for a sand nourishment project with repetitive cross-shore movement. However, the physical features of the North Sea currents take shape of a rotating elliptical current with a minor (cross-shore) and major (alongshore) axis, where the major axis is significantly larger than the minor axis (Figure 6.1). The cross-shore currents reach a maximum of 0.35 [m/s] during neap tide, while the alongshore currents can reach up to 1.2 [m/s] (Rijnsburger et al., 2021) during a spring tide. Harnessing these alongshore currents can potentially result in a greater energy reduction, particularly during a spring tide scenario when these currents reach their maximum magnitude. Instead of the chosen cross-shore sailing route, the vessel's movement during a sand nourishment project can be alongshore if the sediment source is not located directly offshore. It is therefore recommended to explore dredging strategies for sand nourishment project where alongshore movement is involved. Additionally, the alongshore currents can be harnessed during the mobilisation of dredging vessels towards a certain location. Van Oord has for instance undertaken various dredging projects in Zeeland and at the Waddeneilanden, which are located on the southern and northern parts of the Dutch coastline, respectively. In the scenario where the logistics of different dredging projects require dredging vessel mobilisation between Zeeland and the Waddeneilanden, harnessing the alongshore currents can potentially reduce the energy consumption significantly. It is therefore recommended to study sustainable mobilisation along the Dutch Coastline.

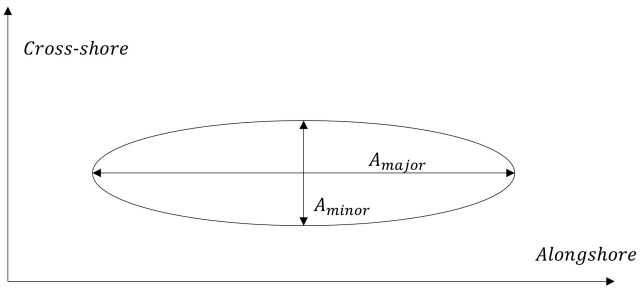

Figure 6.1: Ellips with the major axis in alongshore direction and the minor axis in cross-shore direction

Instead of waiting for the current to grow more favourable in the sailing direction, the sailing speed can also be adjusted in real-time according to the instantaneous current magnitude. When the current is favourable and the vessel is projected to arrive ahead of schedule, reducing the engine power can be considered. The increase in sailing time is not a significant concern since maintaining the same engine power would result in the vessel arriving too early. However, this adjustment can lead to decreased energy consumption due to the lower engine power. This can decrease energy consumption on a dredging project scale or during mobilisation, depending on the logistics of the dredging practices.

Because the aim of the present research was to study the impact of the currents on the energy consumption of a sailing dredging vessel, the other parameters influencing the energy consumption were only addressed in the verification of the model. These other parameters are mainly the water depth, draught and engine power. To optimize the sailing route, and minimize the energy consumption during sailing, these parameters should also be taken into account. A study conducted by Halem (2019) explored this aspect by proposing an algorithm for optimized routing based on various hydrodynamics. It is recommended to further develop this routing optimization algorithm by incorporating the Holtrop and Mennen method (1982), such that it can optimize routing based on energy consumption. Once this algorithm is developed, it can be utilized to explore sustainable dredging strategies.

Another limitation caused by the scope of this study is that it solely addressed the free sailing part of a dredging project. In order to provide a comprehensive assessment of the energy consumption of a sailing vessel, it is recommended to conduct a separate study on the energy consumption during acceleration, deceleration and manoeuvring. This is because the tender market is interested in obtaining the total energy consumption of the entire dredging project, and not just the energy consumed during the free sailing phase.

The scope of the current research solely focused on the impact of coastal currents on energy consumption, while ignoring other external factors that also influence energy consumption. Wind and waves also influence the energy consumption of a sailing vessel, thus it is important to conduct fundamental research on their significance in order to estimate energy consumption. This would also enable a full representation of energy consumption during a dredging project and provide more accurate estimates for tendering.

The present study only considered the North Sea, however, Van Oord undertakes numerous dredging projects around the globe. To be able to operate in different continents, large-scale mobilisation of dredging vessels and equipment is required. It is therefore recommended to conduct a separate research that studies the effect of currents on the energy consumption of dredging vessels outside of the North Sea scope. This can be done by assessing the large-scale ocean currents and run simulations that quantify the energy consumption when harnessing these currents. A study on the effects of these large-scale ocean currents on energy consumption is also of significant value outside the scope of Van Oord, as the findings can also contribute to sustainable maritime transport and therefore a significant reduction of the shipping industry's share in greenhouse gas emissions.

Appendix A

Prandle Derivation

This appendix outlines the derivation of the equations of motion in the phasor form, it serves as additional understanding of the derivation for the tidal-induced current. The start of this derivation is the equation of motion in cartesian form:

$$\frac{\partial u}{\partial t} - fv = -g\frac{\partial \eta}{\partial x} + \frac{\partial}{\partial z}\left(E_z \frac{\partial u}{\partial z}\right) \tag{A.1}$$

$$\frac{\partial v}{\partial t} + fu = -g\frac{\partial \eta}{\partial y} + \frac{\partial}{\partial z}\left(E_z \frac{\partial v}{\partial z}\right) \tag{A.2}$$

By first introducing the velocity vectors expressed in complex vector notation as follows; $\boldsymbol{U} = u + iv$, where x is the real axis and y is the imaginary axis. The velocity vector is then decomposed as two counter rotating phasors as follows:

$$R = R^+ + R^- = u + iv \tag{A.3}$$

R^+ is the counter clockwise rotating phasor and R^- clockwise rotating phasor. They are defined in the complex plane as:

$$R^+ = \left|R^+\right| e^{i\phi^+} e^{+i\omega t}$$

$$R^- = \left|R^-\right| e^{i\phi^-} e^{-i\omega t}$$

where ω is the angular frequency depending on the tidal constituent or combination of tidal constituents, for the current 3D flow field an M2 tide is applied with a tidal period of 12 hours and 25 minutes. ϕ is the phase in the complex plane, i.e. the phase of the tidal propagation. Applying equation A.1 and A.2 to the propagation of a tidal wave yields the general solutions for u and v of the form:

$$u = a\cos\omega t + b\sin\omega t \tag{A.4}$$

$$v = c\cos\omega t + d\sin\omega t \tag{A.5}$$

Noting that the complex definitions of cosine and sinus can formulated as follows:

$$\cos\omega t = \frac{e^{i\omega t} + e^{-i\omega t}}{2}$$
$$\sin\omega t = \frac{e^{i\omega t} - e^{-i\omega t}}{2i}$$

This way the horizontal velocities u and v can be rewritten in complex vectors with clockwise rotating and anti-clockwise rotating phasors with a certain phasor amplitude. Hereafter these complex vectors can be substituted in equation A.1 and equation A.2.

$$u = a\frac{e^{i\omega t} + e^{-i\omega t}}{2} + b\frac{e^{i\omega t} - e^{-i\omega t}}{2i} = \frac{1}{2}(a - ib)e^{iwt} + \frac{1}{2}(a + ib)e^{-iwt}$$

$$v = c\frac{e^{i\omega t} + e^{-i\omega t}}{2} + d\frac{e^{i\omega t} - e^{-i\omega t}}{2i} = \frac{1}{2}(c - id)e^{iwt} + \frac{1}{2}(c + id)e^{-iwt}$$

Now the velocities can be divided in anti-clockwise and clockwise components, respectively R^+ and R^-, as $u + iv = R^+ + R^-$.

$$u + iv = \frac{1}{2}(a - ib)e^{iwt} + \frac{1}{2}(a + ib)e^{-iwt} + \frac{1}{2}(ic + d)e^{iwt} + \frac{1}{2}(ic - d)e^{-iwt}$$

$$u + iv = \frac{1}{2}(a + d + i(c - d))e^{iwt} + \frac{1}{2}(a - d + i(b + c)e^{-iwt}$$

thus,

$$R^+ = \frac{1}{2}(a + d + i(c - d))e^{iwt}$$
$$R^- = \frac{1}{2}(a - d + i(b + c)e^{-iwt}$$

By expanding the equations of motion with equations A.4 and A.5 and forming the summation of [A.1 + i A.2], the equations can be separated resulting in a decoupled system of equations expressed into a anti-clockwise and clockwise rotating motion, respectively:

$$i(f + \omega)R^+ = G^+ + \frac{\partial}{\partial z}\left(E_z\frac{\partial R^+}{\partial z}\right) \tag{A.6}$$

$$i(f - \omega)R^- = G^- + \frac{\partial}{\partial z}\left(E_z\frac{\partial R^-}{\partial z}\right) \tag{A.7}$$

Appendix B

Holtrop and Mennen: Karpov modification

This sections presents the various 6^{th} polynomials that determine the value for a^{**}, D $[m]$ is the water depth and T $[m]$ is the draught.

If $F_{nh} \leq 0.4$:

- If $0 \leq \left(\frac{\mathrm{D}}{T}\right) < 1.75$:

$a^{**} = (-4 \cdot 10^{-12}) \cdot F_{nh}^3 - 0.2143 \cdot F_{nh}^2 - 0.0643 \cdot F_{nh} + 0.9997$

- if $1.75 \leq \left(\frac{\mathrm{D}}{T}\right) < 2.25$:

$a^{**} = -0.8333 \cdot F_{nh}^3 + 0.25 \cdot F_{nh}^2 - 0.0167 \cdot F_{nh} + 1$

- if $2.25 \leq \left(\frac{\mathrm{D}}{T}\right) < 2.75$:

$a^{**} = -1.25 \cdot F_{nh}^4 + 0.5833 \cdot F_{nh}^3 - 0.0375 \cdot F_{nh}^2 - 0.0108 \cdot F_{nh} + 1$

- if $\left(\frac{\mathrm{D}}{T}\right) \geq 2.75$:

$a^{**} = 1$

If $F_{nh} > 0.4$:

- If $0 \leq \left(\frac{\mathrm{D}}{T}\right) < 1.75$:

$a^{**} = -0.9274 \cdot F_{nh}^6 + 9.5953 \cdot F_{nh}^5 - 37.197 \cdot F_{nh}^4 + 69.666 \cdot F_{nh}^3 - 65.391 \cdot F_{nh}^2 + 28.025 \cdot F_{nh} - 3.4143$

- if $1.75 \leq \left(\frac{\mathrm{D}}{T}\right) < 2.25$:

$a^{**} = 2.2152 \cdot F_{nh}^6 - 11.852 \cdot F_{nh}^5 + 21.499 \cdot F_{nh}^4 - 12.174 \cdot F_{nh}^3 - 4.7873 \cdot F_{nh}^2 + 5.8662 \cdot F_{nh} - 0.2652$

- if $2.25 \leq \left(\frac{\mathrm{D}}{T}\right) < 2.75$:

$a^{**} = 1.2205 \cdot F_{nh}^6 - 5.4999 \cdot F_{nh}^5 + 5.7966 \cdot F_{nh}^4 + 6.6491 \cdot F_{nh}^3 - 16.123 \cdot F_{nh}^2 + 9.2016 \cdot F_{nh} - 0.6342$

- if $2.75 \leq \left(\frac{\mathrm{D}}{T}\right) < 3.25$:

$a^{**} = -0.4085 \cdot F_{nh}^6 + 4.534 \cdot F_{nh}^5 - 18.443 \cdot F_{nh}^4 + 35.744 \cdot F_{nh}^3 - 34.381 \cdot F_{nh}^2 + 15.042 \cdot F_{nh} - 1.3807$

- if $3.25 \leq \left(\frac{\mathrm{D}}{T}\right) < 3.75$:

$a^{**} = 0.4078 \cdot F_{nh}^6 - 0.919 \cdot F_{nh}^5 - 3.8292 \cdot F_{nh}^4 + 15.738 \cdot F_{nh}^3 - 19.766 \cdot F_{nh}^2 + 9.7466 \cdot F_{nh} - 0.6409$

- if $3.75 \leq \left(\frac{\mathrm{D}}{T}\right) < 4.5$:

$a^{**} = 0.3067 \cdot F_{nh}^6 - 0.3404 \cdot F_{nh}^5 - 5.0511 \cdot F_{nh}^4 + 16.892 \cdot F_{nh}^3 - 20.265 \cdot F_{nh}^2 + 9.9002 \cdot F_{nh} - 0.6712$

- if $4.5 \leq \left(\frac{\mathrm{D}}{T}\right) < 5.5$:

$a^{**} = 0.3212 \cdot F_{nh}^6 - 0.3559 \cdot F_{nh}^5 - 5.1056 \cdot F_{nh}^4 + 16.926 \cdot F_{nh}^3 - 20.253 \cdot F_{nh}^2 + 10.013 \cdot F_{nh} - 0.7196$

- if $5.5 \leq \left(\frac{\mathrm{D}}{T}\right) < 6.5$:

$a^{**} = 0.9252 \cdot F_{nh}^6 - 4.2574 \cdot F_{nh}^5 + 5.0363 \cdot F_{nh}^4 + 3.3282 \cdot F_{nh}^3 - 10.367 \cdot F_{nh}^2 + 6.3993 \cdot F_{nh} - 0.2074$

- if $6.5 \leq \left(\frac{\mathrm{D}}{T}\right) < 7.5$:

$a^{**} = 0.8442 \cdot F_{nh}^6 - 4.0261 \cdot F_{nh}^5 + 5.313 \cdot F_{nh}^4 + 1.6442 \cdot F_{nh}^3 - 8.1848 \cdot F_{nh}^2 + 5.3209 \cdot F_{nh} - 0.0267$

- if $7.5 \leq \left(\frac{\mathrm{D}}{T}\right) < 8.5$:

$a^{**} = 0.1211 \cdot F_{nh}^6 + 0.628 \cdot F_{nh}^5 - 6.5106 \cdot F_{nh}^4 + 16.7 \cdot F_{nh}^3 - 18.267 \cdot F_{nh}^2 + 8.7077 \cdot F_{nh} - 0.4745$

- if $8.5 \leq \left(\frac{\mathrm{D}}{T}\right) < 9.5$:
  - if $F_{nh} < 0.6$:

  $a^{**} = 1$

  - if $F_{nh} \geq 0.6$:

  $a^{**} = -6.4069 \cdot F_{nh}^6 + 47.308 \cdot F_{nh}^5 - 141.93 \cdot F_{nh}^4 + 220.23 \cdot F_{nh}^3 - 185.05 \cdot F_{nh}^2 + 79.25 \cdot F_{nh} - 12.484$

- if $\left(\frac{\mathrm{D}}{T}\right) > 9.5$:
  - if $F_{nh} < 0.6$:

  $a^{**} = 1$

  - if $F_{nh} \geq 0.6$:

  $a^{**} = -6.0727 \cdot F_{nh}^6 + 44.97 \cdot F_{nh}^5 - 135.21 \cdot F_{nh}^4 + 210.13 \cdot F_{nh}^3 - 176.72 \cdot F_{nh}^2 + 75.728 \cdot F_{nh} - 11.893$

Appendix C

Validation

This Appendix consists of the remaining 9 validation simulations, the caption is repeated here for convenience:

Figure C.1 - Figure C.9: Comparison of the SOG (speed over ground) resulting from the python-based model, including and excluding currents, and the measured SOG from Vessellog (a), the measured water depth D and draught T (b) and the measured effective power P_e and brake horse power P_b (c). The grey shaded areas in (a), (b) and (c) depict the region in which the criteria for free sailing is met. The model outcomes for each increment along the sailing route are presented in a scatter plot, along with the ideal fit (d). The path of the sailing route with the corresponding interpolated time-varying currents (e).

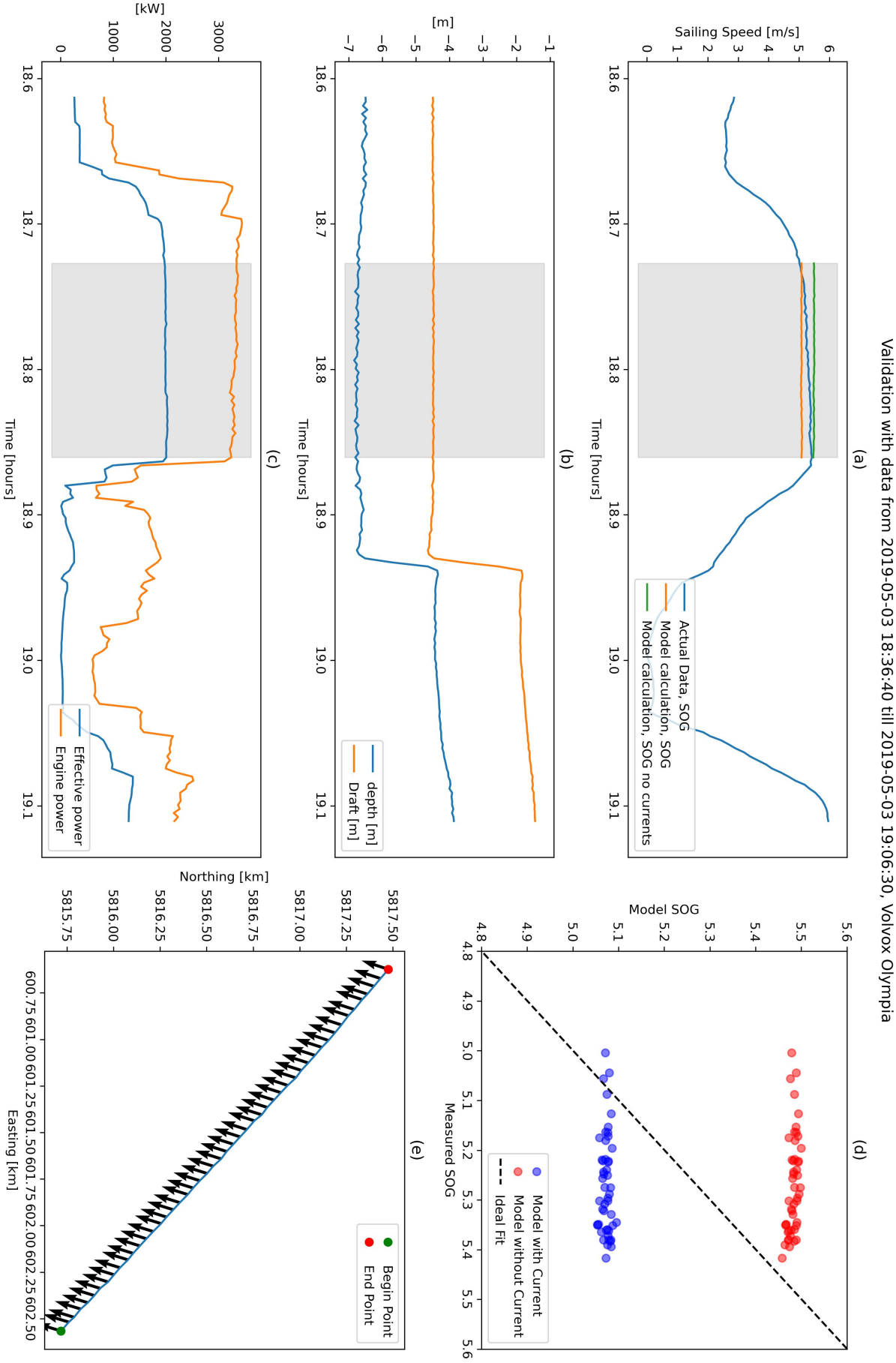

Figure C.1: Validation 2

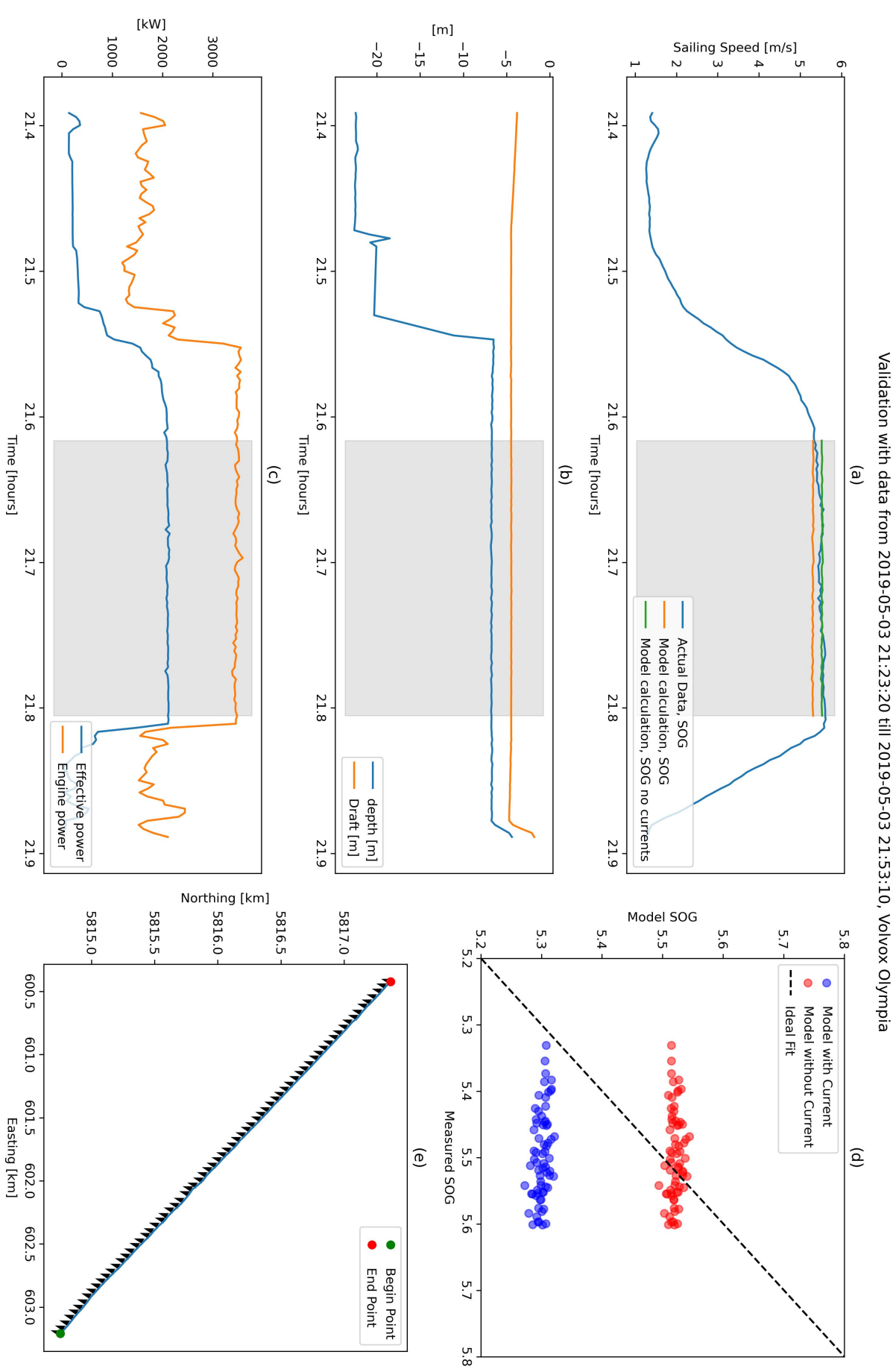

Figure C.2: Validation 3

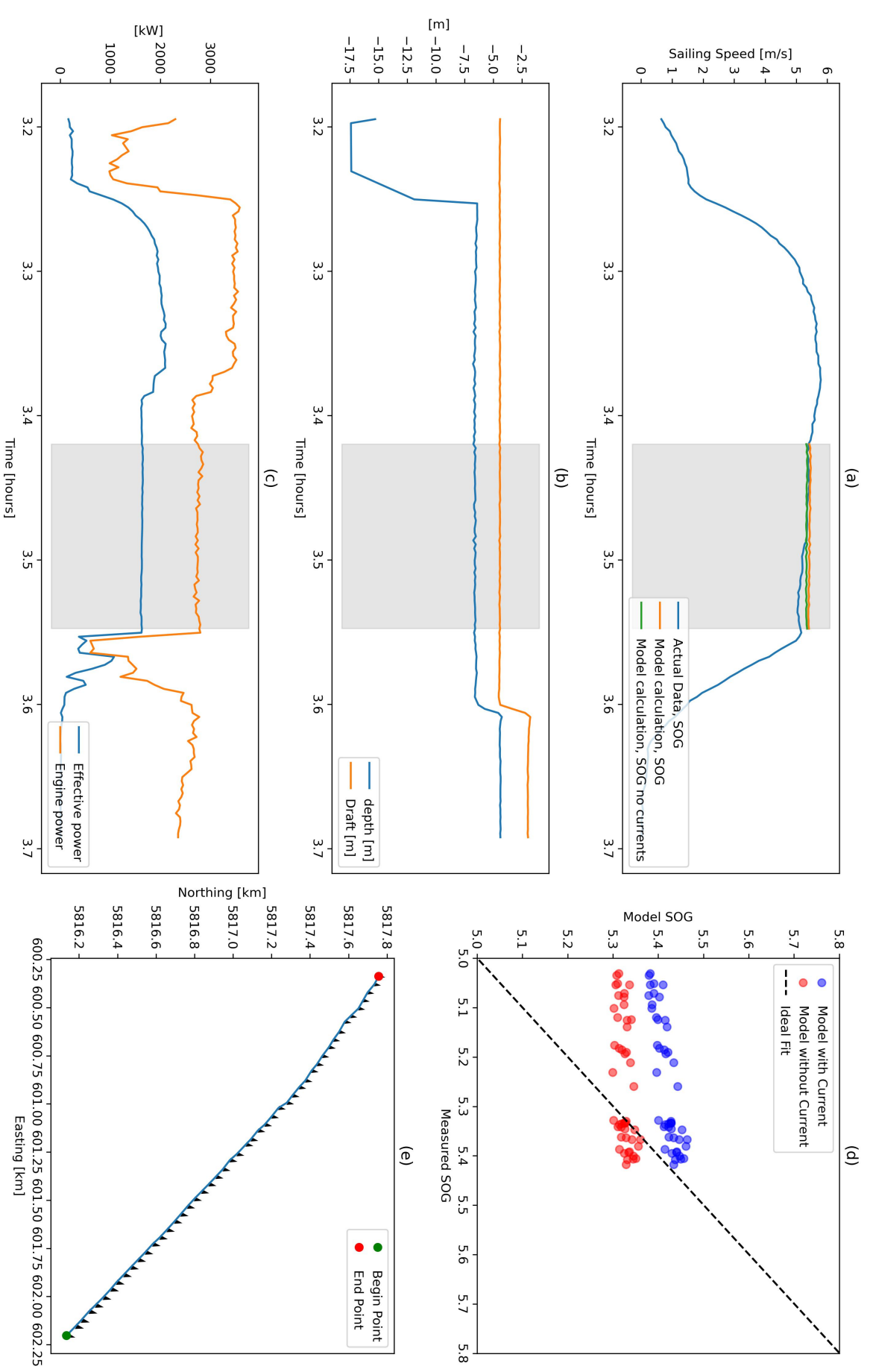

Figure C.3: Validation 4

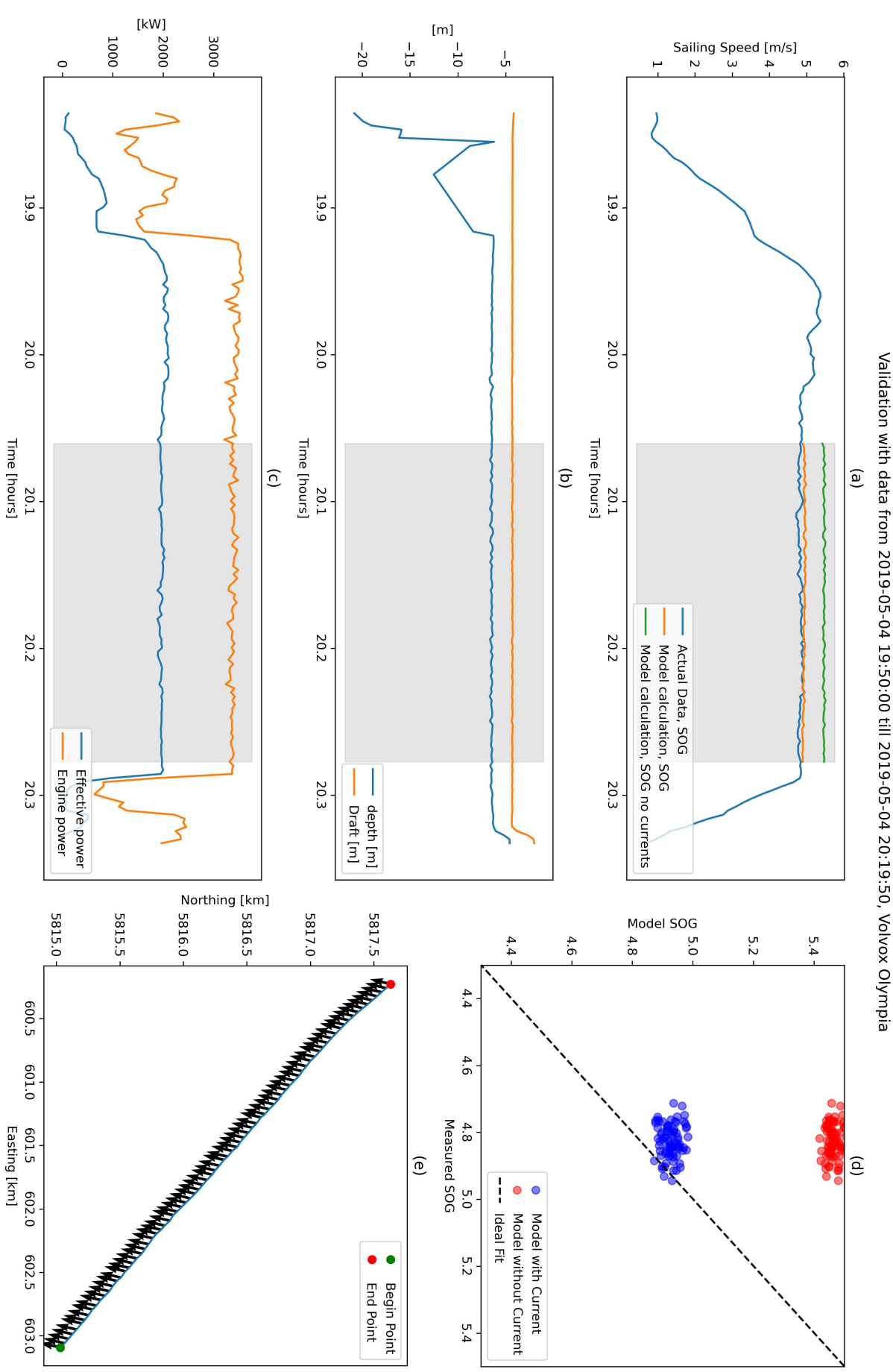

Figure C.4: Validation 5

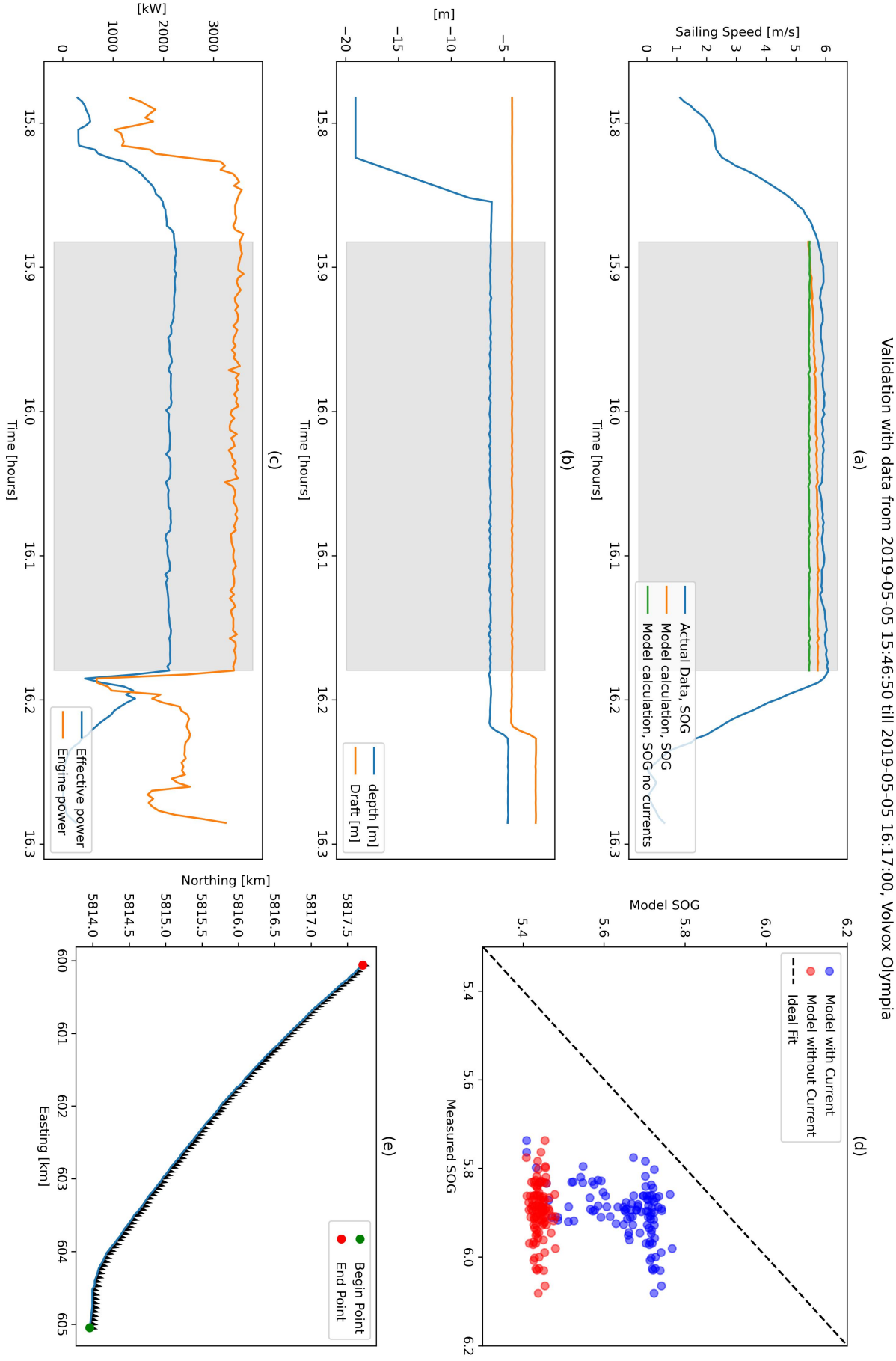

Figure C.5: Validation 6

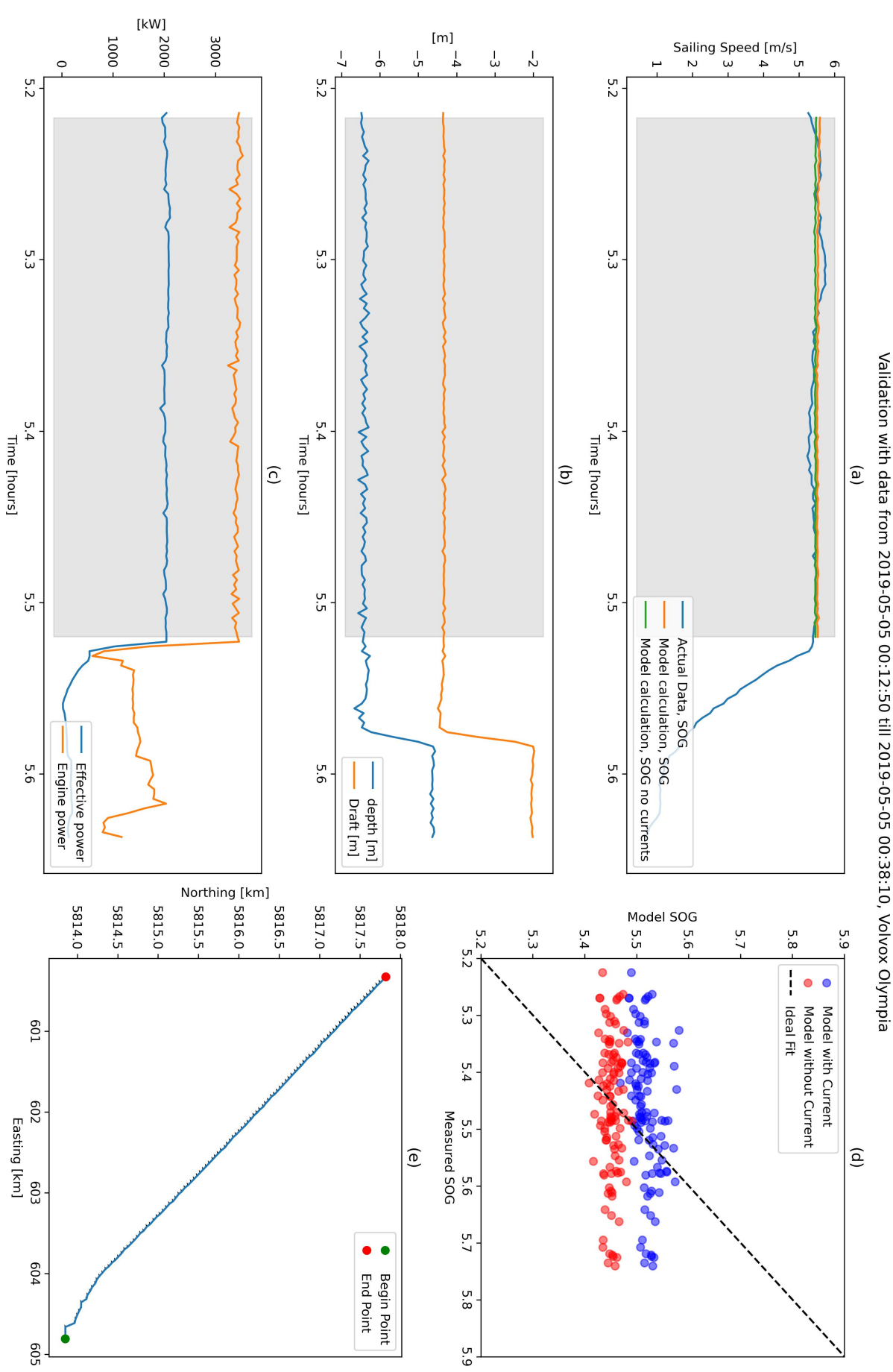

Figure C.6: Validation 7

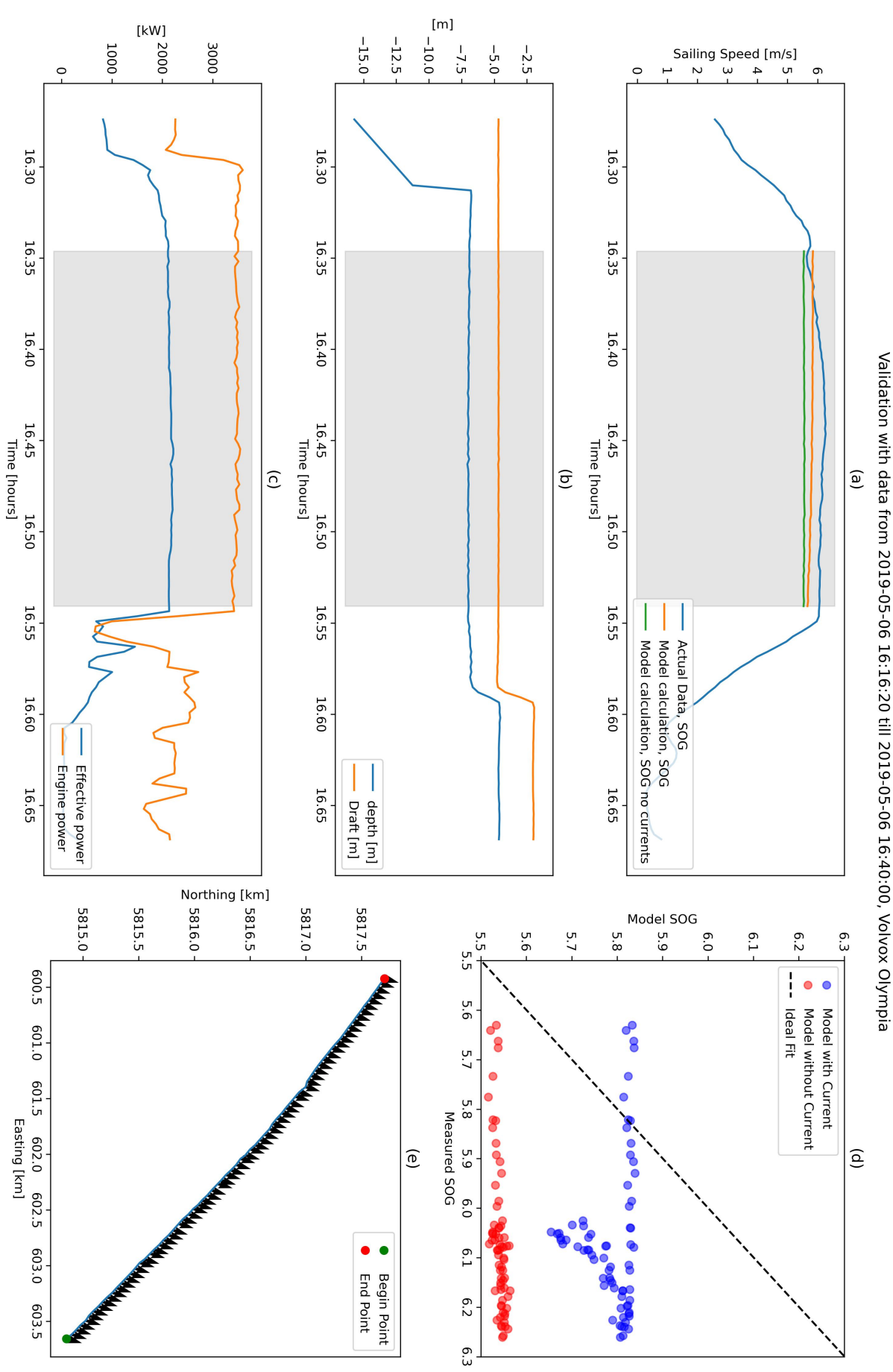

Figure C.7: Validation 8

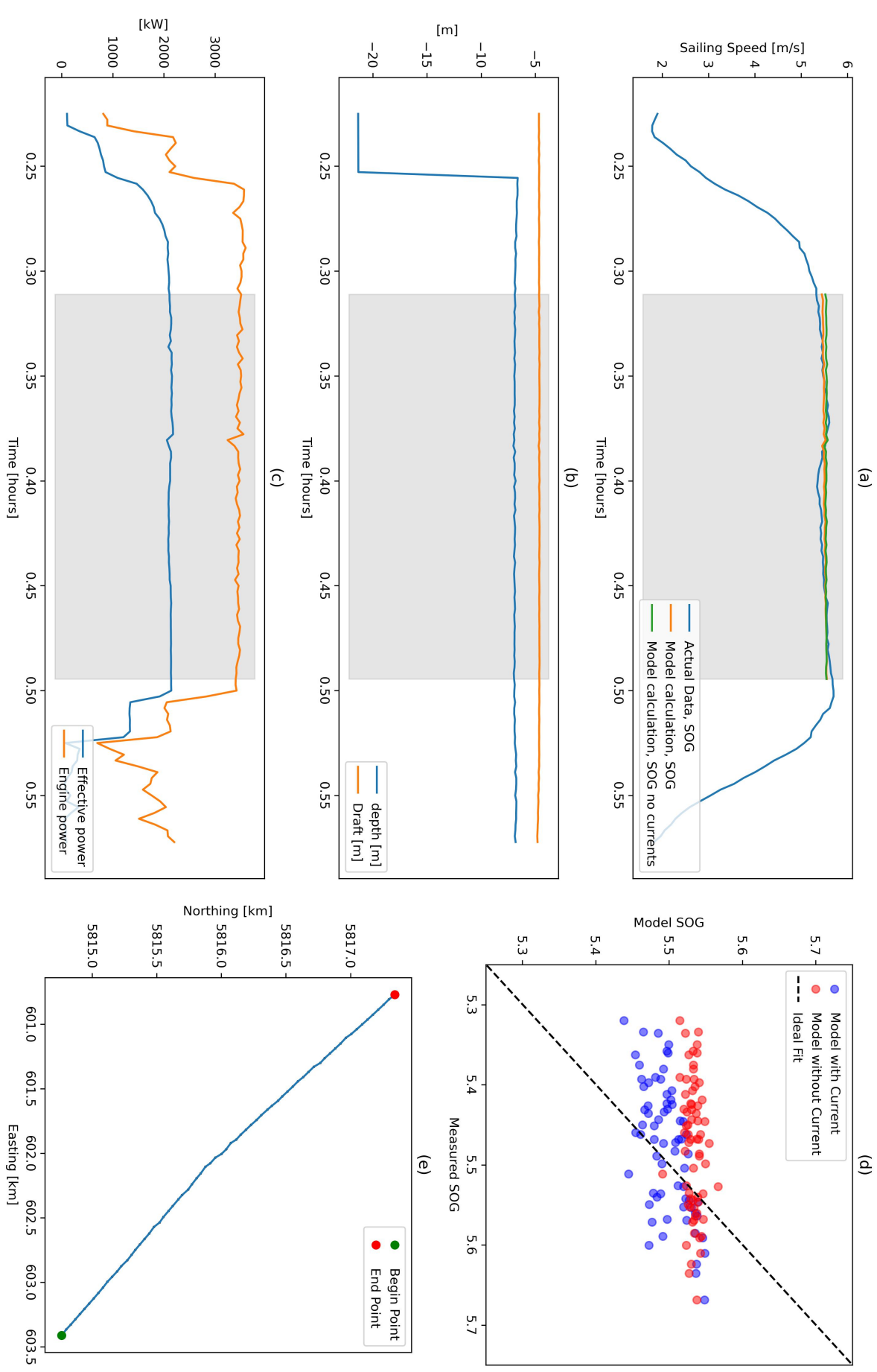

Figure C.8: Validation 9

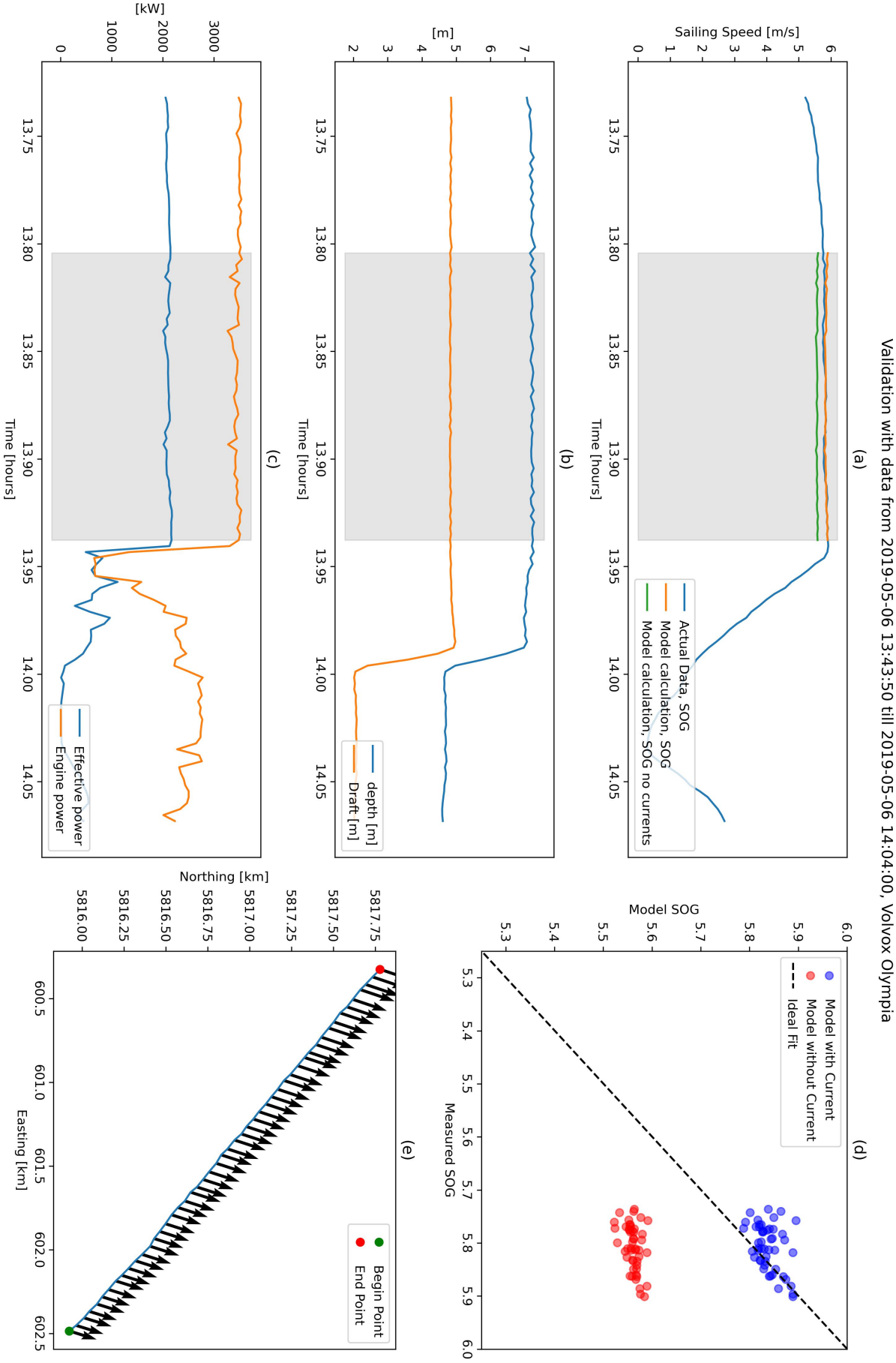

Figure C.9: Validation 10

Appendix D

Dredging Strategy

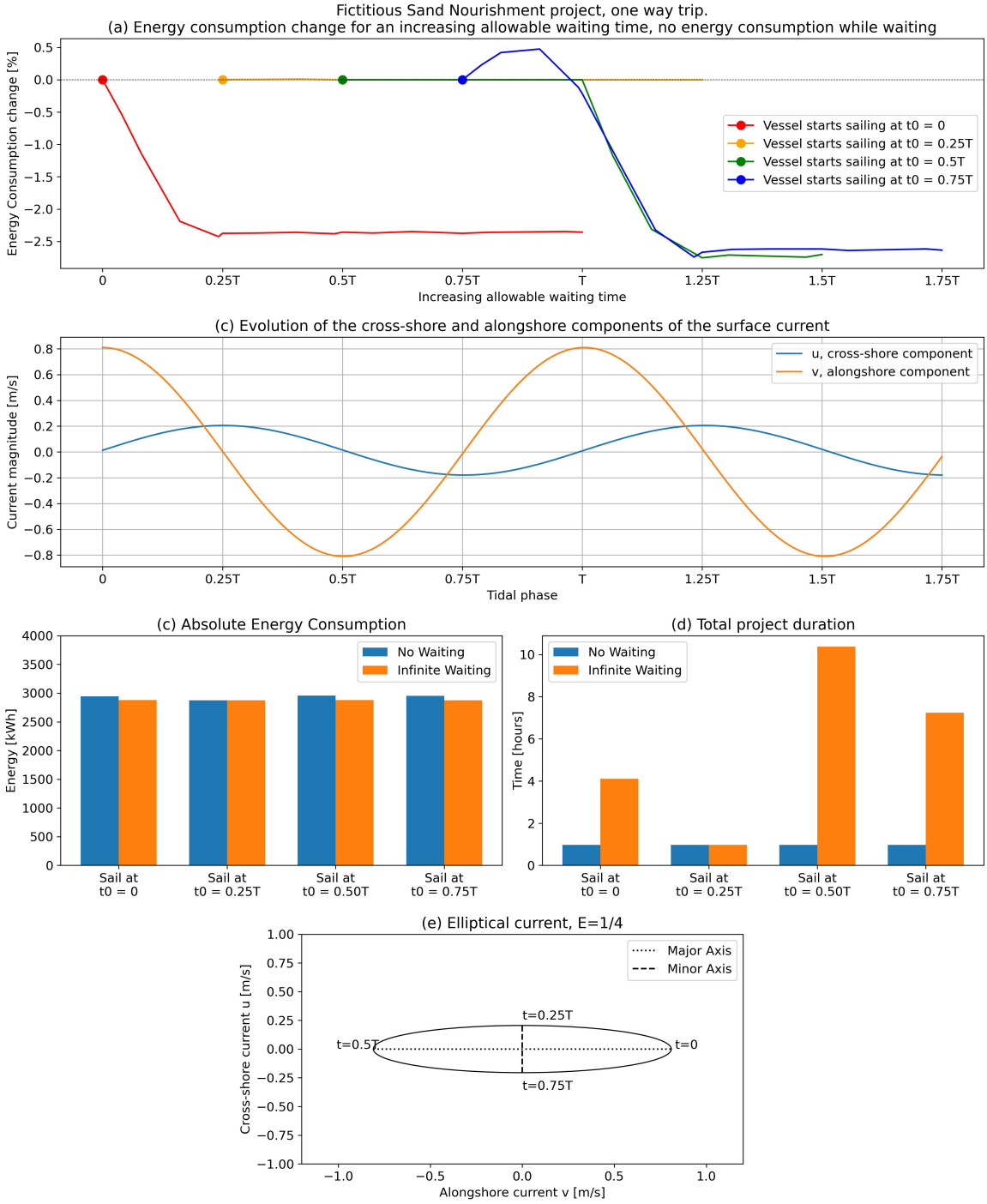

Figure D.1: Results for sailing a one way trip. Relative energy consumption change compared to no allowable waiting time for four different starting times (a), cross-shore and alongshore components at x = -20km (b), absolute energy consumption change (c) and total project duration (d). Ellipticity E = 1/4 (e).

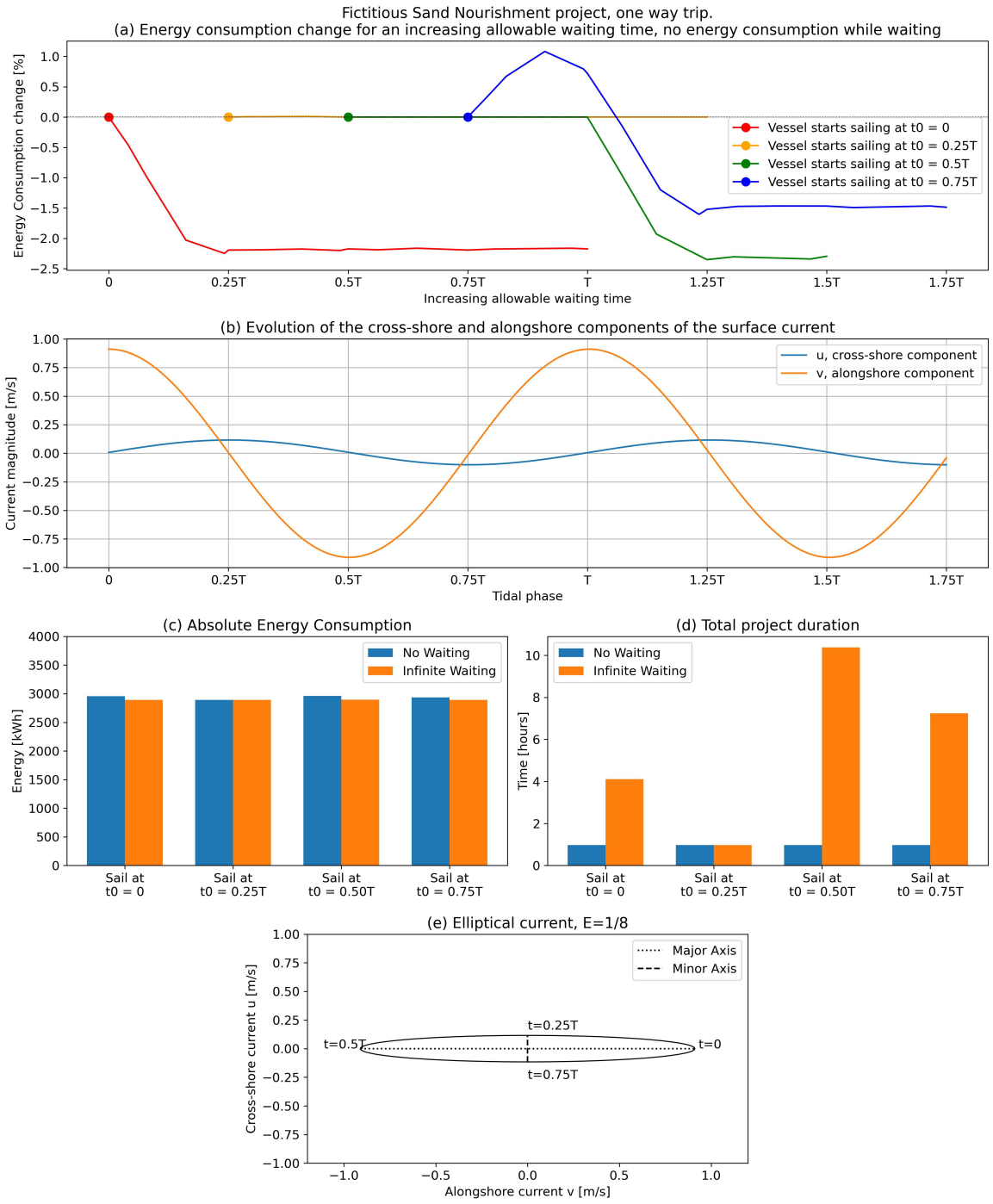

Figure D.2: Results for sailing a one way trip. Relative energy consumption change compared to no allowable waiting time for four different starting times (a), cross-shore and alongshore components at x = -20km (b), absolute energy consumption change (c) and total project duration (d). Ellipticity E = 1/8 (e).

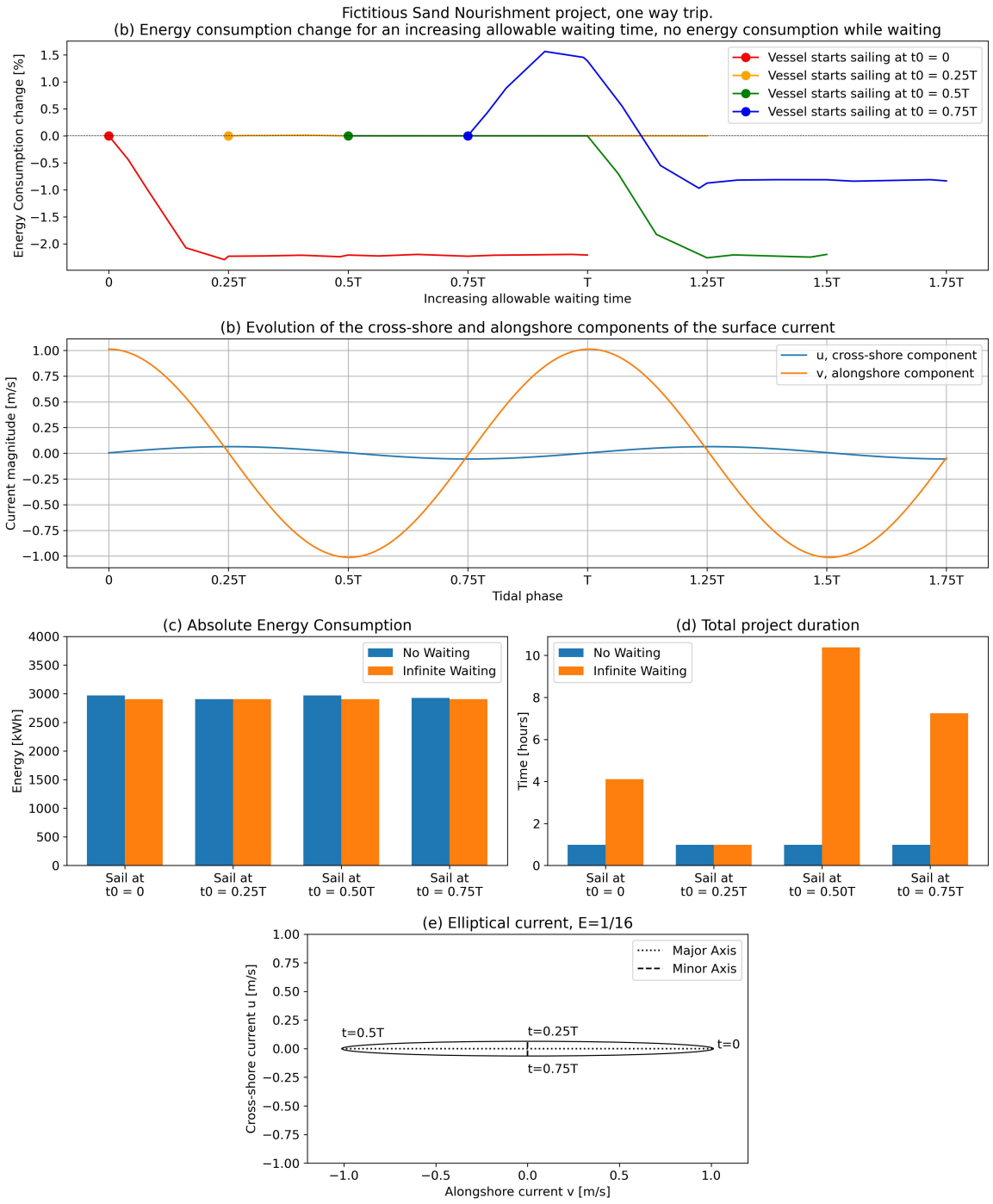

Figure D.3: Results for sailing a one way trip. Relative energy consumption change compared to no allowable waiting time for four different starting times (a), cross-shore and alongshore components at x = -20km (b), absolute energy consumption change (c) and total project duration (d). Ellipticity E = 1/16 (e).

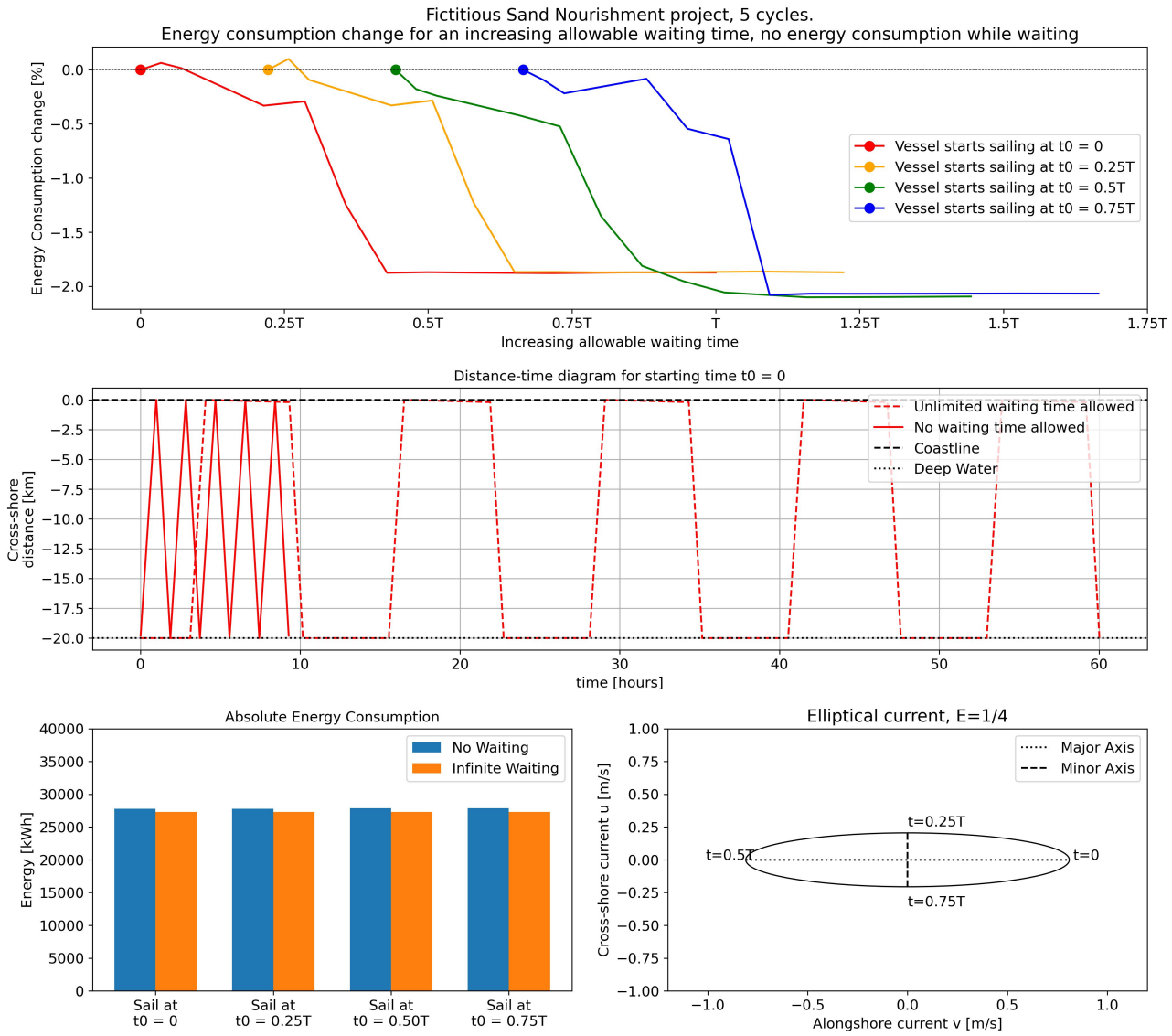

Figure D.4: Results for sailing 5 cycles. Relative energy consumption change compared to no allowable waiting time for four different starting times (top), cross-shore and alongshore components at x = -20km (middle), absolute energy consumption change (bottom left) and ellipticity E = 1/4 (bottom right).

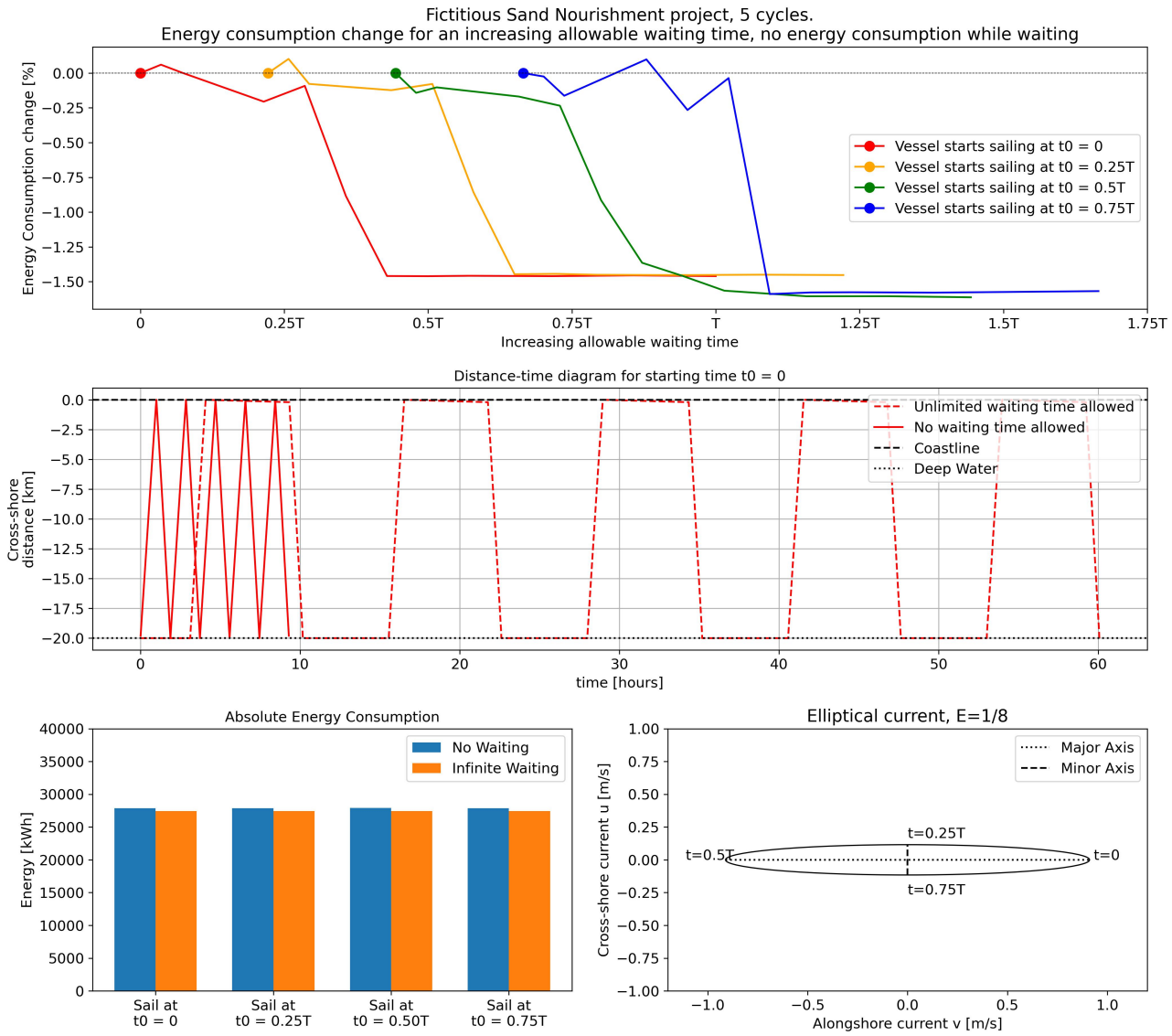

Figure D.5: Results for sailing 5 cycles. Relative energy consumption change compared to no allowable waiting time for four different starting times (top), cross-shore and alongshore components at x = -20km (middle), absolute energy consumption change (bottom left) and ellipticity E = 1/8 (bottom right).

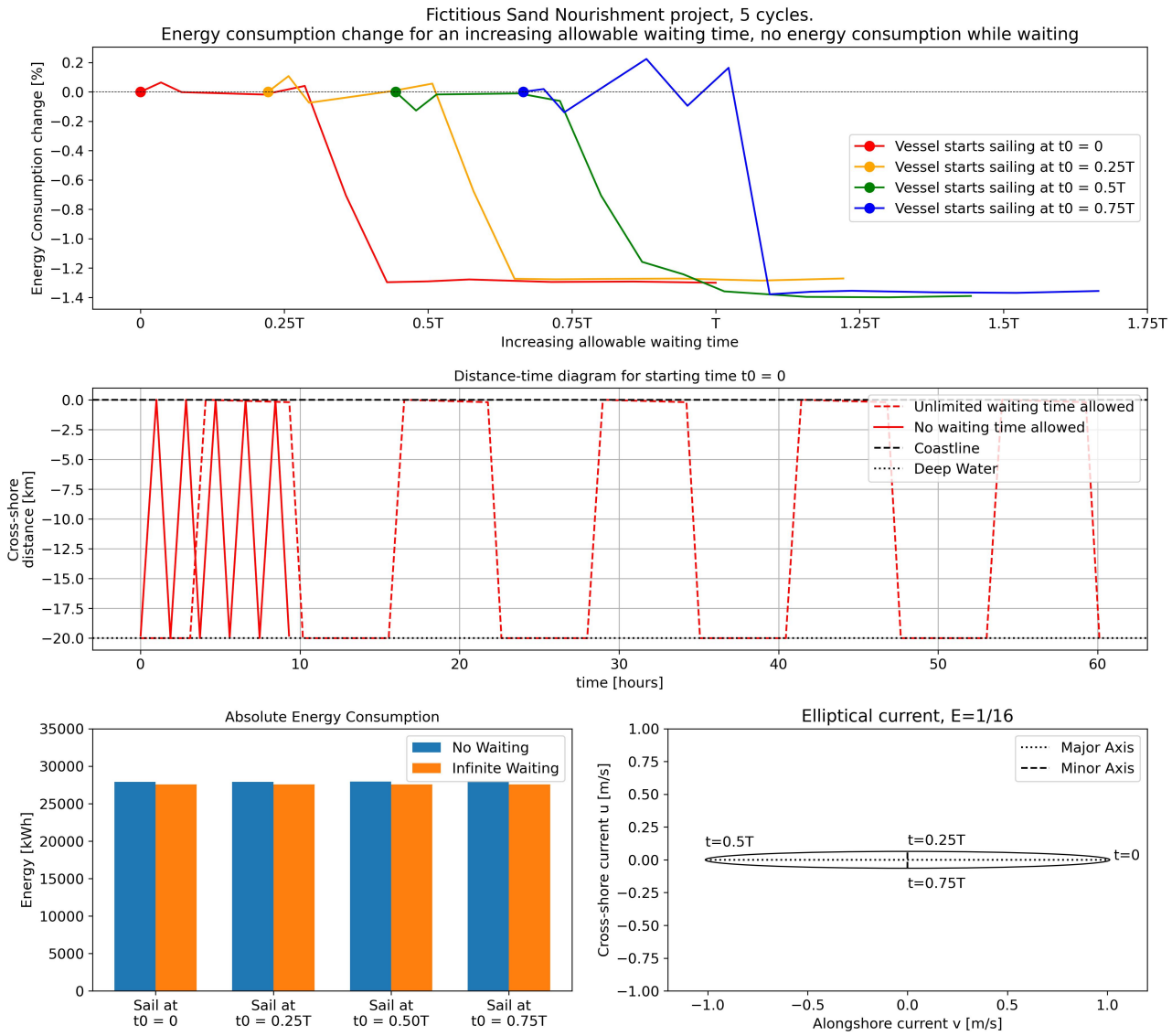

Figure D.6: Results for sailing 5 cycles. Relative energy consumption change compared to no allowable waiting time for four different starting times (top), cross-shore and alongshore components at x = -20km (middle), absolute energy consumption change (bottom left) and ellipticity E = 1/16 (bottom right).

Bibliography

Baresic, D. (2018). Lng as a marine fuel in the eu, transport environment. https://policycommons.net/artifacts/3411429/lng-as-a-marine-fuel-in-the-eu/4210790/fragments/?page=1on30Mar2023.CID:20.500.12592/xn19h5.

Bilt, V. V. D. (2019). Assessing emission performance of dredging projects. https://repository.tudelft.nl/islandora/object/uuid%3Aab6d12ea-34fe-4577-b72c-6aa688e0d1bf.

Bolt, E. (2003). schatting energiegebruik binnenvaartschepen. https://bivas.chartasoftware.com/DocumentManagement/Documents/Document:328.

Chakraborty, S. (2021). How does a rudder help in turning a ship? https://www.marineinsight.com/naval-architecture/rudder-ship-turning/.

Comer, B., Chen, C., and Rutherford, D. (2018). Relating short-term measures to imo's minimum 2050 emissions reduction target. https://theicct.org/publication/relating-short-term-measures-to-imos-minimum-2050-emissions-reduction-target/.

Corbett, J. J. (2007). Estimation, validation, and forecasts of regional commercial marine vessel inventories alternative fuels in marine transportation view project marine highway stakeholder relations view project. https://www.researchgate.net/publication/251440678.

Council of the European Union (2021). Proposal for a regulation of the european parliament and of the council establishing the framework for achieving climate neutrality and amending regulation (eu) 2018/1999 (european climate law). https://data.consilium.europa.eu/doc/document/ST-8440-2021-INIT/en/pdf.

Cullinane, K. and Cullinane, S. (2018). Policy on reducing shipping emissions: Implications for "green ports". https://doi.org/10.1016/B978-0-12-814054-3.00003-7.

de Boer, G. J. (2009). On the interaction between tides and stratification in the rhine region of freshwater influence. http://resolver.tudelft.nl/uuid:c5c07865-be69-4db2-91e6-f675411a4136.

Esmaeilpour, M., Martin, J. E., and Carrica, P. M. (2016). Near-field flow of submarines and ships advancing in a stable stratified fluid. https://doi.org/10.1016/j.oceaneng.2016.06.038.

Esmaeilpour, M., Martin, J. E., and Carrica, P. M. (2018). Computational fluid dynamics study of the dead water problem. https://doi.org/10.1115/1.4037693.

European Commission (2013). Green paper a 2030 framework for climate and energy policies. https://eur-lex.europa.eu/LexUriServ/LexUriServ.do?uri=COM:2013:0169:FIN:en:PDF.

Fetting, C. (2020). The european green deal. https://www.esdn.eu/fileadmin/ESDN_Reports/ESDN_Report_2_2020.pdf.

Flores, R. P., Rijnsburger, S., Horner-Devine, A. R., Kumar, N., Souza, A. J., and Pietrzak, J. D. (2020). The formation of turbidity maximum zones by minor axis tidal straining in regions of freshwater influence. *Journal of Physical Oceanography*, 50:1265–1287.

Forster, H., Nissen, C., Siemons, A., Renders, N., Dael, S., Sporer, M., Tomescu, M., and Agency., E. E. (2021). Trends and projections in europe 2021. https://www.eea.europa.eu/publications/trends-and-projections-in-europe-2021.

Goldsworthy, L. and Goldsworthy, B. (2015). Modelling of ship engine exhaust emissions in ports and extensive coastal waters based on terrestrial ais data - an australian case study. *Environmental Modelling and Software*, 63:45–60.

Halem, J. P. V. (2019). Route optimization in dynamic currents navigation system for the north sea and wadden sea. http://resolver.tudelft.nl/uuid:5d34d333-34fe-4181-95b6-d8d82f72d979.

Heaps, N. S. (1972). Estimation of density currents in the liverpool bay area of the irish sea. *Geophysical Journal of the Royal Astronomical Society*, 30:415–432.

Holtrop, J. and Mennen, G. G. J. (1982). An approximate power prediction method. https://repository.tudelft.nl/islandora/object/uuid:ee370fed-4b4f-4a70-af77-e14c3e692fd4.

Huang, L., Wen, Y., Zhang, Y., Zhou, C., Zhang, F., and Yang, T. (2020). Dynamic calculation of ship exhaust emissions based on real-time ais data. *Transportation Research Part D: Transport and Environment*, 80.

IMO (2020). Fourth greenhouse gas study 2020. https://www.imo.org/en/OurWork/Environment/Pages/Fourth-IMO-Greenhouse-Gas-Study-2020.aspx.

IMO (2022). Imo's work to cut ghg emissions from ships. ://www.imo.org/en/MediaCentre/HotTopics/Pages/Cutting-GHG-emissions.aspx.

IPCC (2023). Ar6 synthesis report: Climate change 2023. https://www.ipcc.ch/report/sixth-assessment-report-cycle/.

ITTC (2002). Ittc- recommended procedures. https://ittc.info/media/2021/75-02-02-02.pdf.

Jalkanen, J.-P., Brink, A., Kalli, J., Pettersson, H., Kukkonen, J., and Stipa, T. (2009). Atmospheric chemistry and physics a modelling system for the exhaust emissions of marine traffic and its application in the baltic sea area. www.atmos-chem-phys.net/9/9209/2009/.

Janssen, D. G. J. (2023). Physics-based energy estimation during the loading phase of a tshd. http://resolver.tudelft.nl/uuid:1f4b81b4-3012-40d1-b7b1-8bff6eab766a.

Koningsveld, V., Werff, M. . V. D., Jiang, S. E. ., Lansen, M. ., Vriend, A. J. . D., Koningsveld, M., Werff, S. E. V. D., Jiang, M., Lansen, A. J., and Vriend, . D. (2021). Part iv-ch 5 performance of ports and waterway systems publication date 2021 document version final published version published in ports and waterways.

Lamers, S. (2022). Improved estimations of energy consumption for dredging activities based on actual data. https://repository.tudelft.nl/islandora/object/uuid:0a41fbed-c2e0-4441-a95b-f8dc42655be1?collection=education.

Lübke, L. (2016). Investigation of a semi-balanced rudder. https://www.researchgate.net/publication/265745623.

Maritmeculture (2020). Form coefficients of a ship with illustrations. https://www.maritmeculture.com/form-coefficients-of-a-ship-with-illustrations/.

Miola, A. and Ciuffo, B. (2011). Estimating air emissions from ships: Meta-analysis of modelling approaches and available data sources. *Atmospheric Environment*, 45:2242–2251.

Moreno-Gutiérrez, J. and Durán-Grados, V. (2021). Calculating ships' real emissions of pollutants and greenhouse gases: Towards zero uncertainties. *Science of the Total Environment*, 750.

Olmer, N. (2017). Greenhouse gas emissions from global shipping, 2013-2015. www.theicct.org.

Pavlenko, N., Comer, B., Zhou, Y., Clark, N., and Rutherford, D. (2020). The climate implications of using lng as a marine fuel. www.theicct.org.

Pietrzak, J. D. (2021). *An introduction to oceanography for civil and offshore engineers.* TU Delft.

Prandle, D. (1982). The vertical structure of tidal currents. *Geophysical Astrophysical Fluid Dynamics*, 22:29–49.

Rijnsburger, S., Flores, R. P., Pietrzak, J. D., Horner-Devine, A. R., Souza, A. J., and Zijl, F. (2021). The evolution of plume fronts in the rhine region of freshwater influence. *Journal of Geophysical Research: Oceans*, 126.

Roh, M.-I. and Lee, K.-Y. (2018). Computational ship design. https://doi.org/10.1007/978-981-10-4885-2_5.

Rotteveel, E. (2013). Investigation of inland ship resistance, propulsion and manoeuvring using literature study and potential flow calculations. http://resolver.tudelft.nl/uuid:330b5f75-8fee-4a68-8e63-13bee8149c84.

Sarris, E. (2023). Naval ship propulsion and electric power systems selection for optimal fuel consumption. https://dspace.mit.edu/handle/1721.1/68573.

Schneekluth, H. and Bertram, V. (1998). Ship design for efficiency and economy. https://doi.org/10.1016/B978-0-7506-4133-3.X5000-2.

Segers, L. J. M. (2021). Mapping inland shipping emissions in time and space for the beneet of emission policy development: a case study on the rotterdam-antwerp corridor. https://repository.tudelft.nl/islandora/object/uuid%3Aa260bc48-c6ce-4f7c-b14a-e681d2e528e3.

Smith, T., Jalkanen, J. P., Anderson, B. A., Corbett, J. J., Faber, J., Hanayama, S., O'Keeffe, E., Parker, S., Johansson, L., Aldous, L., Raucci, C., Traut, M., Ettinger, S., Nelissen, D., Lee, D. S., Ng, S., Agrawal, A., Winebrake, J., Hoen, M., Chesworth, S., and Pandey, A. (2014). Third imo ghg study 2014 executive summary and final report. https://greenvoyage2050.imo.org/wp-content/uploads/2021/01/third-imo-ghg-study-2014-executive-summary-and-final-report.pdf.

Soulsby, R. L. (1983). Physical oceanography of coastal and shelf seas. https://www.sciencedirect.com/bookseries/elsevier-oceanography-series/vol/35/suppl/C.

United Nations (2016). The paris agreement. https://treaties.un.org/Pages/ViewDetails.aspx?src=TREATY&mtdsg_no=XXVII-7-.

van Koningsveld, M., van der Werff, S. E., Jiang, M., Lansen, A. J., and de Vriend, H. J. (2021). Part iv - ch 5 performance of ports and waterway systems. *Ports and Waterways: Navigating a changing world*, pages 433–458.

Van Oord (2019). S.e.a. https://www.vanoord.com/en/sustainability.

Van Oord (2022). Openclsim: Discrete event dredging fleet simulation to optimise project costs mark van koningsveld. https://www.researchgate.net/publication/360852095.

van Terwisga, T. (1989). Weerstand en voortstuwing van bakken, een literatuurstudie. https://repository.uantwerpen.be/docman/irua/6d4648/4027.pdf.

Ventura, M. (2022). Bulbous bow design. http://www.mar.ist.utl.pt/mventura/Projecto-Navios-I/EN/SD-1.5.4-Bulbous%20Bow%20Design.pdf.

Visser, A. W., Souza, A. J., Hessner, K., Simpson, J. H., and Visser, A. W. (1994). Oceanologica acta-vol. 17-n°4 the effect of stratification on tidal current profiles tidal currents stratification vertical viscosity tidal mixing fresh water in a region of freshwater influence.

Vlasblom, W. J. (2007,). Trailing suction hopper dredge. fromhttps://dredging.org/documents/ceda/downloads/vlasblom2-trailing_suction_hopper_dredger.pdf.

Wang, C., Corbett, J. J., and Firestone, J. (2006). Modeling energy use and emissions from north american shipping: an application of ship traffic, energy and environment model (supporting information). http://www.epa.gov/otaq/ngm.htm.

Zeng, Q., Thill, C., Hekkenberg, R., and Rotteveel, E. (2019). A modification of the ittc57 correlation line for shallow water. *Journal of Marine Science and Technology (Japan)*, 24:642–657.